

RECENT DEVELOPMENTS IN

# mechanical testing

 | STP 608

AMERICAN SOCIETY FOR TESTING AND MATERIALS

# RECENT DEVELOPMENTS IN MECHANICAL TESTING

A symposium  
presented at the  
Seventy-eighth Annual Meeting  
AMERICAN SOCIETY FOR  
TESTING AND MATERIALS  
Montreal, Canada, 22-27 June 1975

ASTM SPECIAL TECHNICAL PUBLICATION 608  
A. K. Schmieder, symposium chairman

List price \$14.50

04-608000-23



AMERICAN SOCIETY FOR TESTING AND MATERIALS  
1916 Race Street, Philadelphia, Pa. 19103

© by AMERICAN SOCIETY FOR TESTING AND MATERIALS 1976  
Library of Congress Catalog Card Number: 76-11471

**NOTE**

**The Society is not responsible, as a body,  
for the statements and opinions  
advanced in this publication.**

**Printed in Lutherville-Timonium, Md.  
Sept. 1976**

## Foreword

The symposium on Recent Developments in Mechanical Testing was presented at the Seventy-eighth Annual Meeting of the American Society for Testing and Materials held in Montreal, Canada, 22-27 June 1975. Committee E-28 on Mechanical Testing sponsored the symposium. A. K. Schmieder, General Electric Company, presided as symposium chairman.

## **Related ASTM Publications**

**Instrumented Impact Testing, STP 563 (1974), \$21.75, 04-563000-23**

**Evaluation of Wear Testing, STP 446 (1969), \$7.75, 04-446000-23**

## **A Note of Appreciation to Reviewers**

This publication is made possible by the authors and, also, the unheralded efforts of the reviewers. This body of technical experts whose dedication, sacrifice of time and effort, and collective wisdom in reviewing the papers must be acknowledged. The quality level of ASTM publications is a direct function of their respected opinions. On behalf of ASTM we acknowledge with appreciation their contribution.

*ASTM Committee on Publications*

## **Editorial Staff**

Jane B. Wheeler, *Managing Editor*

Helen M. Hoersch, *Associate Editor*

Charlotte E. DeFranco, *Senior Assistant Editor*

Ellen J. McGlinchey, *Assistant Editor*

# Contents

<b>Introduction</b>	1
<b>Evaluating Engineering Alloys in Compression</b> —R. CHAIT AND C. H. CURLL	3
Loading and Specimen Considerations for Homogeneous Deformation	4
Lubricants to Minimize End Effects	6
Other Techniques Investigated to Minimize End Effects	9
Recommendations and Closing Comments	12
<b>Rational Basis and New Methods for Proportional Limit, Machine Stiffness, Critical Stress Intensity, and Crack Velocity Measurements</b> —R. B. CLOUGH	20
Tensile Machine Kinetics in System Prior to Tightening and Alignment	22
Tensile Machine Kinetics in a System Which is Aligned and Tightened	23
Determination of Proportional Limit	24
Proportional Limit Under Multiaxial Stress	26
Stiffness of Constant Crosshead Velocity Machines	28
Stiffness of Constant Load Rate Machines	30
Stiffness of Constant Strain Rate Machines	31
Machine Stiffness Effects on Load-Cycling Rate Sensitivity of the Stress	33
Crack Motion	35
Variability of Machine Stiffness	40
Conclusion	40
Discussion	42
<b>Results of a Round Robin Test Program on Hardness Conversion of Ferritic Stainless Steels</b> —T. G. HEBERLING	45
Round Robin Test Procedure	46
Results	47
Conclusions	52
Subsequent ASTM Actions	53
<b>Static Mean Stress and Cyclic Yield Strength</b> —G. F. WEISSMANN AND J. A. DAVIS	55
WT-Bend Tester	55
Test Results	61
Summary and Conclusions	65
<b>Use and Reproducibility of a Gage to Measure the Lateral Expansion of Charpy V-Notch Impact Specimens</b> —J. M. HOLT	67
Lateral Expansion Gage	68

Materials and Experimental Work	71
Results and Discussion	75
Summary and Conclusions	88
<b>Determination of Plastic or Creep Strains by Grids—M. J. MANJOINE</b>	91
Procedure	92
Experimental Work	97
Discussion	100
Conclusion	104
<b>Stress Relaxation in Bending—P. PARIKH AND E. SHAPIRO</b>	106
Test Procedure	106
Results and Discussion	109
Conclusions	112
<b>Comparison of Manual to Automatic Unloading During Relaxation Tests—</b>	
A. K. SCHMIEDER AND R. S. ROBINSON	118
Materials Tested	119
Equipment Used	119
Testing Procedure	121
Procedure for Selecting the Magnitude of Stress Step Down	122
Results of Tests	124
Discussion	126
Conclusions	131

# Introduction

---

Many areas of mechanical testing, such as fatigue, fracture toughness, and creep, have professional specialists in one area alone and an effective means of disseminating and preserving technical information in that area. This symposium is designed to perform the same function for those areas which deal with data that are widely used but do not require the attention of a professional specialist in each single area in most laboratories. It follows that the person interested in one paper of this group will probably also be interested in several others. The symposium seemed to be an efficient way of making this specialized information on a variety of subjects available to the rather limited group who would find it directly applicable to their work. It is our hope that this publication will keep the information available for these people and for new people who will work with this group of tests in the future.

More specifically, this volume contains two papers related to tensile properties, two on relaxation, and one each on topics related to compression, hardness, and impact testing, and one on the use of grids to measure strain at elevated temperature. The functional classifications are almost as numerous as the types of tests. These are to:

1. Preserve for the use of future task groups detailed information which was used to arrive at a current test standard or recommended practice. Examples are the paper on hardness conversions and the paper on measurement of lateral expansion of impact specimens.

2. Provide a convenient reference which may be listed in revisions of recommended practices for the convenience of those that need more detailed information on the test methods. Examples are the two papers on relaxation and that on compression.

3. Describe test methods which have been found to be useful as supplements or replacements for the methods published in the standards. Examples are the papers on proportional limit, on cyclic yield strength, and on the use of strain grids at high temperatures.

4. Provide a comprehensive summary of a well-established area of testing. An example is the paper on compression testing.

The number of discussions of new test methods indicates that the technical community finds them interesting and stimulating. This, combined with the mercenary advantage of early application of improved methods, would seem to be ample justification for their continued publication. On the other hand, the wisdom of printing detailed statistics and refinements of technique concerning test methods that are well established may well be questioned. However, all of these test methods are reviewed after five years, if not sooner, and many are revised. Those who have served on the task groups charged with revision will probably remember the frustration of trying to determine what facts, if any, led to certain preferences and numerical values. Yet, it would be impractical to record all the workshop discussions and fragmentary evidence used and even difficult to pass it on to the next task group, to say nothing of the monumental tasks of editing the material into useful order and easily understood statements. Just to hammer out a five-page recommended practice every five years is as much writing as most engineers would be willing to undertake. This type of symposium is proposed as a suitable stimulus to get at least part of this voluminous information put into good order with clear language and stored in a readily accessible form. This will make the work of future task groups much easier in the parts covered and focus their efforts on those parts where least is known. The need for factual data is greater now than in the past because of the added requirement of a section on precision and accuracy in all standards and recommended practices.

Similar symposia are planned at five-year intervals or sooner if the available material justifies a shorter interval. Members of all task groups to revise standards or practices and task groups conducting round robins are urged to order the factual material and fully describe the test methods. They may have confidence that the effort will be helpful to many following groups through a publication similar to this.

*A. K. Schmieder*

Manager, Material Testing, Materials and Processes Laboratory, General Electric Co., Schenectady, N. Y. 12345; symposium chairman.

## Evaluating Engineering Alloys in Compression

---

**REFERENCE:** Chait, R. and Curll, C. H., "Evaluating Engineering Alloys in Compression," *Recent Developments in Mechanical Testing, ASTM STP 608*, American Society for Testing and Materials, 1976, pp. 3-19.

**ABSTRACT:** Testing in compression has several attractive features when compared to the more frequently employed tension test. To take full advantage of these features, it is necessary to obtain deformation that is as close to homogeneous as possible. This paper describes how homogeneous compression can be obtained, paying particular attention to specimen dimensions and lubrication techniques. Comparison is made to deformation under nonhomogeneous conditions. Stress-strain curves obtained in compression for various engineering materials are presented. These curves represent uniform or homogeneous compression. For some metals, there is excellent agreement between the compressive flow curves and those obtained in tension, provided the latter is corrected for necking. However, it is shown that, for high-strength steels, there is not the expected agreement between the compressive and tensile flow curves. The resistance to compressive deformation is greater than to tensile deformation. This effect, termed a strength differential effect, is shown to be independent of the amount of plastic strain. However, it is affected by temperature, since it increases as the temperature is lowered.

**KEY WORDS:** mechanical tests, compression tests, deformation, stresses, strains, lubrication, tensile properties, compressive properties

Compression testing of engineering materials has been attractive to many investigators for several reasons. First, there may be a desire to avoid the tensile instability phenomenon (necking) that occurs when the strain hardening no longer compensates for the decrease in cross-sectional area. When this phenomenon occurs, a triaxial state of stress develops, and necking corrections [1,2]<sup>2</sup> must be utilized to obtain a uniaxial flow stress. This phenomenon also serves to limit ductility since void initiation begins under tensile loading soon after necking [3]. It is possible, under compressive deformation, to avoid this phenomenon and obtain uniaxial stress-

<sup>1</sup> Supervisory materials engineer and general engineer, respectively, Army Materials and Mechanics Research Center, Watertown, Mass. 02172.

<sup>2</sup> The italic numbers in brackets refer to the list of references appended to this paper.

strain data not only beyond necking but beyond the tensile fracture strain as well. This determination of stress-strain data at large plastic strains is of interest to those engaged in metal working and fabrication where operations such as forging and rolling essentially involve large compressive deformation. For alloys that behave in a rather brittle fashion and fracture in tension before reaching the tensile yield strength, compressive deformation offers the possibility of extending the ductility range so that stress-strain data can be characterized adequately. A case in point is the flow curve obtained for a brine-quenched 0.72 percent C steel [4]. With these characteristics and uses of the compression test in mind, the objective of this paper is to discuss and summarize the more salient features of the compression test. The factors that influence the determination of mechanical properties of engineering metals and alloys utilizing the compression test are emphasized. Stress-strain curves representing homogeneous deformation are presented and compared to those obtained in tension.

### Loading and Specimen Considerations for Homogeneous Deformation

Deformation under compressive loading should be as close to homogeneous or uniform deformation as possible, and, to achieve this goal, consideration must be given to loading techniques and specimen dimensions. To promote axial loading of a cylindrical specimen, a ball seat adapter of the type proposed by in der Schmitzen [5] is suggested as part of the ASTM Compression Testing of Metallic Materials at Room Temperature (E 9-70 (1973)). Also, to help ensure concentric loading, ASTM Method E 9 specifies that for cylindrical test specimens, "the ends of a specimen shall be plane and perpendicular to the axis and the sides of the specimen within 0.25 degrees" and that "the ends shall be parallel with 0.02 percent of the length or 0.001 in., whichever is less." Accurate machining and the ball seat adapter just mentioned, coupled with centering washers and aligning collars such as shown in Fig. 1, can be employed to obtain concentric loading. It should be noted that the alignment can be checked by means of strain gages bonded to the specimen. The differences of the gages during elastic loading can be used as an indication of concentricity.

The selection of proper specimen dimension to avoid a buckling instability is also important. The critical stress for the onset of elastic buckling,  $\sigma_{cr}$ , is given by the Euler relationship

$$\sigma_{cr} = C\pi^2 E / (h/\rho)^2 \quad (1)$$

where  $E$  is the modulus of elasticity,  $h$  the specimen height,  $\rho$  the radius of gyration of the column cross section, and  $C$  the end fixity coefficient. The latter is close to the theoretical value of 4 for compression of a column

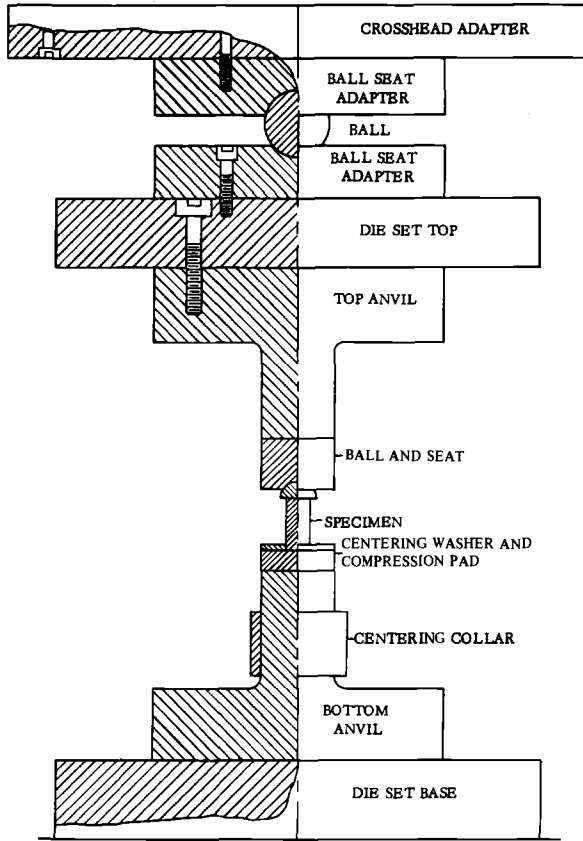


FIG. 1—Compression testing apparatus.

with fixed ends [6]. For the compression of a cylindrical specimen of diameter  $d$ ,  $\rho = d/4$ , reducing Eq 1 to

$$\sigma_{cr} = \frac{\pi^2 E_t}{4(h/d)^2} \quad (2)$$

where  $E_t$  is the tangent modulus replacing  $E$ , since deformation is not restricted to the elastic region. With  $E_t$  defined as  $d\sigma/de$ , utilizing the power law stress-strain relationship  $\sigma = Ke^n$ , Eq 2 may be rewritten as

$$\sigma_{cr} = \left[ \frac{\pi^2 n}{4(h/d)^2} \right]^n \times K \quad (3)$$

where  $n$  and  $K$  are the strain hardening exponent and coefficient, respectively, obtained from the engineering stress-strain curve.

It can be seen that the possibility of buckling instability increases with increasing  $h/d$  ratio. An  $h/d$  ratio of 3 is recommended by ASTM Method E 9-70 (1973) for determining the general compressive strength of metallic materials. However, this ratio may not preclude buckling. For example, with many of the high-strength steels, the critical buckling stress may be reached after a relatively small amount of deformation of a specimen with  $h/d = 3$ . From Eq 3 a critical buckling stress of approximately 200 ksi is calculated for 410 martensitic stainless steel. This stress level is achieved after less than 5 percent deformation. Therefore, it is well to note Polakowski's recommendation [7] that specimens with an  $h/d$  ratio of 1.6 to 2.0 be used to preclude buckling. Most of the investigations involving the compressive deformation of high-strength steels [8-12] utilize specimens with  $h/d$  ratios less than that recommended in ASTM Method E 9-70 (1973). The same statement can be made for elevated temperature tests not only of steel but for nonferrous metals and alloys [13-16].

#### Lubricants to Minimize End Effects

Reduced  $h/d$  ratios to avoid buckling instability must be balanced against the increased influence of the end effect as the  $h/d$  ratio decreases. The friction that occurs between the specimen and anvil restricts plastic flow near the specimen-anvil interface, resulting in a convex shape to the initially straight-sided specimen and a nonzero circumferential stress. A cylindrical specimen with this barrel shape is shown in Fig. 2. The following discussion emphasizes lubricants that have been used effectively to minimize end effects.

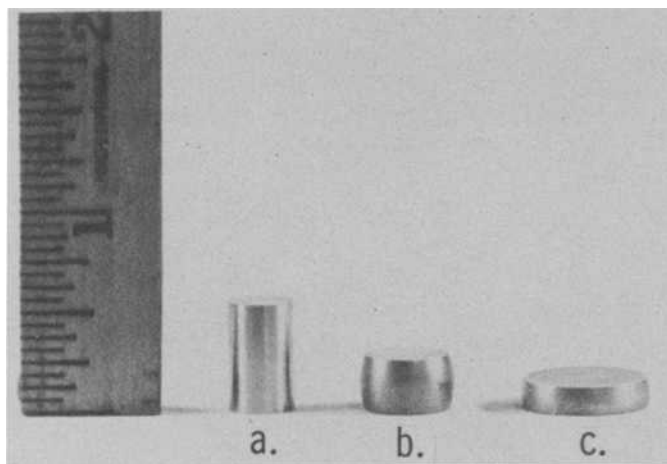


FIG. 2—Comparison of homogeneous compression and barreled specimen: (a) initial specimen, (b) barreled specimen without lubricant, and (c) homogeneous compression with lubricant.

### Lubrication with Teflon

Jovane [17], employing periodic lubrication, obtained stress-strain curves for both steel and aluminum using the following lubricants: molybdenum disulfide, lanolin, phosphate coating, and 0.003-in.-thick Teflon. Of these lubricants, Teflon was the most effective in reducing friction, as evidenced by the fact that barrelling was observed for all lubricants, with the exception of Teflon.

Additional investigations evaluating Teflon as a lubricant involve compressing aged maraging steel specimens of various  $h/d$  values (approximately 2 percent) and measuring the flow stress. The results are shown in Fig. 3. Using the coefficient of friction value from Ref 18,  $\mu = 0.04$ , the resultant frictional contribution can be estimated with the analysis of Siebel [19], as detailed by Hill [20]. Here, the distribution of the axial compressive stress,  $\sigma$ , at a radius,  $r$ , is

$$\sigma = \sigma_0 \exp \left[ \frac{\mu(d - 2r)}{h} \right] \quad (4)$$

where  $\sigma_0$  is the uniaxial flow stress obtained under frictionless conditions. Integrating Eq 2 to provide the mean compressive stress,  $\sigma_c$ , gives

$$\sigma_c = \sigma_0 \left[ 1 + \frac{\mu d}{3h} \right] \quad (5)$$

As shown in Fig. 3, Eq 3 with  $\mu = 0.04$  relates the variation in compressive flow stress to  $h/d$ . For example, from this analysis, the frictional contribution to the measured flow stress is approximately 1 percent for  $h/d = 1.65$ .

Quantitative studies support Teflon's effectiveness as a lubricant [21,22]. Utilizing pins embedded in one of the anvils, the coefficient of friction between each pin and the walls of the cavity was measured. In this way, the effectiveness of ten lubricants, including mineral oil, caprylic and oleic acid,

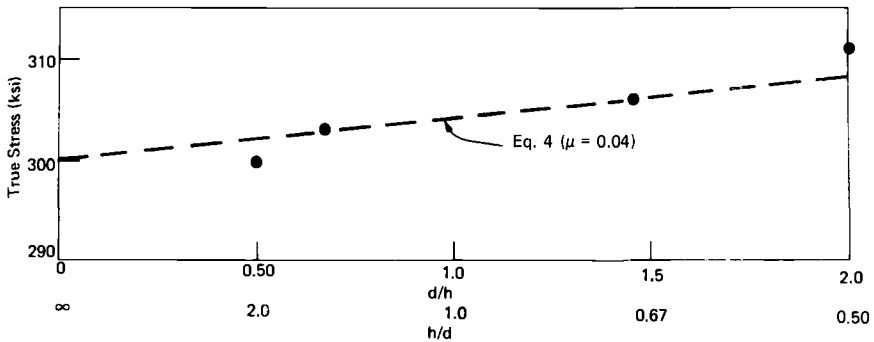


FIG. 3—Effect of specimen dimension on room-temperature compressive flow stress of homogeneously deformed maraging steel (reduction = 2 percent).

stearic acid, sodium stearate soap, lead, and Teflon, was evaluated. With all lubricants, the shear and normal stresses were measured. It was found that the low-shear-strength solid film such as Teflon resulted in the lowest shear and normal stresses [21]. As a result, Lee et al [22] concluded that employing Teflon film as a lubricant led to a condition that was very close to "frictionless." It should be noted that, with the techniques of using instrumented pressure-sensitive pins in the compression platen to monitor the distribution of the normal and shear stress, it was found that Eq 4 described the stress distribution across the interface of a specimen lubricated with Teflon film and reduced 10 percent in height [21].

Teflon's effectiveness as a lubricant has led to its wide and varied use in recent years. Trozera [23] utilized the compressive strain hardening behavior to develop a relationship, useful in wire drawing, involving the stress, coefficient of friction, and die angle. The same author [24] evaluated the accuracy of tensile necking correction factors discussed earlier via a comparison with the true stress-true strain curve obtained in compression. Finally, Hosford [25] utilized Teflon in a plane-strain compression test that provided information on single crystal deformation, while Tomlinson and Talbot [26] were able to evaluate flow curves obtained from hardness measurements.

Hsü [27] has examined the use of Teflon as a lubricant and has made some interesting observations. Upon loading, it was observed that first the Teflon is extruded between the specimen and anvil and along the sides of the specimen. Following the extrusion, the specimen punctures the Teflon and traps a thin film between it and the anvil. During the extrusion, the Teflon acts as a pressurized lubricant producing a net outward force and a saucer shape at the end of the specimen. With a single sheet of Teflon, longitudinal and circumferential strains that are produced are characteristic of the ideal homogeneous deformation. In contrast, using double sheets of Teflon did not result in uniform deformation near the center of the specimen, especially at high reductions.

### *Elevated Temperature Lubricants and Testing Techniques*

To gain information on metal forming characteristics, compression tests have been conducted at elevated temperatures. For these tests, Teflon is not suitable, and other lubricants have been utilized. Up to 100°C, oil has been used [13]. Between room temperature and 400°C, Hockett [28] has successfully used molybdenum disulfide powder in oil for the deformation of uranium. In this temperature range, graphite grease has also been used [14]. Powdered glass has been utilized as a lubricant for the compressive deformation of steel [14,29] and silicon-iron [16] at temperatures up to approximately 1000°C.

One of the reasons for the successful employment of the just mentioned lubricants has been the use of concentric grooves placed in the ends of

the specimen to retain the lubricant despite substantial reductions. This technique has been employed with lead [13], uranium and aluminum [15,28], silicon-iron [16], and Armco iron [29]. However, it has been emphasized that the groove depth, groove spacing, and included angle are critical, and what is optimum for one material may not be optimum for another [15]. For example, seventy-four 0.004-in.-deep grooves/in., thirty-two 0.002-in.-deep grooves/in., and sixty-six 0.004-in.-deep grooves/in. have been used for uranium and aluminum [28], lead [13], and silicon-iron [16], respectively. The author has attempted to adapt this technique to the room-temperature deformation of high-strength steels and has found that regardless of spacing, depth, and included angle, end splaying could not be prevented. Presumably, this was due to the radial pressure that resulted from the entrapped lubricant [13].

### Other Techniques Investigated to Minimize End Effects

In addition to the "concentric groove" technique, there have been other suggestions designed to overcome end effects that have employed modifications to the cylindrical test specimen. As discussed by Polakowski [7], these techniques do not necessarily provide homogeneous deformation. For example, Siebel and Pomp [30] proposed the use of a conical-ended specimen, resulting in an axially directed force. However, the determination of the angle may be difficult. In addition, Polakowski [7] disclaims the fact that a specimen of this geometry will lead to homogeneous compression since the effect of the cone is to bend the inner fibers of the material to the outside, decreasing the load necessary for the deformation. Therefore, seemingly homogeneous compression "is caused not so much by the alleged elimination of friction as by the incidental and unstable equilibrium between the axial and radial stresses, the resistance of the material to deformation, and the friction." Two additional specimen designs which have been suggested are: (a) stacked specimens as suggested by Meyer and Nehl [31] and (b) dumbbell-shaped specimens similar to those used in creep experiments [32]. As evidenced by the flow curves shown in Fig. 4a and the final appearance of the specimen shown in Fig. 5, both geometries exhibited nonuniform deformation.

Specimens that have undergone barrelling can be utilized in conjunction with a correction factor to provide accurate flow stress data. In a derivation similar to that for the triaxial state of stress that exists in a necked tensile specimen [1], Read et al [4] suggest that the relationship between the mean stress based on the cross sectional area at the maximum diameter,  $\sigma_c$  (barrelling), and  $\sigma_0$  is

$$\sigma_c \text{ (barrelling)} = \sigma_0(1 - r/4R) \quad (6)$$

where  $R$  is the radius of curvature of the barrelled section, and  $r$  is the radius of the largest cross section. By utilizing this correction factor, one can

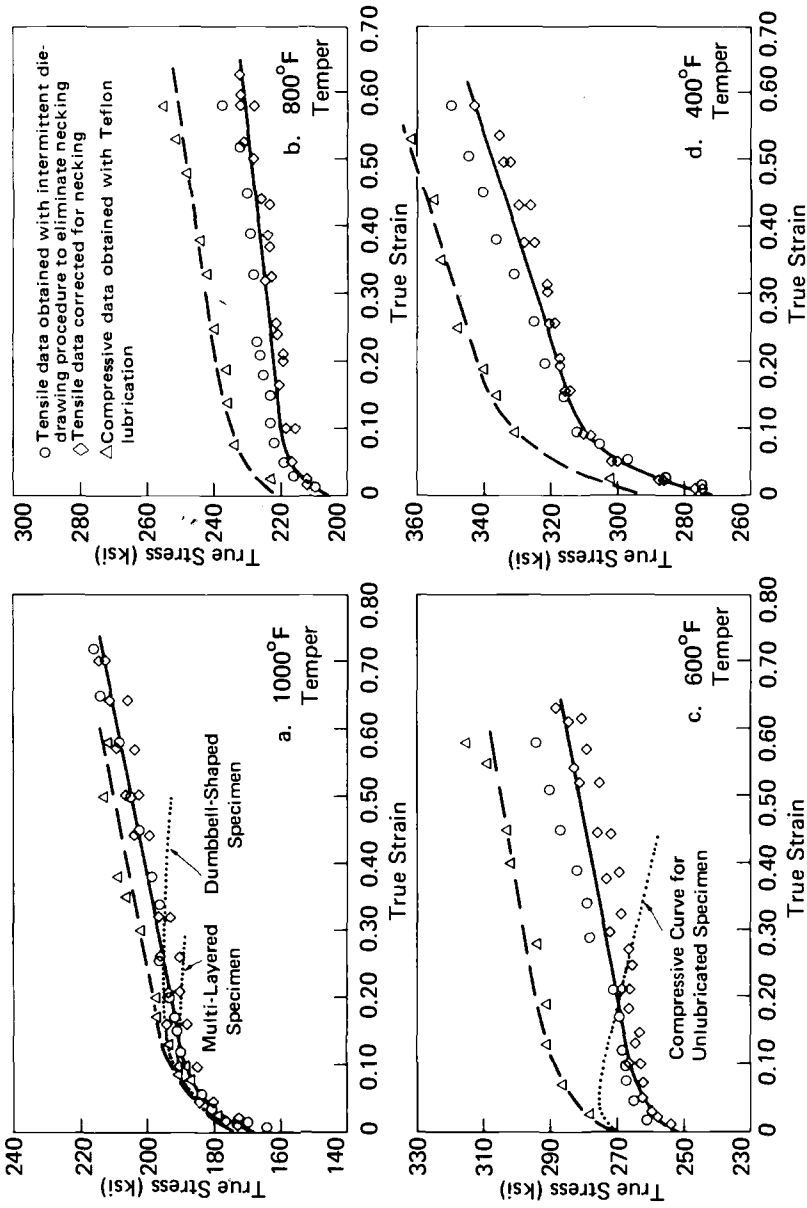


FIG. 4—Room-temperature tensile and compressive flow curves for 4340 steel quenched and then tempered at (a) 1000°F, (b) 800°F, (c) 600°F, and (d) 400°F.

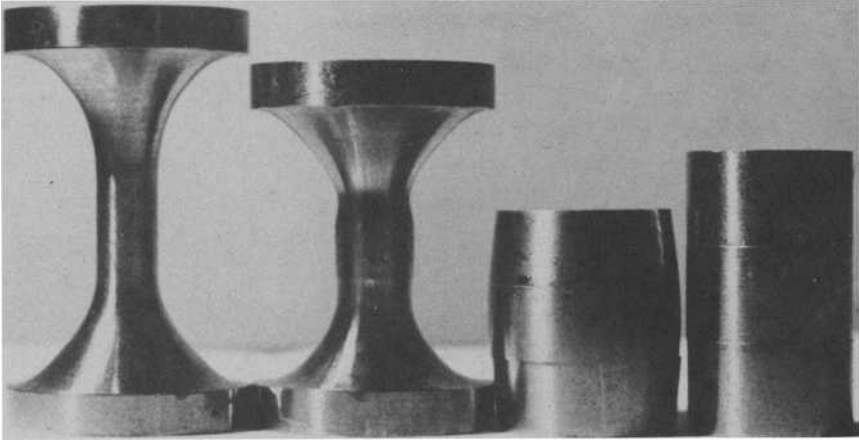


FIG. 5—Nonhomogeneous compression of (a) dumbbell-shaped specimen and (b) multi-layered specimen.

compensate for barrelling as long as  $r/R < 0.1$  and  $h/d > 1.5$  [4]. Note that this behavior is in contrast to that described by Eq 5 which states that, prior to the onset of barrelling,  $\sigma_c$  increases with an increase in friction. Along with other data [15,17], this appears to substantiate Polakowski's claim [7] that "the resistance to homogeneous deformation was higher than to nonhomogeneous deformation and consequently that an increase of friction would have to cause a decrease of the resistance to compression." It was reasoned that, with nonuniform deformation, the outer fibers bend like an axially loaded beam, reducing the resistance to further deformation. In support of this view, Polakowski noted that using a remachining technique of Taylor and Quinney [33] to remove the bent layers gave flow stresses that were greater than those determined from a single-step compressive procedure.

The validity of Polakowski's hypothesis has a bearing on a technique proposed by Cook and Larke [34] which is based on the fact that a specimen of infinite height should represent deformation under frictionless conditions. Specifically, it involves a graphic technique where the flow stress is obtained for an average strain by extrapolating the compressive stress to  $d/h = 0$  ( $h/d = \infty$ ). By varying the amount of reduction and  $h/d$  ratio, it was possible to construct a flow curve claimed to be representative of frictionless conditions. However, it is shown in Fig. 6 that the data of Cook and Larke lie below the stress-strain curve obtained with effective lubrication. Therefore, in agreement with the Polakowski hypothesis, such an extrapolation technique does not appear to compensate for inadequate lubrication to produce flow stress data representative of the frictionless condition.

## Recommendations and Closing Comments

### *Recommendations*

From the preceding section, it can be seen that meaningful stress-strain data can be obtained under compressive loading, provided that proper consideration is given to a number of important factors. Among these are:

1. Concentric loading.
2. Accurate specimen machining.
3. Proper  $h/d$  ratio.
4. Adequate lubrication.

The first two of the factors just listed are given adequate coverage in ASTM Method E 9-70 (1973). However, to avoid buckling with the higher strength materials,  $h/d$  in the range 1.5 to 2.0 is recommended. For cylindrical specimens, Teflon film has been shown to be an effective room-temperature lubricant and should be used to minimize frictional end effects.

Up to this point, discussion has emphasized the more common method of compression testing which utilizes a simple cylindrical specimen. An alternate approach taken by some investigators is based on the use of a flat-ring-type compression specimen. Compressive deformation of this specimen will produce dimensional changes that are dependent on the frictional conditions. These dimensional changes have been incorporated into an analysis of Avitzur [35] and utilized to study friction conditions in terms of the friction factor,  $m$ , ( $m = \tau/\tau_0$  where  $\tau$  is the interfacial shear stress and  $\tau_0$  is the shear strength of the material) [36]. These studies have been extended to the determination of a stress-strain curve via theoretical equations which relate the average compressive stress and dimensional change to the flow stress [37]. With this technique and specimens with outside diameter/inside diameter/height ratios of 6/3/0.5 and 6/3/1, compressive flow curve data have been obtained that agree very well with similar data taken from cylindrical ( $h/d = 2$ ) specimens [39]. While this test method involves the use of several specimens, it does eliminate time-consuming remachining and relubrication and, for this reason, should be examined closely as an alternative for cylindrical specimens.

### *Sheet Materials*

Many times it is not possible to obtain a cylindrical or a ring-type specimen. For example, when conducting compression tests of specimens taken from sheet material, thin specimens must be used, and buckling is a distinct possibility. To prevent buckling, a fixture such as shown in Fig. 7 which supports the specimen is required. This fixture is similar to that of Budington [40] except that an extensometer is used. The knife edge move-

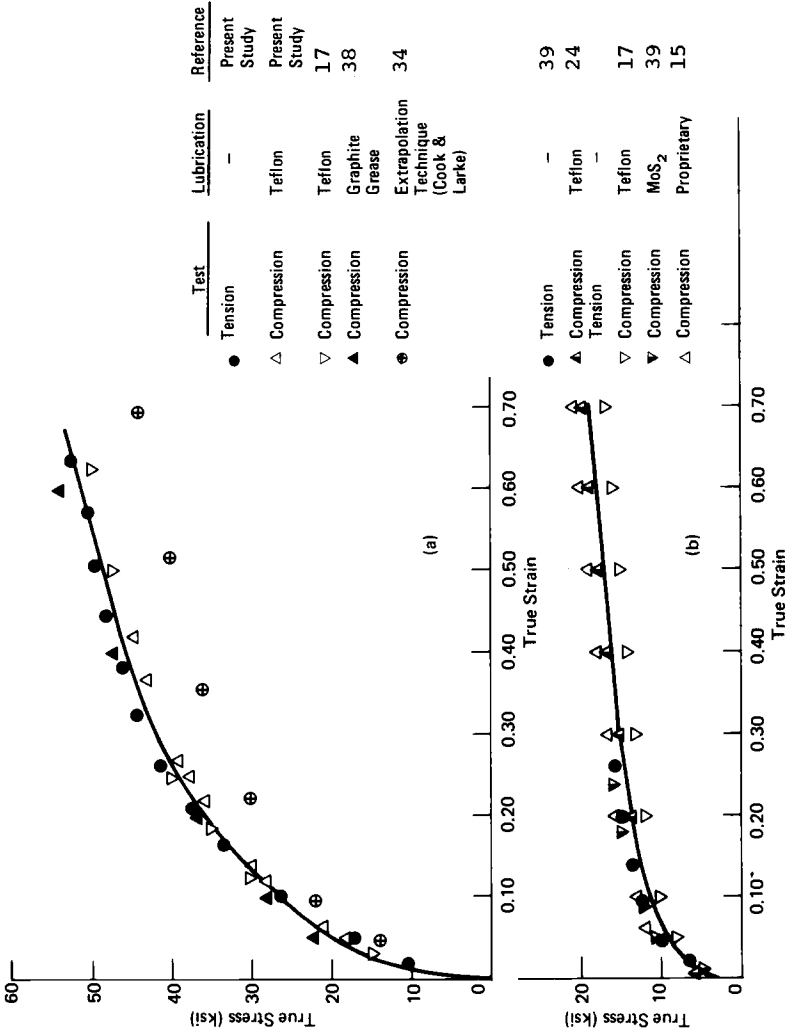


FIG. 6—Room-temperature tensile and compressive flow curves for (a) annealed copper and (b) annealed aluminum.

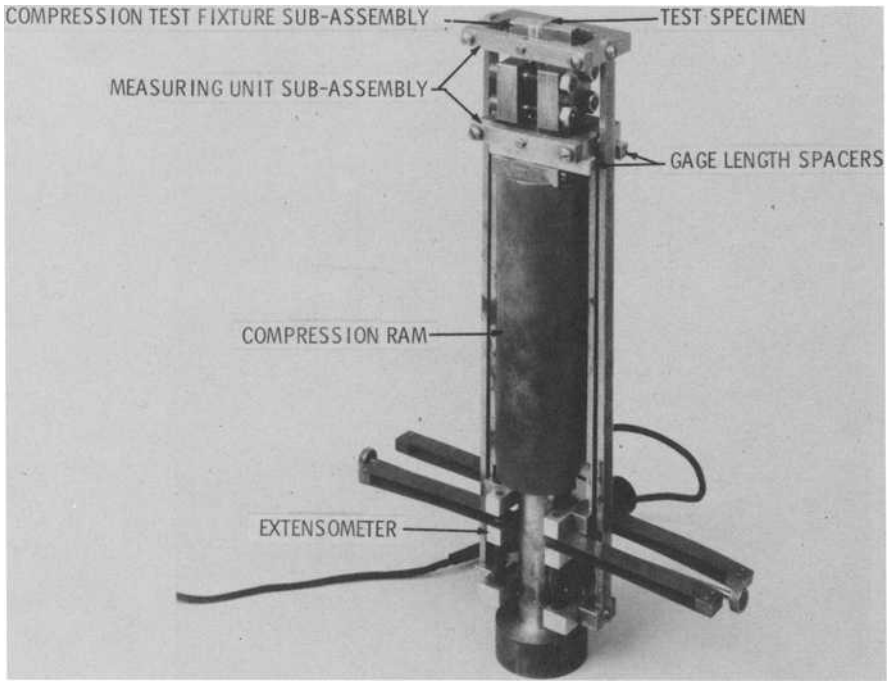


FIG. 7—Sheet compression test fixture assembly.

ment is transferred by connecting arms through a pivot and microformer to produce a calibrated voltage signal which is sent to a balancing microformer to simultaneously record the load-deflection curve and null balance the microformer cores.

#### *Comparison of Compression and Tension Data—The SD Effect*

After giving the necessary attention to the factors just listed, stress-strain curves of some materials agree exactly with those obtained in tension. Such materials are copper (Fig. 6a) and 1100-0 aluminum (Fig. 6b). The curve obtained by the extrapolation method of Cook and Larke is not considered for the reasons noted earlier. With many materials, however, there is growing evidence that one does not obtain agreement between flow curves obtained in tension and compression. Some data on high-strength steels illustrate this point. Compressive flow curves were obtained by deforming cylindrical specimens having a diameter of 0.333 in. and an  $h/d$  ratio of approximately 1.65. Homogeneous compressive deformation was achieved by coupling the renewal of the 0.002-in.-thick Teflon film lubricant with a remachining technique similar to that of Taylor and Quinney [33]. Remachining was necessary since the Teflon film punctures around the rim of

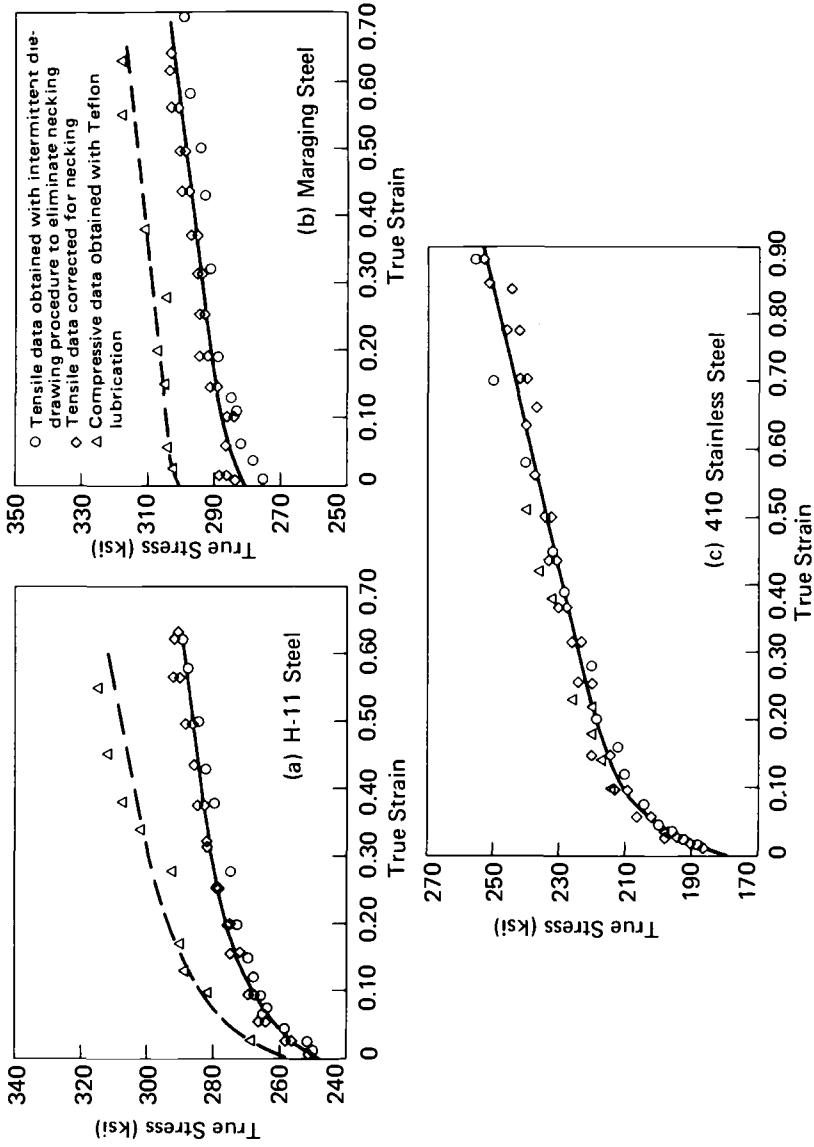


FIG. 8—Room-temperature tensile and compressive flow curves for (a) H-11 steel, (b) 18Ni (300) maraging steel, and (c) 410 stainless steel.

the specimen, as noted earlier. The remachining closely restored the original  $h/d$  ratio.

Results of these tests are shown in Fig. 4 for quenched and tempered 4340 steel and in Fig. 8 for H-11 steel, maraging steel, and 410 martensitic stainless steel. Also, shown in Figs. 4 and 8 are the corresponding stress-strain curves obtained in tension. The uniaxial flow stresses in tension were obtained either by utilizing a necking correction factor discussed previously or a die-drawing procedure which eliminated the neck. The resultant tensile curves are parallel to those obtained in compression but lie considerably below the compressive flow curves. This observation is referred to as the strength-differential (SD) effect [41]. Several observations concerning the SD effect can be made. First, the SD effect does not appear to be affected by the amount of plastic strain. It remains essentially constant regardless of substantial deformation, as shown in Fig. 9. Also, as the test temperature decreases, the SD increases, as shown in Fig. 10. Because the magnitude of the SD is not greatly affected by large plastic strain, it is highly unlikely that microcracking, residual stress, retained austenite, or Baushinger effect contribute significantly to the SD of ultra-high-strength steels. More promising is the recent suggestion that the SD could be interpreted in terms of a solute/dislocation interaction model where nonlinear elastic strains resulting from the distortion of the lattice around the interstitial atom lead to a greater interstitial-dislocation binding energy in compression than in tension [41]. Precipitation of carbon from solution during the tempering process does not negate its application to microstructures of tempered martensite

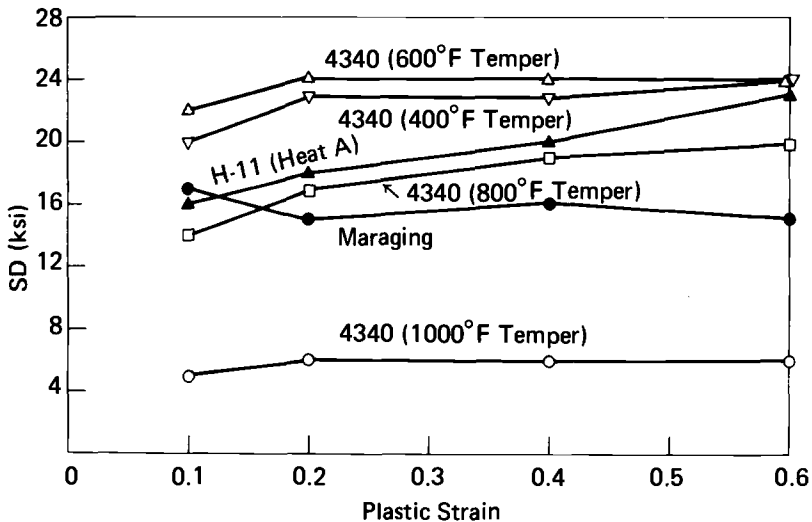


FIG. 9—The effect of plastic strain on the strength differential.

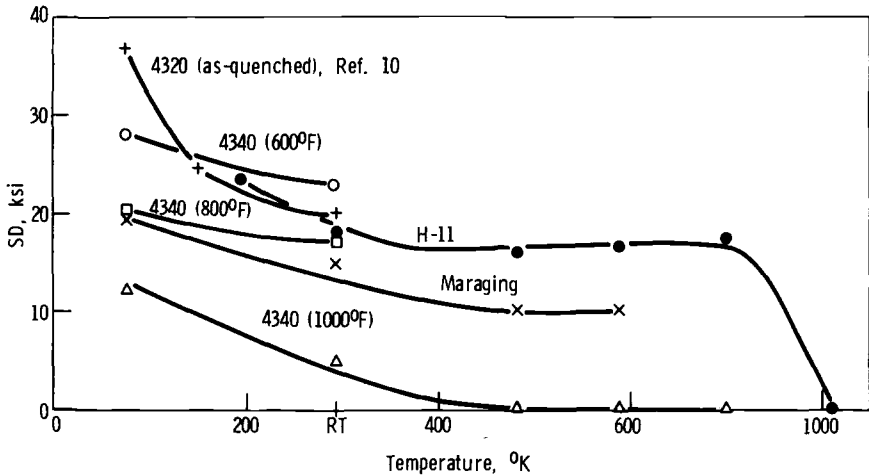


FIG.10—SD as a function of test temperature for 4340 steel (tempering temperature shown in parenthesis), H-11 steel, and 18Ni (300) maraging steel.

since the interaction may now involve carbon atmospheres adsorbed at dislocations [41]. This approach has also been taken to explain the SD effect in aged maraging steel [10,11].

Prompted by the just mentioned nonlinear elastic approach, Pampillo and Davis [42] suggest an effective modulus interpretation where, at sufficient large elastic strains, the elastic modulus is higher in compression than in tension. This arises from an increase in internal stress during compression while, during tension, the internal stress decreases. To account for the temperature dependence of the SD, a thermal component associated with the double kink mechanism of dislocation motion is suggested [12]. Here, the hydrostatic component increases the activation energy for dislocation motion.

Events on a microstructural level are involved in the SD of some other materials. For example, the compressive deformation of a series of annealed magnesium-aluminum alloys ranging from 0 to 9 percent aluminum occurred by large-scale twinning [43]. Since twinning was minimal under tensile deformation, SD was appreciable. The SD effects observed with zirconium and titanium alloys may also involve differences in the ease of twinning between compression and tension [44,45]. The SD of TD nickel (a dispersion-strengthened alloy containing 2 volume percent  $\text{ThO}_2$  particles dispersed in a nickel matrix) has been attributed to the stress concentration at the particle-matrix interface during tensile deformation [46]. Backofen et al [47] have shown that, for an austenitic stainless steel, tensile deformation promoted an austenite-to-martensite transformation to a greater degree than did compressive loading, thus producing an SD effect.

### Acknowledgment

The author expresses his appreciation to R. P. Papirno for reviewing the manuscript and offering many helpful suggestions, particularly concerning the complex subject of specimen buckling. Also, the contribution of J. Fehling in obtaining much of the tensile data used for the flow curves of the high-strength steels is acknowledged.

### References

- [1] Bridgman, P. W., *Transactions*, American Society for Metals, Vol. 32, 1944, p. 553.
- [2] Beeuwkes, R., Jr., private communication; see also Warnas, A. A., "A Relation Between Maximum Load and Necking in a Tensile Test and a Necking Correction for Flow Stress," Technical Report, AMRA 64-35, Army Materials and Mechanics Research Center, Watertown, Mass., Oct. 1964.
- [3] Sullivan, C. P., "A Review of Some Microstructural Aspects of Fracture in Crystalline Materials," Bulletin No. 122, Welding Research Council, May 1967.
- [4] Read, T. A., Markus, H., and McCaughey, J. M. in *Fracturing of Metals*, American Society for Metals, Metals Park, Ohio, 1948, p. 228.
- [5] in der Schmitt, W., *Transactions*, American Institute of Mining, Metallurgical, and Petroleum Engineers, Vol. 221, April 1961, p. 409.
- [6] Papirno, R. and Gerard, G., "Investigation of Creep Buckling of Columns and Plates—Part III: Creep Buckling Experiments with Columns of 2024-0 Aluminum Alloy," Technical Report, WADC TR 59-416, Part III, Air Force Materials Laboratory, Dayton, Ohio, March 1961.
- [7] Polakowski, N. H., *Journal of the Iron and Steel Institute*, Vol. 163, Nov. 1949, p. 250.
- [8] Leslie, W. C. and Sober, R. J., *Transactions*, American Society for Metals, Vol. 60, 1967, p. 459.
- [9] Rauch, G. C. and Leslie, W. C., *Metallurgical Transactions*, Vol. 3, Feb. 1972, p. 373.
- [10] Chait, R., *Metallurgical Transactions*, Vol. 3, Feb. 1972, p. 365.
- [11] Kalish, D. and Rack, H. J., *Metallurgical Transactions*, Vol. 3, Aug., 1972, p. 2289.
- [12] Fletcher, F. B., *Metallurgical Transactions*, Vol. 5, April 1974, p. 905.
- [13] Loizou, N. and Sims, R. B., "The Yield Stress of Pure Lead in Compression," *Journal of Mechanics and Physics of Solids*, 1953.
- [14] Alder, J. F. and Phillips, V. A., *Journal of the Institute of Metals*, Vol. 83, 1954, p. 80.
- [15] Hockett, J. E., *Transactions*, American Institute of Mining, Metallurgical, and Petroleum Engineers, Vol. 239, July 1968, p. 969.
- [16] English, A. T. and Backofen, W. A., *Transactions*, American Institute of Mining, Metallurgical, and Petroleum Engineers, Vol. 230, April 1964, p. 396.
- [17] Jovane, F., "Some Static Compression Test to Large Strain," National Engineering Laboratory Report, Nov. 1963.
- [18] Rabinowicz, E. in *Friction and Wear of Materials*, Wiley, New York, 1965, p. 82.
- [19] Siebel, E., *Stahl und Eisen*, 1923, Vol. 43, p. 1295.
- [20] Hill, R. in *The Mathematical Theory of Plasticity*, Oxford University Press, London, 1950, p. 277.
- [21] Pearsall, G. W. and Backofen, W. A., *Transactions*, American Society for Metals, Vol. 85B, Feb. 1963, p. 68.
- [22] Lee, D., Sata, T., and Backofen, W. A., *Journal of the Institute of Metals*, Vol. 93, 1964, p. 418.
- [23] Trozera, T. A., *Transactions*, American Society for Metals, Vol. 57, March 1964, p. 309.
- [24] Trozera, T. A., *Transactions*, American Society for Metals, Vol. 56, 1963, p. 780.
- [25] Hosford, W. F., *Acta Metallurgical*, Vol. 14, Sept. 1966, p. 1085.
- [26] Tomlinson, W. J. and Talbot, K., *Journal of Material Science*, 1968, p. 655.
- [27] Hsü, T. C., *Materials Research and Standards*, Vol. 9, 1969, p. 20.
- [28] Hockett, J. E., *Proceedings*, American Society for Testing and Materials, Vol. 59, 1959, p. 1309.

- [29] Uvira, J. L. and Jonas, J. J., *Transactions, American Institute of Mining, Metallurgical and Petroleum Engineers*, Vol. 242, Aug. 1968, p. 1619.
- [30] Siebel, E. and Pomp, A., *Mitteilungen Kaiser-Wilhelm Institute für Eisenforschung*, 1928, Vol. 10, p. 55.
- [31] Meyer, H. and Nehl, F., *Stahl und Eisen*, Vol. 45, 1925, p. 1961.
- [32] Yerkovich, L. A. and Gurnieri, G. J., *Proceedings, American Society for Testing and Materials*, Vol. 55, 1955, p. 732.
- [33] Taylor, G. I. and Quinney, H., *Proceedings, Royal Society*, Vol. 143, 1934, p. 307.
- [34] Cook, M. and Larke, C., *Journal of the Institute of Metals*, Vol. 71, 1945, p. 371.
- [35] Avitzur, B. in *Metal Forming: Processes and Analysis*, McGraw-Hill, New York, 1968.
- [36] De Pierre, V., Saul, G., and Male, A. T., "The Relative Validity of Coefficient of Friction and Interface Friction Shear Factor For Use in Metal Deformation Studies," Technical Report AFML-TR-70-243, Air Force Materials Laboratory, Oct. 1970.
- [37] Saul, G., Male, A., Tand DePierre, V., "A New Method for the Determination of Material Flow Stress Values Under Metalworking Conditions," Technical Report AFML-TR-70-19, Air Force Materials Laboratory, March 1970.
- [38] Atkins, A. G. and Tabor, D., *Journal of Mechanics and Physics of Solids*, Vol. 13, 1965, p. 149.
- [39] Lindholm, U. S., Yeakley, L. M., and Bessey, R. L., "An Investigation of the Behavior of Materials Under High Rates of Deformation," Technical Report AFML-TR-68-194, Air Force Materials Laboratory, July 1968.
- [40] Budington, R. A., "Compression Testing Procedures for Titanium," Interim Technical Report 1, Titanium Corporation of America, April 1967.
- [41] Hirth, J. P. and Cohen, M., *Metallurgical Transactions*, Vol. 1, Jan. 1970, p. 3.
- [42] Pampillo, C. A. et al., *Scripta Metallurgica*, Vol. 6, 1972, p. 765.
- [43] Lenhart, R., "The Deformation of Polycrystalline Mg-Al Alloys," Technical Report WADC TR 55-112, Electric Research Laboratory, May 1955.
- [44] Snowden, K. U., *Scripta Metallurgica*, Vol. 5, 1971, p. 467.
- [45] Chait, R., *Scripta Metallurgica*, Vol. 7, April 1973, p. 351.
- [46] Olsen, R. J. and Ansell, C. S., *Transactions, American Society for Metals*, Vol. 62, Sept. 1969, p. 711.
- [47] Powell, G. W., Marshall, E. R., and Backofen, W. A., "Strain Hardening of Austenite Stainless Steel," *Transactions, American Society for Metals*, Vol. 50, p. 478.

R. B. Clough<sup>1</sup>

# Rational Basis and New Methods for Proportional Limit, Machine Stiffness, Critical Stress Intensity, and Crack Velocity Measurements

---

**REFERENCE:** Clough, R. B., "Rational Basis and New Methods for Proportional Limit, Machine Stiffness, Critical Stress Intensity, and Crack Velocity Measurements," *Recent Developments in Mechanical Testing, ASTM STP 608*, American Society for Testing and Materials, 1976, pp. 20-44.

**ABSTRACT:** This paper is a summary of some new measurement techniques that have been developed recently at the National Bureau of Standards for measurement of proportional limit of elasticity, machine stiffness, critical stress intensity, and crack velocity. These seemingly unrelated measurements all result from the rational basis of a single type of equation relating specimen and machine kinetics. In a regime of linear elasticity, the concept of a limit beyond which the specimen elastic gage length displacement is no longer proportional to load is referred to as proportional limit if the gage length begins to exhibit plastic deformation, and is referred to in a precracked specimen as critical stress intensity if the crack begins to extend in length. Multiaxial plastic yielding is also discussed. Machine stiffness and crack velocity are other measurements which can be obtained through the specimen-machine equation. The relationship of the new stiffness measurement to the International Standards Organization (ISO) proposed method and advantages of the new method are discussed. Methods of measuring stiffness in constant load rate and constant strain rate tests are outlined. A method of measuring the proportional limit or critical stress intensity which does not use a displacement gage of any type is also given; this should prove useful in hostile environments. Other related topics discussed include loading transients and rate sensitivity.

**KEY WORDS:** mechanical tests, measurement, proportional limit, determination of stress, crack propagation, plastic deformation

This paper presents a summary of several new mechanical test techniques for measurement of proportional limit of elasticity, machine stiffness, critical stress intensity, and crack velocity. These seemingly unrelated

<sup>1</sup> Metallurgist, Engineering Mechanics Section, Mechanics Division, National Bureau of Standards, Washington, D. C. 20234.

measurements all have the same rational basis: a single type of equation relating machine and specimen kinetics.

A central feature is a new method of measuring the proportional limit of elasticity or, equivalently, the critical stress intensity if the specimen is precracked. Therefore, it is assumed that the specimen exhibits a regime of linear elasticity and that subsequently the specimen exhibits either plastic deformation or, if precracked, the crack extends. It is important to point up that proportional limit implies such a regime of linear elasticity, whereas the concept of elastic limit permits nonlinear elasticity [ASTM Definition of Terms Relating to Methods of Mechanical Testing (E 6-66 (1973))] [1].<sup>2</sup> In the strictest sense, linear elasticity—Hooke's law—is a mathematical convenience corresponding to dropping second order differentials of displacement. The practical usefulness of this approximation is attested, for example, by the success of structural design methods. In the same way, as has often been pointed up [2], the elastic limit generally decreases as strain resolution increases. Thus, in the strictest sense, a true elastic or proportional limit (zero plastic strain), if it exists at all, might correspond to extremely low stress and, hence, be unusable in many applications. A common difficulty in attempting to measure such a low elastic limit or proportional limit in the usual types of tension testing systems is that it is below or of the same order as the magnitude of forces involved in tightening interfaces and aligning components of the testing system. Some design value of a proportional limit is still needed, once this true elastic limit is exceeded (in alignment and so forth), so that one is forced to adopt some effective definition. The proportional limit which is measured in this paper is such an effective proportional limit, since it assumes that the material obeys Hooke's law up to some critical stress above which plastic deformation occurs. The linear and nonlinear behavior of stress and strain are described by two equations. The linear behavior is described by Hooke's law and corresponds to the regime of tightening and aligning the system. The nonlinear region or the region of plastic deformation is described by a specimen-machine equation which makes no assumptions about the shape of the nonlinearity, that is, it does not assume any particular material constitutive equation as is usually done in back-extrapolation methods of determining a proportional limit. These same considerations also apply to measurements of critical stress intensity for crack extension, where it is assumed that specimen compliance is constant (linear behavior) up to a critical load above which load and extension become nonlinear as the crack extends. Related techniques of measuring crack velocity under different loading situations are presented and discussed.

The machine stiffness is related directly to the slope of the specimen-machine equation, and experimental measurements of stiffness are dis-

<sup>2</sup> The italic numbers in brackets refer to the list of references appended to this paper.

cussed in relation to other methods, including that proposed by the International Standards Organization (ISO).

Consideration is also given to machine effects in activation volume determination by crosshead speed cycling as well as a simple graphical comparison of various mechanical tests such as creep, constant crosshead speed or constant load rate tension tests, and stress relaxation with fixed crossheads or with constant specimen length.

**Tensile Machine Kinetics in System Prior to Tightening and Alignment**

The new methods described in this paper arise from a consideration of interactions between the specimen and the test system. These are more conveniently understood if stress rate and strain rate are plotted, as shown in Fig. 1 [3], for a constant crosshead velocity tension test. As described previously, there are two regions, both linear in the rate plane: one of elasticity described by Hooke's law and the other of plasticity described by the stiffness of the tensile machine. Elastic deformation proceeds rapidly from the origin along Line *oa* to the vicinity of Point *a*, which describes most of the duration of elastic straining. As plastic flow begins, the rela-

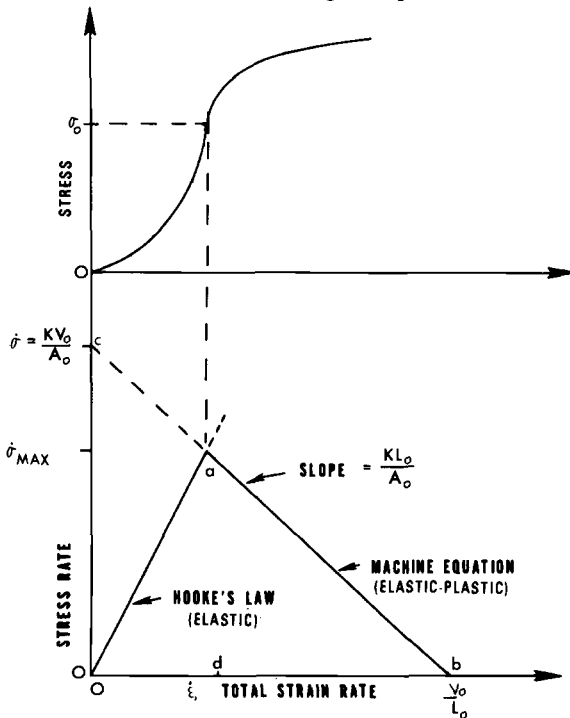


FIG. 1—Schematic diagram of stress rate versus total strain rate at constant crosshead speed.

tionship between stress rate and strain rate is represented by Line *ab*. The intersection of these two lines then corresponds to the proportional limit.

These will be described in more detail later. At small loads, the specimen is only loosely aligned in the system, so that specimen and machine behavior are only related indirectly. At zero load, the specimen stress rate is zero. At the first discernible load rate, the specimen load rate is given by the differential form of Hooke's law with respect to time

$$\dot{\sigma} = E\dot{\epsilon}_e \quad (1)$$

where  $\dot{\sigma}$  is stress rate,  $E$  is Young's modulus, and  $\dot{\epsilon}_e$  is the elastic strain rate of the specimen. This relation characterizes the rapid elastic deformation along Line *oa* in Fig. 1.

### Tensile Machine Kinetics in a System Which is Aligned and Tightened

Relationships between measurable quantities, such as crosshead velocity, machine stiffness, load rate, and strain rate, are now derived for a tensile machine which has been loaded to the extent that interfaces have tightened sufficiently, and components are aligned sufficiently so that within our measurement resolution the system stiffness is approximately constant. Loading is slow enough so that inertial forces are small. The total distance between crossheads,  $X_t$ , is a function of force  $F$  and time  $t$  and is the sum of  $X_s$ , the specimen reduced section length, and  $X_m$ , the remaining length of machine between crosshead which includes the pull rods, grips, and so forth. This gives the equation  $X_t = X_m + X_s$ . Taking the differential of  $X_t$  with respect to time and expanding

$$\frac{dX_t}{dt} = \frac{dX_m}{dt} + \frac{dX_s}{dt} = \frac{dX_m}{dF} \frac{dF}{dt} + \frac{dX_s}{dt} \quad (2)$$

This equation is the rational basis for all the methods mentioned. Next, the following definitions are made:

- $V \equiv (dX_t/dt) =$  crosshead velocity,
- $K \equiv (dF/dX_m) =$  machine stiffness,<sup>3</sup>
- $\dot{\sigma} \equiv (dF/A_0dt) =$  stress rate,
- $A_0 \equiv$  initial cross-sectional area of specimen,
- $\dot{\epsilon} \equiv (dX_s/L_0dt) =$  total strain rate of specimen, and
- $L_0 \equiv$  initial specimen gage length.

<sup>3</sup> Notationally, the  $K$  utilized throughout the text is the reciprocal of the  $K$  defined in ISO 2573. Here,  $K$  is defined dimensionally as (force/length) and is called stiffness, while the  $K$  in ISO 2573 is defined as (length/force). In the United States, the ratio of (length/force) is usually called compliance.

If the dimensional changes are small, there is no appreciable difference between engineering and true values of stress and strain. Using the definitions just listed, Eq 2 can be written

$$\dot{\sigma} = \frac{KV}{A_0} - \frac{KL_0}{A_0} \dot{\epsilon} \quad (3)$$

with the condition that the machine be tightened and aligned. This condition gives a maximum stress rate, combining Eq 3 and 1, as

$$\dot{\sigma} \leq \dot{\sigma}_{\max} = \frac{KVE}{A_0E + L_0K} \quad (4)$$

at the intersection of the lines for Eqs 3 and 1. Equation 1 applies at the earliest stages of loading, up to the point at which either the specimen and machine are tightened and aligned or plastic flow occurs. Equation 3 applies to a tightened and aligned system, for both elastic and plastic flow.

### Determination of Proportional Limit

Figure 1 depicts the kinetics of a constant crosshead velocity test ( $V = V_0$ , a constant, for example, a screw-driven machine). The specimen is initially at rest (Point  $o$ ). Elastic deformation then proceeds rapidly along Line  $oa$  according to Hooke's law (Eq 1) during the process of machine tightening and alignment. This process is completed at Point  $a$ , at which Eq 3 becomes valid while the specimen continues to deform elastically. Point  $a$  characterizes the major portion of elastic loading. When plastic deformation occurs and Eq 1 no longer holds, the stress rate decreases according to Eq 3, which remains valid. This may be shown by writing the total strain rate as the sum of an elastic strain rate and a plastic strain rate

$$\dot{\epsilon} = \dot{\epsilon}_e + \dot{\epsilon}_p \quad (5)$$

Substituting Eqs 5 and 1 into Eq 3, we have at crosshead velocity  $V_0$

$$\dot{\sigma} = \frac{V_0}{ML_0} - \frac{\dot{\epsilon}_p}{M} \quad (6)$$

where  $M$  is an elastic constant of the system

$$M \equiv \frac{A_0}{KL_0} + \frac{1}{E} \quad (7)$$

For a given crosshead velocity ( $V_0$ ), the maximum value of Eq 6 is given by elastic loading ( $\dot{\epsilon}_p = 0$ ) and corresponds to Point  $a$  on Fig. 1. With the onset of plastic deformation, the plastic strain rate, according to Eq. 6, causes a decrease in the stress rate. Therefore, the proportional limit ( $\dot{\epsilon}_p = 0$ ) corresponds to Point  $a$  or maximum stress rate as a function of

strain rate. By also monitoring the stress as a function of total strain rate (shown in the upper half of Fig. 1), the proportional limit ( $\sigma_0$ ) is obtained graphically. Note that the technique is not useful if the slope of the stress versus total strain rate curve is too steep at this point, so that the point of intersection with the vertical line is difficult to resolve. Such a vertical slope, it should be noted also, is predicted for an ideal system which aligns and tightens to a load-independent stiffness at low loads and obeys Hooke's law over a substantial region of stress.

Figure 2 is taken from previous work at the National Bureau of Standards on the determination of proportional limit in mild steel specimens [3]. Load rate and strain rate were differentiated or double-differentiated or both electronically with respect to time, using simple operational amplifier circuitry. These amplifiers were null calibrated, and a maximum output

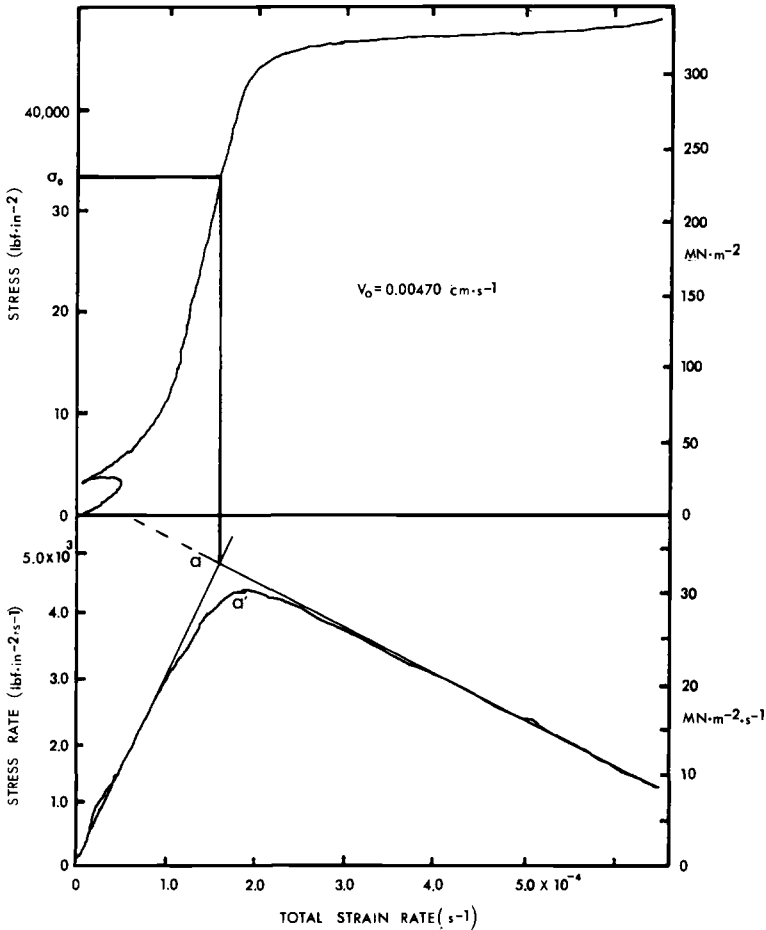


FIG. 2—Rate relationships and determination of proportional limit in steel specimen [3].

voltage alarm was installed to ensure that the differentiations were linear and accurate. As can be seen from Fig. 2, there is a rounding off of the peak described ideally by Point *a*. The cause of this effect has not been established, although it is suggested that contributing factors may arise from machine-specimen misalignment, tightening of machine interfaces, straightening of the specimen if bent, and from the statistical or heterogeneous nature of yielding.

The method for the determination of proportional limit given here has a rational basis as the intersection of lines representative of perfect elastic specimen behavior and plastic flow. It has the following advantages:

1. It is nonarbitrary in the sense that no arbitrary microplastic flow law is postulated, as may be used in back-extrapolation methods.
2. Machine and loading abnormalities, such as loading alignment, are accounted for by a complete display of the appropriate parameters.
3. No unloading is required, and the technique is dynamic. Since no unloading is required, there is no specimen relaxation during unloading and loading which would affect the measured value.

An unusual feature of a variant of the present method, which may be an advantage in certain circumstances such as in extreme environments—extreme temperatures, nuclear radiation, extreme pressure, or hostile chemicals—is that no strain gages need be used for measuring specimen deformation. With reference to Fig. 1, note that the stress rate increases on Line *oa* and decreases along Line *ab* so that the proportional limit corresponds to maximum stress rate. Accordingly, the second derivative of stress or load with respect to time is positive along Line *oa*, goes through zero at Point *a* (the proportional limit), and is negative along Line *ab*. Again, following the previous comment, the second derivative of stress would be zero over a substantial stress range where Hooke's law applies, the machine stiffness is load independent, and the machine is aligned at low stress. Figure 3, taken from Ref 3, shows this method of measuring proportional limit in a mild steel specimen.

Figure 4 demonstrates, in a schematic way, the effect of type of machine on proportional limit determination. Here, a constant load rate machine is used so that plastic deformation occurs along the constant load rate line.

### Proportional Limit Under Multiaxial Stress

The previously discussed method of measuring proportional limit may be readily extended to measuring proportional limit under multiaxial stresses [4]. Determination of the proportional limit along any one axis is sufficient to locate the flow surface for those stresses. The method is similar to that just described. If proportional loading is used, a constant load rate is em-

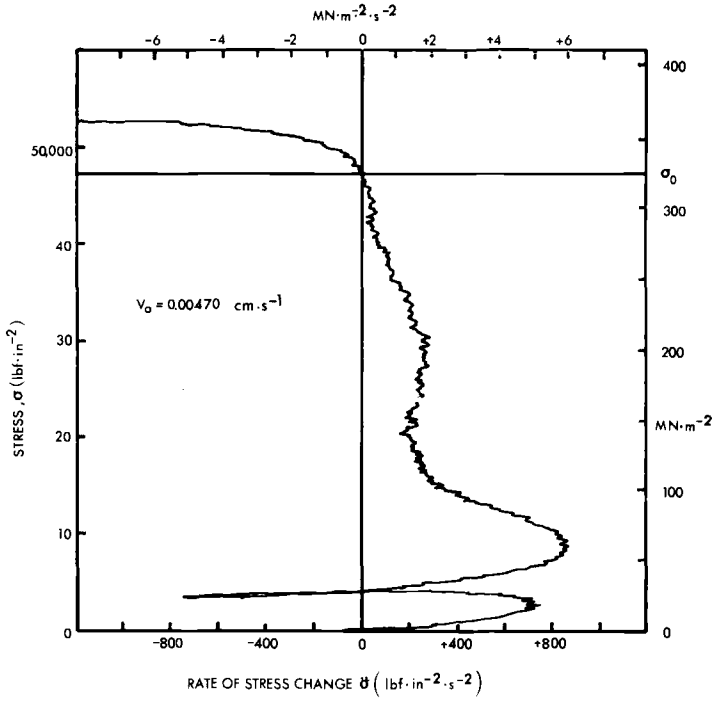


FIG. 3—Definition of proportional limit according to  $\partial^2\sigma/\partial t^2 = 0$  (0.5 percent plastic strain) [4].

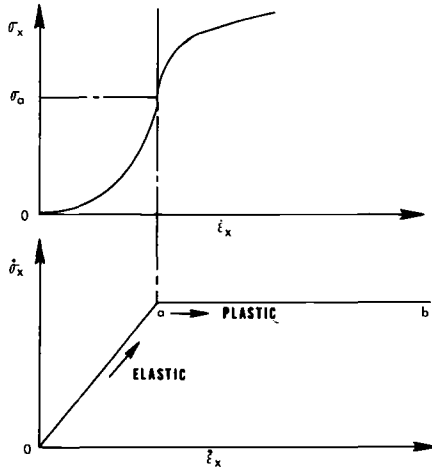


FIG. 4—Proportional limit determination in machine with constant load rate control.  $\sigma_0$  is the proportional limit of  $\sigma_x$  [4].

ployed, and the schematic of Fig. 4 is then applicable. In the case where no plastic strain rate develops along a given direction, as in the plane-strain situation, a nonzero strain rate axis (preferably the largest strain rate expected) is monitored.

As an example, consider biaxial loading ( $\sigma_z \equiv 0$ ). Then the total strain rate along the  $x$  axis is

$$\dot{\epsilon}_x = (C_x + C_y R)\dot{\sigma}_x + \dot{\epsilon}_x^p \quad (8)$$

where  $C_x$  and  $C_y$  are elastic constants of the specimen, and  $R = (\dot{\sigma}_y/\dot{\sigma}_x)$  is the stress rate ratio from which the orthogonal principal stress is calculated. If  $R$  is held constant (proportional loading), then a plot of  $\dot{\epsilon}_x$  versus  $\dot{\sigma}_x$  will become linear, according to Hooke's law, up to the proportional limit. As  $\dot{\epsilon}_x^p$  becomes nonzero, linearity will fail beyond the proportional limit, as in Fig. 4.

### Stiffness of Constant Crosshead Velocity Machines

Subsequent to plastic yielding of the specimen in the constant crosshead velocity test, there is a linear relationship between stress rate and total strain rate (Eq 3 and Fig. 1). The zero total strain rate intercept on the stress rate axis ( $\dot{\sigma}_i$  in Fig. 1) has been proposed [3] as a method for the determination of the machine stiffness through

$$(K)_i = \frac{\dot{\sigma}_i A_0}{V_0} \quad (9)$$

The load-time slope method [5] differs from this. Load is recorded as a function of time, and the maximum slope is taken. This would ideally correspond to Point  $a$  in Fig. 1. If the corresponding stress rate is  $\dot{\sigma}_a$ , the load-time slope method gives the stiffness as

$$(K)_a \equiv \left( \frac{V}{\dot{\sigma}_a A_0} - \frac{L_0}{A_0 E} \right)^{-1} \quad (10)$$

which is obtained directly from Eqs 3 and 4 by taking  $\dot{\sigma}_a = \dot{\sigma}_{\max}$ . A difficulty arises in practice, however, as shown in Fig. 2. The ideal maximum stress rate ( $\dot{\sigma}_a = \dot{\sigma}_{\max}$ ) is often not reached, so that erroneously low values of machine stiffness may be calculated from the maximum slope ( $\dot{\sigma}_a A$ ) of the load-time curve. In a previous study [3], values of machine stiffness calculated by the load-time slope method without correction were of the order of 10 percent low. However, by displaying the stress rate versus total strain rate curve, one can correct for this effect by using values of  $\dot{\sigma}_a$  adjusted to equal  $\dot{\sigma}_{\max}$ .

The method of measuring stiffness proposed by the ISO, which at this writing is still in draft form [6], is a convenient method of stiffness measure-

ment since the stiffness is defined as a *ratio* of strain rates, and therefore no absolute determination of them is necessary. It is possible to derive the ISO equation for stiffness from the present analysis. In the ISO-proposed method, the strain versus time curve is recorded for a mild steel specimen with a flat lower yield plateau. Then the relative slope or strain rate in the elastic region is divided into the relative slope or strain rate on the yield plateau (which will be the steepest slope) from which the stiffness is obtained. The derivation is as follows. The elastic strain rate corresponds to the maximum stress rate  $\dot{\sigma}_{\max}$  (Eq 4) divided by Young's modulus, or  $\dot{\epsilon}_a = \dot{\sigma}_{\max}/E = KV_0/(A_0E + L_0K)$ . This corresponds (Fig. 1) to the relative length of Line *od*, irrespective of whether or not the maximum stress rate is actually obtained. The second slope, taken during lower yield plateau straining, corresponds to the strain rate at Point *b*, given by  $\dot{\epsilon}_p = V_0/L_0$  or equivalently by the relative length of Line *ob*. Here, the ratio is defined as

$$H \equiv \frac{\dot{\epsilon}_b}{\dot{\epsilon}_a} = \frac{|ob|}{|od|} = \frac{A_0E + L_0K}{L_0K} \quad (11)$$

so that

$$(K)_{b,d} \equiv \frac{A_0E}{L_0(H - 1)} \quad (12)$$

This is the reciprocal of the expression employed in the ISO method since *K* is defined in that document in units of (length/force), which is conventionally called compliance in the United States. In the United States, the letter *K* usually stands for the spring rate or spring constant, such as in the expression (force) = *K* × (displacement), and is called stiffness, a larger value of stiffness implying a larger force required for a given displacement. Equation 12 demonstrates the compatibility of the present analysis with the ISO definition.

A possible disadvantage of the ISO method is the requirement of the flat lower yield plateau so that Point *b* is reached in Fig. 1. Any oscillation or variation of stress in that region will give rise to an error as deformation proceeds back along Line *ba* or never reaches Point *b*. Since the slope of the line is proportional to stiffness, this error should be greater in less stiff machines. This is not a problem with the present method (Eq 9) since these variations are displayed and accounted for. The present method thus permits machine stiffness measurements on specimens of work-hardening materials or those with no flat lower yield stress, such as plastics and non-ferrous metals.

A comparison of machine stiffness values at constant crosshead velocity as measured by the three methods [3] is given in Table 1. If the stress rates corresponding to the rounded-off curve are used in the load-time slope method, one obtains somewhat lower values than those corresponding to

TABLE 1—Results of machine stiffness measurements at constant crosshead velocity.

Method	lbf/in.		MN/m
A. Load-time slope method (Eq 10 at Point $a'$ )	573 000	$(K)_{a'}$	100
B. Improved load-time slope method (Eq 10 at Point $a$ )	644 000	$(K)_a$	113
C. Present method (Eq. 9 at Point $c$ )	643 000	$(K)_i$	113
D. ISO British method (Eq 12 at Points $o$ , $b$ , and $d$ )	646 000	$(K)_{d,b}$	113

the peak at Point  $a$ . If the latter values are substituted into Eq 10, there is good agreement.

### Stiffness of Constant Load Rate Machines

The previously discussed methods are applicable to test machines with constant crosshead velocity. In this section, a constant load rate mode of operation is examined. Equation 3 can be reformulated as

$$K = \frac{\dot{\sigma}A_0}{V - L_0\dot{\epsilon}} \quad (13)$$

In many cases, the load rate ( $\dot{\sigma}A_0$ ) is only nominally constant, so that stiffness measurement generally requires simultaneous measurements of load rate, crosshead velocity, and total strain rate, with the stiffness calculated according to Eq 13. If, however, the load rate is satisfactorily constant, such as shown in Fig. 4, only continuous measurements of crosshead velocity and total strain rate are needed (Eq 13). From this or Eq 3 these are related by the expression

$$V = \frac{\dot{\sigma}A_0}{K} + L_0\dot{\epsilon} \quad (14)$$

so that a method analogous to the constant crosshead velocity test method may be developed. Such a test would appear as in Fig. 5. The crosshead velocity passes through two stages exactly analogous to those for the stress rate in the constant crosshead velocity test (Fig. 1). At low loads, Eq 14 is not valid, due to lack of tightness and possible misalignment. Crosshead velocity and strain rate are both zero at the start of the test, but they may not be proportional during the alignment and tightening stage, so that only the linear stage described by Eq 14 is shown in Fig. 5. This is extrapolated to zero strain rate as shown in Fig. 5, and the stiffness is found from the zero strain rate intercept  $V_i$

$$(K)_i \equiv \frac{\dot{\sigma}A_0}{V_i} \quad (15)$$

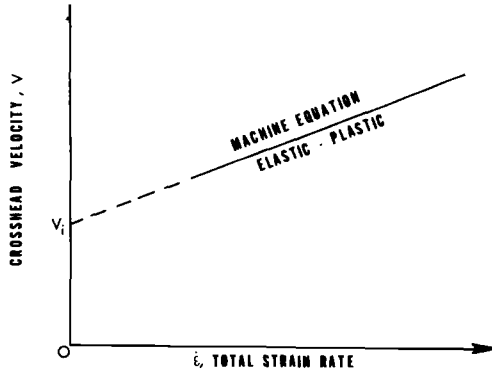


FIG. 5—Crosshead speed in a constant load rate test (shown in Fig. 4).

If  $K$  is large, a load rate should be used which is large enough to give a measurable value of  $V_i$ . So far, this method has not been utilized.

### Stiffness of Constant Strain Rate Machines

If a closed-loop type of test machine with appropriate feedback is used, a specimen can be tested at constant strain rate. The method here is virtually identical to that used at constant load rate. Equation 14 applies, except that now the crosshead velocity is a function of the variable load rate. The test would appear as in Fig. 5, except that stress rate is monitored and is the horizontal axis instead of strain rate. The stiffness is then given by the zero stress rate intercept  $V_i$ :

$$(K)_\dot{\epsilon} = \frac{L_0 \dot{\epsilon}}{V_i} \quad (16)$$

and again, if  $K$  is large, a sufficiently large strain rate should be employed to give a measurable value of  $V_i$ . So far, this method has not been utilized.

### Strain Rate Transients and Other Mechanical Effects

A stress rate versus total strain rate diagram is useful in demonstrating and comparing the characteristics of various types of mechanical tests. In these diagrams, certain features of tests emerge that are not apparent otherwise. Figure 6 is a schematic stress rate versus total strain rate diagram for a typical tensile load-unload constant crosshead velocity test. The specimen is loaded from rest, Point  $o$ , plastically yields at Point  $a$ , and undergoes plastic deformation up to Point  $b$ . Here, the crosshead velocity is suddenly changed ( $b'$ ) from  $+V_0$  to  $-V_0$  so that Eq 2 becomes

$$\dot{\sigma} = -\frac{KV_0}{A_0} - \frac{L_0 K}{A_0} \dot{\epsilon} \quad (17)$$

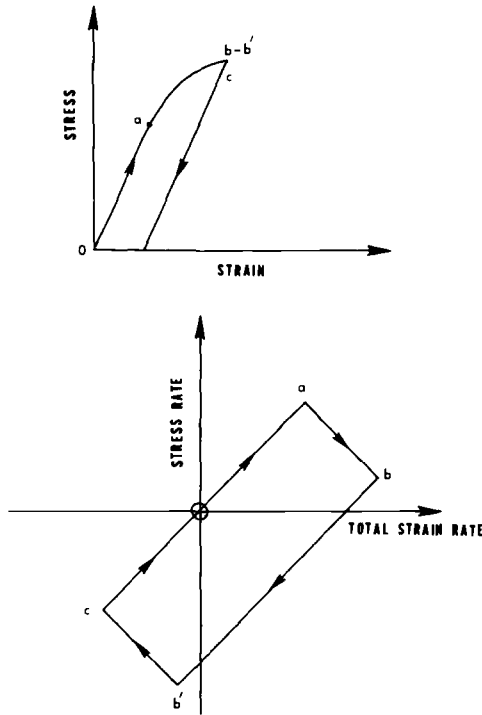


FIG. 6—Schematic of stress rate versus total strain rate for load-unload constant crosshead velocity test.

and there is a sudden change in elastic strain rate from  $b$  to  $b'$ . Since the load is positive, one must expect some additional small plastic strain rate from  $b'$  to  $c$ , along with elastic contraction from Point  $c$  so that the loop closes at rest again at Point  $o$ . Important features of such an analysis are the demonstration of transient strain rate or stress rate effects, such as the sudden contraction of  $b$  to  $b'$ , as well as the necessity of plastic strain rate ( $b'c$ ) to close the loop.

As another example of transient effects, consider the crosshead velocity cycling test depicted in Fig. 7. Such a test is often used to obtain the strain rate sensitivity of the flow stress, which will be discussed next in terms of the activation volume for plastic flow. The transient effects, as shown, are quite complicated.

It is instructive to compare the schematic stress rate versus total strain rate diagram for various types of mechanical tests, such as shown in Fig. 8. One is able to graphically compare creep tests, tension tests, and stress relaxation tests on a single diagram. There is a great difference in tension tests at constant crosshead velocity, constant stress rate, and at constant total strain rate. The stress relaxation test at constant total specimen strain

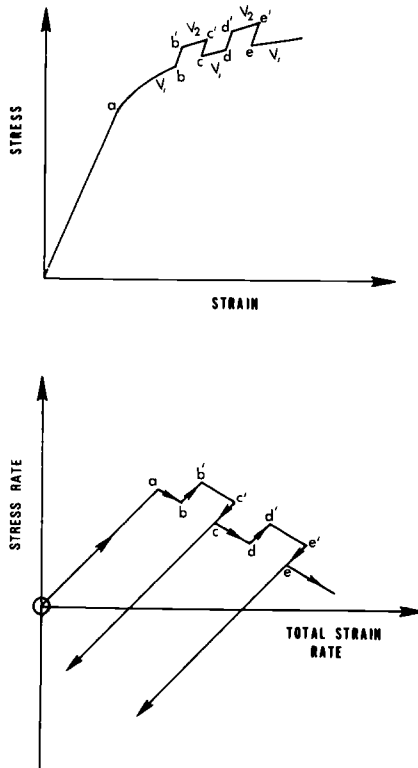


FIG. 7—Schematic of stress rate versus total strain rate for crosshead velocity cycling tests (activation volume determination).

(Line *do*) differs from the stress relaxation test at fixed crossheads (zero velocity). The creep test appears as a special case of a tension test at constant load rate with the load rate being zero.

### Machine Stiffness Effects on Load-Cycling Rate Sensitivity of the Stress

The strain rate sensitivity of the flow stress is an important parameter which is used to characterize the flow behavior of materials. For example, it is proportional to the activation volume for plastic flow, which gives the average area on an atomic scale swept out by mobile dislocations thermally activated from barrier to barrier [7]. The measurement is made ordinarily by observing changes in flow stress as the moving crosshead is cycled between fixed velocities, usually differing by about an order of magnitude. The activation volume can be written [7] as  $v^* = 2kT(\partial \ln \dot{\epsilon}_p / \partial \sigma)_T$  where  $k$  is Boltzmann's constant,  $T$  is absolute temperature, and  $(\partial \ln \dot{\epsilon}_p / \partial \sigma)_T$  is the strain rate sensitivity of the flow stress. It is assumed that the mobile

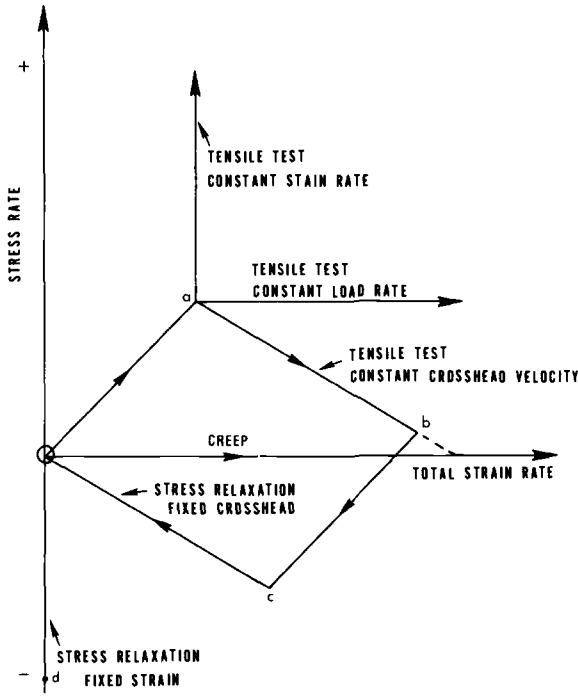


FIG. 8—Comparison of tension tests with creep and stress relaxation tests.

dislocation density does not change. The plastic strain rate may be written, from Eq 6, as

$$\dot{\epsilon} = \frac{V}{L_0} - M\dot{\sigma} = \frac{V}{L_0} - M\theta\dot{\epsilon}_p \quad (18)$$

where  $M$  is an elastic constant of the system defined by Eq 7, and  $\theta = (d\sigma/d\epsilon_p)$  is the rate of work hardening. Then, solving for the plastic strain rate

$$\dot{\epsilon}_p = \frac{V}{L_0(1 + M\theta)} \quad (19)$$

so that the true activation volume is

$$v_{\text{true}}^* = 2kT \frac{\partial \ln \dot{\epsilon}_p}{\partial \sigma} = 2kT \left[ \frac{\partial \ln V}{\partial \sigma} - \frac{\partial \ln (1 + M\theta)}{\partial \sigma} \right] \quad (20)$$

The first term is obtained by cycling the crosshead velocity and observing the change in flow stress; the second is an error term due to the machine. Let  $\theta_i$  be the rate of work hardening at velocity  $V_i$  and  $\Delta\sigma = \sigma_2 - \sigma_1$  be the change in stress (for example, segment  $b - b'$  in Fig. 7) for an incremental

increase in crosshead velocity from  $V_1$  to  $V_2$ . The condition for the measurement to be accurate is

$$v_{\text{true}}^* \cong 2kT \left( \frac{\partial \ln V}{\partial \sigma} \right)_T \quad (21)$$

so that

$$\frac{\partial \ln V}{\partial \sigma} \gg \frac{\partial \ln (1 + M\theta)}{\partial \sigma} \quad (22)$$

This will be met approximately if

$$\ln \left( \frac{V_2}{V_1} \right) \gg \ln \left( \frac{1 + M\theta_2}{1 + M\theta_1} \right) \quad (23)$$

This condition is generally fulfilled for plastic strains larger than about  $10^{-4}$  where the rate of work hardening becomes less than  $M^{-1}$ . In the microstrain region, however,  $\theta$  can be quite large, and the correction term becomes significant. Generally, crosshead velocities are changed by a factor of about ten ( $V_2/V_1 \sim 10$ ). If  $M\theta \gg 1$ , then a change in work hardening rate of the order of ten ( $\theta_2/\theta_1 \sim 10$ ) would be necessary for errors to arise. In experimental work, Arsenault and co-workers [8] have used changes in true plastic strain rate measured on the specimen instead of changes in crosshead velocity to evaluate activation volumes in the microstrain region, thus eliminating machine effects.

### Crack Motion

The discussion so far has dealt with a specimen which can deform plastically. With minor changes, a similar procedure can be developed to determine the onset of crack motion and measure crack velocity. While the terminology differs, an equation similar to that for plastic flow is derived from the rational basis of Eq 2. If the specimen does not undergo significant plastic deformation but contains a crack perpendicular to the load axis, the onset of crack extension corresponds to the limit of proportionality between load and extension. Plane-strain crack motion is generally fairly abrupt, that is, brittle. In plane stress, however, the onset of crack motion is gradual (Fig. 9) so that a method of determining the proportional limit is very useful. For the specimen (which could be a compact precracked tension specimen) we have, following Eq 2, which has served as the rational basis of these techniques

$$V = \frac{dX_m}{dt} + \frac{dX_s}{dt} = C_m \dot{F} + \dot{X}_s \quad (24)$$

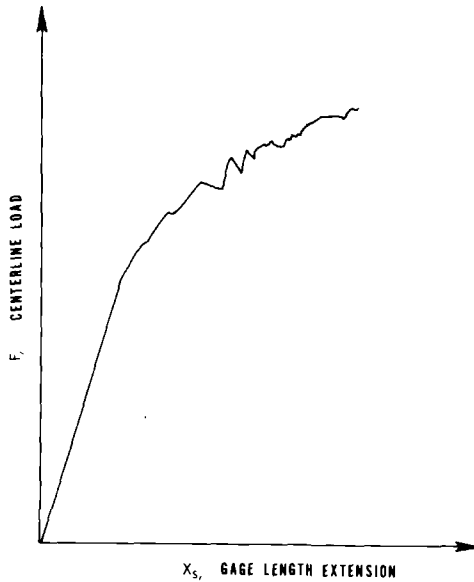


FIG. 9—Load-extension diagram for typical crack extension in precracked plane-stress crack specimen.

where  $C_m \equiv K^{-1}$  is the machine compliance.  $\Delta X_s$  is the change in specimen gage length, which could be the crack opening displacement. It is assumed, as it was previously, that  $\dot{C}_m = 0$ , that is, that the machine is perfectly elastic. This gives

$$\dot{F} = \frac{V - \dot{X}_s}{C_m} \quad (\text{tightened and aligned system}) \quad (25)$$

for the condition of crack opening. This applies only to an aligned and tightened system. At lower loads, during tightening and alignment, the load rate is given by

$$\dot{F} = \frac{\dot{X}_s}{C_s} \quad (\text{low loads}) \quad (26)$$

where  $C_s \equiv \Delta X_s/F$  is the specimen compliance. Comparison of these two equations, as depicted in Fig. 10 for a constant crosshead velocity test, shows that, as the load is increased from zero, at first the load rate increases with increasing specimen extension rate as the system tightens and aligns (Eq 26). Once the “proportional limit”—the critical load for crack extension—is reached, the load rate begins to decrease with increasing specimen extension rate. Then simultaneous monitoring of the load rate, the gage length displacement rate, and the load enables one to determine the critical load for crack extension. The critical load (or proportional limit,  $F_c$ ) is, in this case, that at maximum load rate as a function of displacement rate.

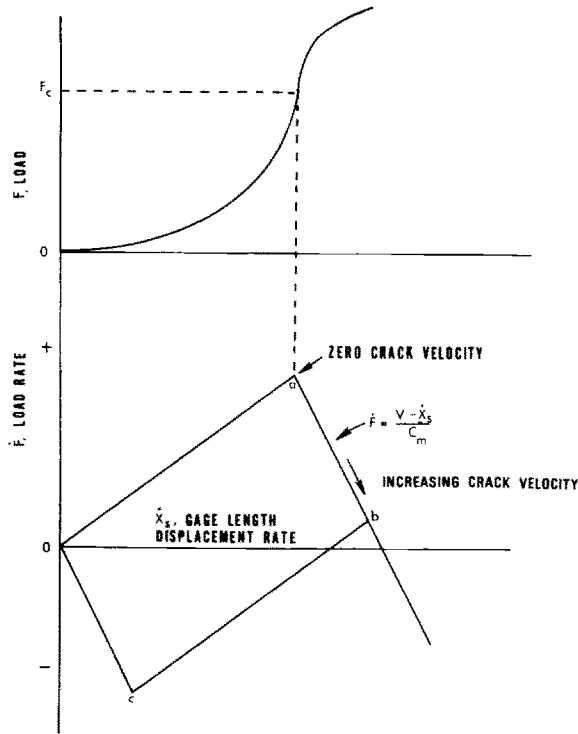


FIG. 10—Schematic of gage length displacement rate versus load and load rate for pre-cracked tension specimen at constant crosshead velocity.

It may be that the critical stress intensity is desired for crack extension in an extreme environment, such as extreme temperatures, high pressure, nuclear radiation, or hostile chemicals. Then the variant just described for measuring proportional limit at  $\ddot{F} = 0$  depicted for plastic yielding in Fig. 3 may be used.

Irwin and Kies [9] have given a method of determining the critical crack extension force in terms of change in specimen compliance and load. Ignoring Poisson effects, this is

$$G_c = \frac{F_c^2}{2B} \frac{dC_s}{da} = \frac{K_{Ic}^2}{E} \quad (27)$$

where

- $G_c$  = critical crack extension force,
- $B$  = specimen width,
- $a$  = crack length,
- $E$  = Young's modulus,
- $K_{Ic}$  = critical stress intensity factor, and
- $F_c$  = proportional limit.

The crack velocity can then be obtained in the following manner. By definition  $\Delta X_s \equiv C_s F$  so that  $\dot{X}_s = \dot{C}_s F + C_s \dot{F}$ . Substituting this expression for  $\dot{X}_s$  into Eq 25, after rearrangement, the crack velocity may be written

$$v_c = \frac{V - C_t \dot{F}}{F(dC_s/da)} \quad (28)$$

where  $C_t \equiv C_m + C_s$  is the total system compliance,  $\dot{C}_s = (dC_s/da)v_c$ , and  $v_c \equiv (da/dt)$ . A typical plot of change in specimen compliance with crack length is given in Fig. 11; it shows that, for small crack extensions of the original crack length  $a_0$ ,  $(dC_s/da)$  is nearly constant.

Consider three types of crack motion: (a) irregular motion corresponding to Fig. 9, (b) creep at constant load, and (c) stress relaxation crack growth. Figure 12 gives a schematic representation of crack motion and velocity distribution during the irregular type of load-extension behavior which is often observed in plane-stress specimens. As given in Eq 28, the crack velocity is a sensitive function of the loading rate, which varies considerably, going from positive to negative values. As the load rises on a load jog, the load rate is positive, so that the velocity is less; as the load falls, the load rate is negative, so that the crack velocity is faster. Thus, the crack velocity is predicted to oscillate. It can be shown that  $v_c$  will be nonnegative. Also, since stress wave effects were omitted from the theory, only velocities much less than the elastic wave velocities are considered.

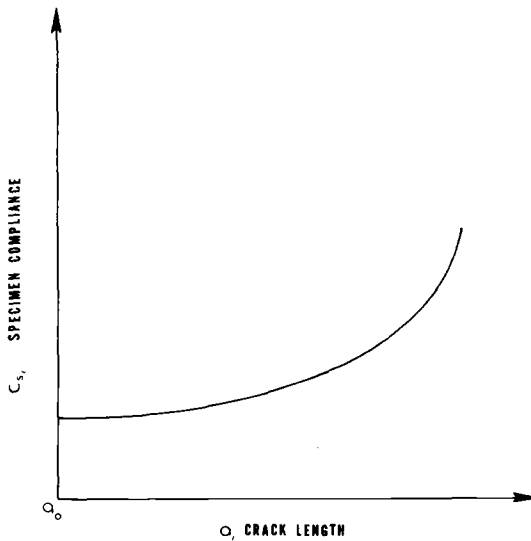


FIG. 11—Schematic of specimen compliance versus crack length for typical precracked tension specimen.

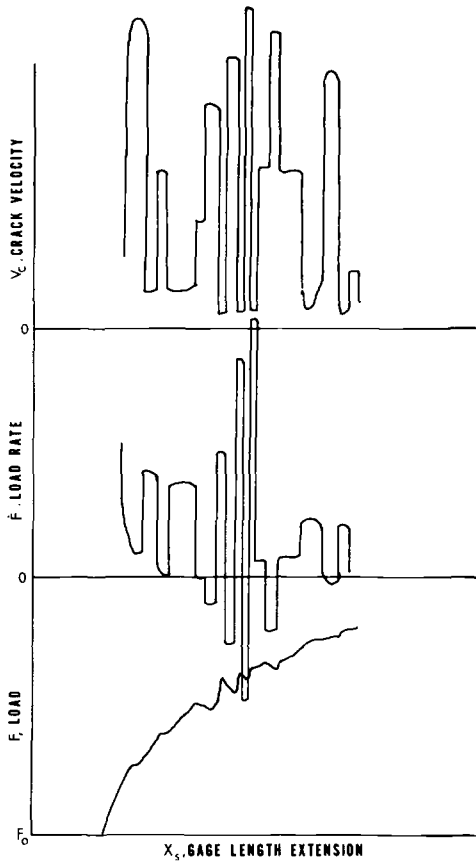


FIG. 12—Schematic of crack velocity versus gage length extension for typical precracked tension specimen.

At constant load, Eq 28 reduces to

$$v_c = \frac{V}{F(dC_s/da)} \quad (\text{constant load}) \quad (29)$$

so that the crack velocity, if  $(dC_s/da)$  is relatively constant, is proportional to the crosshead or descending weight velocity. In stress relaxation ( $V = 0$ ) Eq 28 reduces to

$$v_c = - \frac{C_i \dot{F}}{F(dC_s/da)} \quad (\text{stress relaxation}) \quad (30)$$

so that the velocity decreases with  $d(\ln F)/dt$ . Equations 29 and 30 are equivalent to those derived by Evans [10] for these cases.

### Variability of Machine Stiffness

Suppose the machine stiffness can vary with time. Then it can be shown that Eq 28 must be written

$$v_c = \frac{V - C_s \dot{F} - F \dot{C}_m}{F(dC_s/da)} \quad (31)$$

In the stress relaxation test, the familiar problem of machine relaxation is equivalent to an increase in the machine compliance, giving a finite positive value for  $\dot{C}_m$ . Thus, the true value of  $v_c$  will be somewhat smaller than that calculated according to Eq 28. The conventional method of substituting a hard, rigid specimen and measuring load relaxation, then subtracting this as being the "machine relaxation" can be shown to be incorrect by a simple argument. Certainly, one expects the machine to relax less when a nonrigid specimen is present since the relaxation of the specimen is taking up some of the slack.

An advantage of the present technique is that one may continuously monitor the machine compliance during the stress relaxation experiment. In this test,  $V = 0$ , and Eq 25 gives

$$\dot{F} = - \frac{\dot{X}_s}{C_m} \quad (\text{if } \dot{C}_m = 0) \quad (32)$$

which is represented by the Line  $co$  in Fig. 10. If  $\dot{F}$  versus  $\dot{X}$  is a straight line, then  $C_m$  is a constant. The variability of machine stiffness during plastic deformation or crack extension at constant crosshead velocity will result similarly in the nonlinearity of Line  $ab$  in Fig. 1 (plasticity) or Line  $ab$  in Fig. 10 (crack extension). Analytic techniques for evaluating machine contributions in these situations remain to be developed.

### Conclusion

Ordinarily, the pertinent mechanical parameters in the tension test are considered to be stress and strain. By considering the rate of change of these parameters with respect to time, together with the interaction of a specimen with the tensile machine, entirely new useful relationships emerged. These allowed definitions of new test methods which have certain advantages for measuring proportional limit for plastic flow, machine stiffness, critical load for crack motion, and crack velocity. A consideration of the mechanics of the tension test led to a rational basis for a new method of measuring proportional limit for plastic deformation. A variant which is potentially useful for proportional limit as well as for critical load measurement in extreme environments would not require a strain gage on the specimen.

A new method of measuring machine stiffness was given for constant crosshead speed (which includes stress relaxation), constant load rate, and constant strain rate conditions. Measurements made with the constant crosshead speed technique were compared with those made by other methods. The load-time slope method generally gave erroneously low values of stiffness, and the reason for this was given. The proposed method of measuring machine stiffness can be used on materials which have no lower yield point plateaux (plastics, nonferrous metals, etc.). Since a continuous display of the important mechanical parameters is provided, loading abnormalities, etc., become apparent, and variations in machine stiffness during the test (if present) are monitored. The latter is a useful check on machine relaxation during stress relaxation tests. Transient effects were discussed, and various common mechanical tests were displayed comparatively on a single plot in the stress rate-strain rate plane.

The analysis of crack velocity in terms of external kinetic parameters (load, load rate, and crosshead velocity) was given in general and for the special cases of creep and stress relaxation. The case of irregular crack motion at constant crosshead velocity was also discussed. The possibility of change in machine compliance (machine relaxation) during crack velocity measurements was examined, and suggestions were made concerning the solution of this problem.

### *Acknowledgment*

Dr. E. R. Fuller has provided useful insights on crack velocity measurements.

### **References**

- [1] Weissman, G. F., *Experimental Mechanics*, Vol. 15, 1975, pp. 96-101.
- [2] Wonsiewicz, B. C. and Hart, R. R., *Journal of Testing and Evaluation*, Vol. 1, No. 5, Sept. 1973, pp. 412-514.
- [3] Clough, R. B., *Journal of Testing and Evaluation*, Vol. 3, No. 2, March 1975, pp. 143-146.
- [4] Clough, R. B., *Journal of Testing and Evaluation*, Vol. 4, No. 2, March 1976, pp. 139-140.
- [5] Hockett, J. E. and Gillis, P. P., *International Journal of Mechanical Sciences*, Vol. 13, 1971, pp. 251-275.
- [6] "Determination *K*-Values of a Tensile Testing System," ISO Draft International Standard 2573, International Standards Organization, 1972, available from American National Standards Institute, New York.
- [7] Conrad, H. in *Mechanical Behavior of Materials at Elevated Temperatures*, J. E. Dorn, Ed., McGraw-Hill, New York, 1961, pp. 149-217.
- [8] Carnahan, R. E., Arsenault, R. J., and Stone, G. A., *Transactions of the Metallurgical Society*, American Institute of Mining, Metallurgical, and Petroleum Engineers, Vol. 239, 1967, pp. 1193-1199.
- [9] Irwin, G. R. and Kies, J. A., *Welding Journal Research Supplement*, Vol. 33, 1954, pp. 193s-198s.
- [10] Evans, A. G., *Journal of Materials*, Vol. 7, 1972, pp. 1137-1146.

## DISCUSSION

---

*B. C. Wonsiewicz*<sup>1</sup> (*written discussion*)—The proportional limit has a precise definition, as defined by the American Society for Testing and Materials (ASTM) and general practice. The quantity measured by the author is *not* the proportional limit, and it has an uncertain relation to any other commonly defined mechanical property. Would not a new name be in order?

Further, variations in the machine stiffness constant,  $K$ , or a nonlinear machine response would seem to make the quantity determined a function of the particular machine employed as well as the material tested.

*R. B. Clough* (*author's closure*)—Since the theme of our symposium is recent developments in mechanical testing, it seems appropriate to introduce a new method for measuring proportional limit which has certain advantages, as I have indicated. Proportional limit is defined by the 1975 ASTM Standards as “the greatest stress which a material is capable of sustaining without any deviation from proportionality of stress to strain (Hooke’s law).” This ASTM definition is followed by an instructive note:

Many experiments have shown that values observed for the proportional limit vary greatly with the sensitivity and accuracy of the testing equipment, eccentricity of loading, the scale to which the stress-strain diagram is plotted, and other factors. When determination of proportional limit is required, the procedure and the sensitivity of the test equipment should be specified.

The proportional limit is always an idealization, since every perfect-elastic (defect-free) materials in reality have nonzero second- and third-order elastic constants. But rather than dismiss the use of proportional limit, since in practice it is found to be a useful quantity, we retain the concept, keeping in mind that it is an idealization. A basic assumption of our method, like any other, is that Hooke’s law—that is, stress being proportional to strain—applies up to the proportional limit. Therefore, the method is designed around the strict definition of proportional limit just discussed (see Eq 1). Since no material obeys Hooke’s law exactly, all proportional limit methods really measure some “effective proportional limit.” This is the stress one would have obtained had the material shown a linear elastic region. You may call my method “effective proportional limit” if you wish, but this would therefore also apply to other proportional limit methods. It would seem simpler to drop the modifier “effective” but keep the idealization in mind.

<sup>1</sup> Member of the Technical Staff, Bell Laboratories, Murray Hill, N. J. 07974.

Although the technique employed here is novel, it employs the strict definition of proportional limit just discussed. If you examine the method closely, you will see that it is the stress rate and strain rate counterpart to conventional stress and strain methods in which the time rate form of Hooke's law is used (Eq 1). It states that the proportional limit corresponds to the stress at maximum stress rate. Therefore, if one plots load versus time, such as is given often as an output in a conventional constant cross-head velocity test, the procedure would correspond to taking the load at maximum stress rate  $(\partial\sigma/\partial t)_{\max}$ , the maximum slope of the load-time diagram. Usually, this curve has a sigmoidal shape due to "tailing" at low loads and to plastic deformation above the proportional limit, so that the stress rate goes through a maximum at the proportional limit. On the other hand, the slope of the stress-strain curve has a constant value of  $(\partial\sigma/\partial\epsilon) = E$  up to the proportional limit. The strain rate is elastic and is proportional to the stress rate through  $E$  up to the proportional limit. This gives the line  $Oa$  in Fig. 1. Then, during elastic deformation, the relationship  $\dot{\sigma} = E\dot{\epsilon}$  holds in general and gives  $\dot{\sigma}_{\max} = E\dot{\epsilon}_{\max}$  at the proportional limit. At higher stresses, the addition of a plastic strain rate causes this relationship to fail due to simultaneous deviation by all three quantities, but it holds at the proportional limit and shows the equivalence between this and the conventional method. Here, we note the deviation of  $(\dot{\sigma}, \dot{\epsilon})$  from linearity; in the conventional method, we note the deviation of  $E$  from its constant value.

On your second point, let me show that, if there are effects on the proportional limit due to machine stiffness or specimen geometry, they are only indirectly present, due to the fact that the material possesses a rate sensitivity of the flow stress. Furthermore, since I have demonstrated the equivalence of this method with the usual stress-strain methods through Hooke's law, such effects, usually quite small for most materials at room temperature, are also to be expected in the usual methods. To show this, I will make use of Fig. 1 of the text. A first examination would seem to indicate that a change in machine stiffness, for example, would cause a shift in Point  $a$  and hence cause a sharp change in proportional limit by projection to the stress versus strain rate curve. This would be an erroneous (although quite natural) conclusion, due to the fact that a shift in Point  $a$  is occasioned by a shift in the entire stress versus strain rate curve. Let me indicate one of the ways to show this. Although not brought up in the text (but shown schematically in the upper curve of Fig. 1), the proportional limit corresponds to the inflection point in the  $(\sigma, \dot{\epsilon})$  curve. Therefore, a shift in Point  $a$  must correspond to a similar shift in the inflection point of the  $(\sigma, \dot{\epsilon})$  curve, so that the  $(\sigma, \dot{\epsilon})$  curve also must shift. This should have a negligible effect on the corresponding stress at the inflection point in relatively strain-rate-insensitive materials. In the limit, for an idealized strain rate independent material, the  $(\sigma, \dot{\epsilon})$  curve is horizontal at the proportional limit, giving no effect.

To indicate why the proportional limit corresponds to the inflection point in the  $(\sigma, \dot{\epsilon})$  curve for an ideal case, consider the following. We can write the slope of  $(\sigma, \dot{\epsilon})$ , following the chain rule, as

$$(\partial\sigma/\partial\dot{\epsilon}) = \frac{(\partial\sigma/\partial t)}{(\partial\dot{\epsilon}/\partial t)} = \dot{\sigma}/\ddot{\epsilon}$$

In the elastic region,  $\ddot{\epsilon} = \ddot{\sigma}/E$  so that

$$(\partial\sigma/\partial\dot{\epsilon})_e = E\dot{\sigma}/\ddot{\sigma} \quad \text{if } \sigma \leq \sigma_0$$

And during plastic deformation (that is, above the proportional limit), one can show from Eq 3 of the text that  $\ddot{\epsilon} = -A_0/KL_0$  so that

$$(\partial\sigma/\partial\dot{\epsilon})_p = -KL_0\dot{\sigma}/A_0\ddot{\sigma} \quad \text{if } \sigma > \sigma_0$$

Now Fig. 3 shows that  $\ddot{\sigma}$  is finite and positive below the proportional limit, goes suddenly through zero at the proportional limit, and becomes finite and negative above the proportional limit. According to this, since  $\dot{\sigma}$  is always positive, the slope  $(\partial\sigma/\partial\dot{\epsilon})_e$  increases during loading until it becomes theoretically infinite at the proportional limit as  $\ddot{\sigma}$  goes to zero, decreasing to a finite positive slope  $(\partial\sigma/\partial\dot{\epsilon})_p$  as  $\ddot{\sigma}$  becomes finite and negative during plastic deformation. (Of course, this is the ideal case, and the infinite slope is not reached in practice, as Fig. 2 shows.) The curvature of  $(\sigma, \dot{\epsilon})$  is positive below the proportional limit and negative above, corresponding to the slope increasing with increasing strain rate below, and decreasing with increasing strain rate above the proportional limit. Thus, the proportional limit corresponds to the inflection point.

The effect of nonlinear machine response, for example, variable cross-head speed or stiffness, would be predicted by an argument similar to the one just discussed. In this case, one would use maximum stress rate and the inflection point in the stress versus strain rate curve to obtain the proportional limit.

T. G. Heberling<sup>1</sup>

## Results of a Round Robin Test Program on Hardness Conversion of Ferritic Stainless Steels

---

**REFERENCE:** Heberling, T. G., "Results of a Round Robin Test Program on Hardness Conversion of Ferritic Stainless Steels," *Recent Developments in Mechanical Testing, ASTM STP 608*, American Society for Testing and Materials, 1976, pp. 45-54.

**ABSTRACT:** A round robin program was conducted to determine the hardness conversions for ferritic stainless steels. Each of six participating laboratories conducted hardness tests on specimens representing nine grades, each having varying amounts of cold reduction. Conversions were established to the Rockwell B scale from Rockwell 15T, 30T, 45T, and A scales.

In all cases, the Wilson Chart (Chart No. 52—Wilson Instruments Division, American Chain and Cable Company) conversion fits the least squares round robin data line better than does the ASTM Method E140 austenitic conversion. The Wilson Chart conversion line falls within the 95 percent confidence band of the round robin data for the conversions to Rockwell B from Rockwell 30T, 45T, and A. For the 15T to Rockwell B conversion, the Wilson line falls outside the 95 percent confidence limits for values below HRB 80.

As a result of this round robin program, a joint task group was organized under ASTM Subcommittees A-01.13 and E-28-06 to determine what changes should be made in the hardness conversion tables in ASTM Methods A 370 and E 140. The recommendations of this task group are currently being balloted.

**KEY WORDS:** hardness, ferritic stainless steels, mechanical tests

In discussions on the subject of hardness conversion with representatives of various companies, it was discovered that uncertainty exists as to the proper conversion procedure for ferritic stainless steels. This round robin program was initiated to determine whether hardness conversions for these steels can be accomplished using existing charts or whether they exhibit unique conversion relationships requiring a different conversion procedure.

<sup>1</sup> Senior staff metallurgist, Research and Technology, Armco Steel Corp., Middletown, Ohio 45043.

### Round Robin Test Procedure

Six laboratories took part in the round robin test program. Participating companies included Allegheny Ludlum Steel Corporation, Armco Steel Corporation, Carpenter Technology Corporation, Cyclops Corporation, United States Steel Corporation, and Wilson Instrument Division of American Chain and Cable Company (ACCO).

Thirty-four sheet specimens (3 by 3 in.) of various ferritic stainless grades supplied by Armco were tested. These specimens, including Types 405, 409, 410, 430, 436, 442, 446, Armco 400, and Armco 18SR, had cold reductions ranging from 0 to 15 percent. Each specimen was scribed into nine 1 in. squares which were coded to identify the location of each laboratory's hardness readings.

Before any tests were made on the specimens, each hardness machine used in the program was calibrated using standard hardness blocks donated by Wilson Instrument Division of ACCO. The set of ten blocks, representing the low and high end of each scale studied, was circulated to the participating laboratories along with the specimens.

All laboratories made five hardness determinations on each standard test block. If the average of these five readings was within the required limits indicated on the block, the machine was considered to be in calibration. If the initial average was outside these limits, the machine was adjusted and the procedure repeated until proper calibration was obtained. Once all machines were in calibration, no further corrections were made for testing machine variation.

After calibration was completed, hardness tests were made in the appropriate square of each specimen. Five readings were taken on each of the A, 15T, 30T, 45T, and B scales. The Rockwell B scale was selected as the reference scale, and the averages of the five readings obtained on the superficial and A scales were then plotted versus average Rockwell B to obtain the conversion relationships.

All specimens used in this study had very smooth cold-rolled or annealed and pickled surfaces. To avoid introducing an additional variable, specimens were given no surface preparation other than a thorough cleaning with a solvent.

The round robin conversion data obtained by the six laboratories were computer plotted and the best conversion lines established using the method of least squares. These conversion lines were then compared to the Wilson Chart (No. 52) conversions for ferritic steels and the ASTM Method E 140-72<sup>2</sup> (Table 7) conversions for austenitic stainless steel sheets.

Comparison of the round robin conversion lines with the Wilson Chart was a problem because the Wilson conversions are not perfectly linear.

<sup>2</sup> ASTM Hardness Conversion Tables for Metals (Relationship Between Brinell Hardness, Vickers Hardness, Rockwell Hardness, Rockwell Superficial Hardness, and Knoop Hardness) (E 140-72).

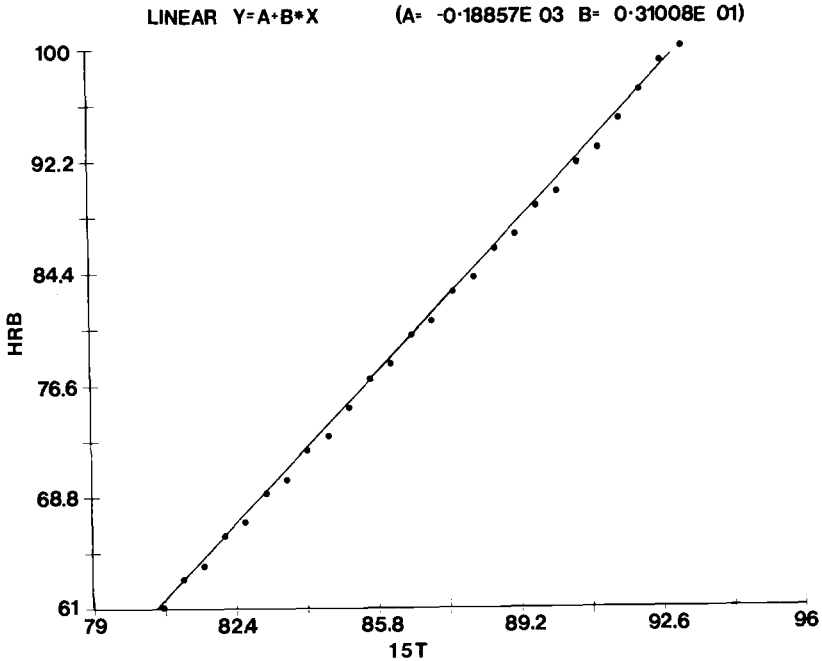


FIG. 1—Least squares plot of Wilson Chart conversion values for 15T to Rockwell B.

The method decided upon was to computer plot the least squares line for the conversion points listed in the chart. This line was then considered to be the “Wilson conversion line” in the comparisons. The computer plots for the conversions from the Rockwell 15T, 30T, 45T, and A scales to the Rockwell B scale are presented in Figs. 1–4, respectively.

Comparison with ASTM Method E 140 austenitic conversion was made using the original least squares equations obtained by ASTM Subcommittee E-1.06 in 1966, upon which ASTM Method E 140 Table 7 is based.<sup>3</sup>

## Results

The conversion relationships determined in the round robin program from 15T, 30T, 45T, and Rockwell A to Rockwell B are shown in Figs. 5–8, respectively. The least squares line is plotted through the data points along with the 95 percent confidence limits (shown as dashed lines) for an average of two hardness readings.<sup>4</sup> In other words, one can be 95 percent confident that the average of duplicate readings of a future hardness determination

<sup>3</sup> Heyer, R. H., private communication to P. J. Todkill, 13 July 1966 (Mr. Heyer was the chairman of ASTM Subcommittee E-01.06 on Conversion Equations for Austenitic Stainless Steels).

<sup>4</sup> *Statistical Methods in Research and Production*, 3rd ed., O. L. Davies, Ed., Hafner Publishing Co., New York, 1961, p. 170.

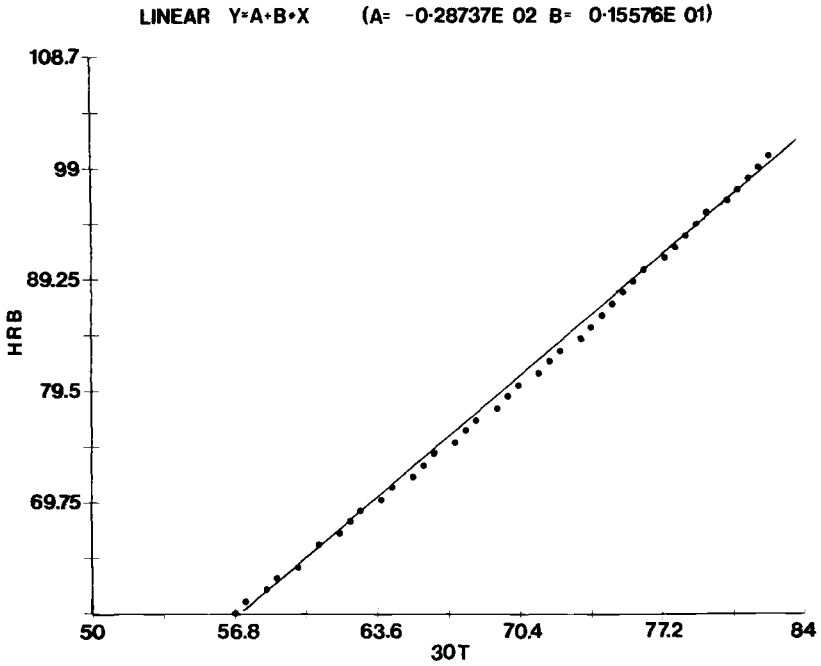


FIG. 2—Least squares plot of Wilson Chart conversion values for 30T to Rockwell B.

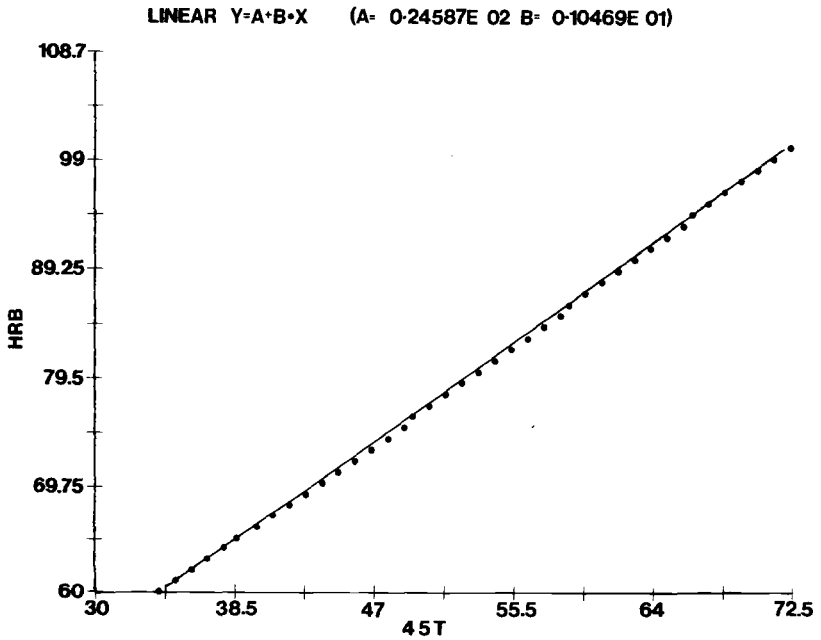


FIG. 3—Least squares plot of Wilson Chart conversion values for 45T to Rockwell B.

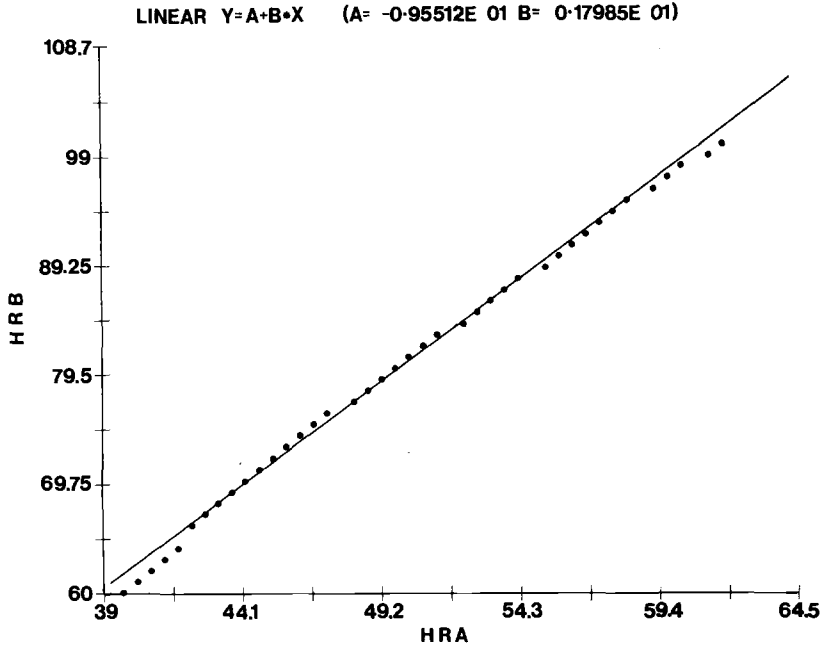


FIG. 4—Least squares plot of Wilson Chart conversion values for Rockwell A to Rockwell B.

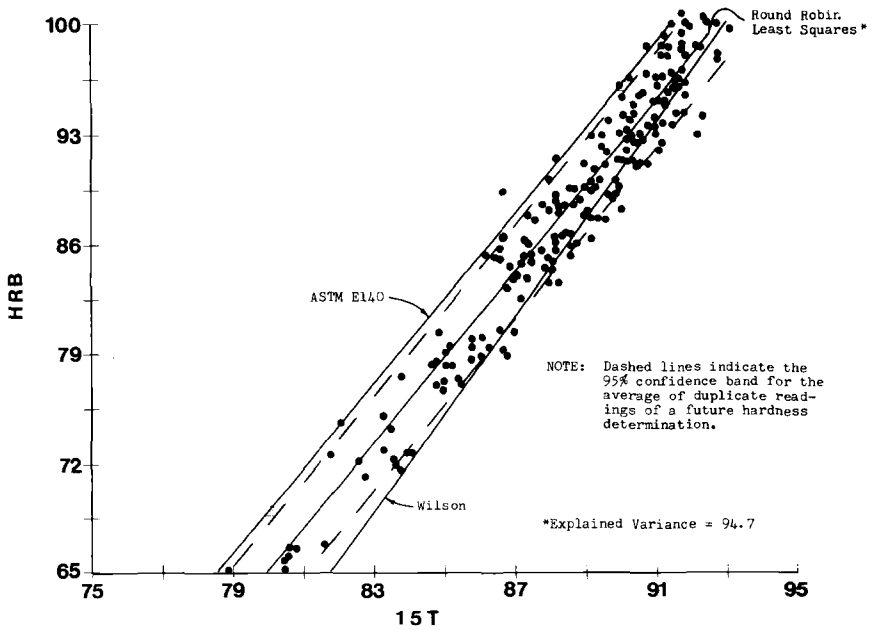


FIG. 5—Round robin test results 15T to Rockwell B.

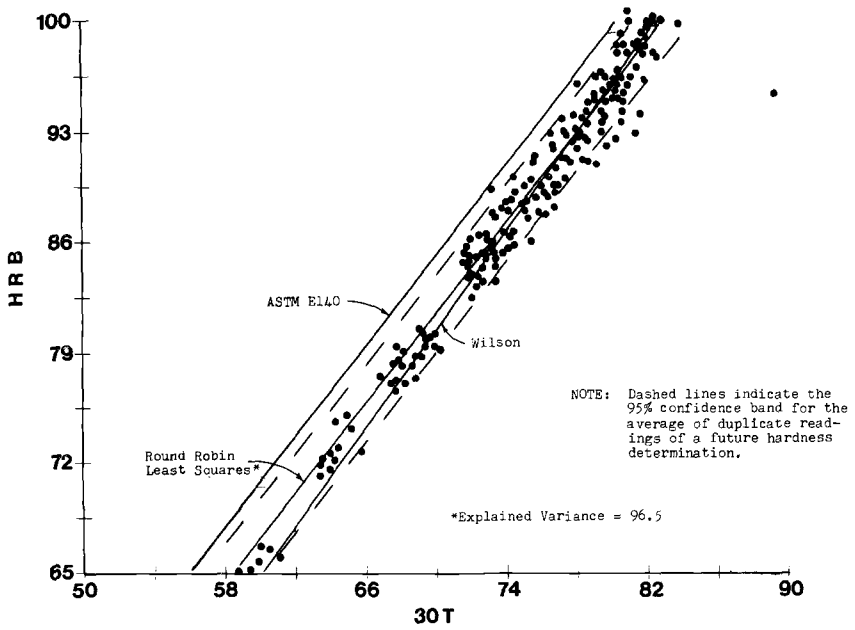


FIG. 6—Round robin test results 30T to Rockwell B.

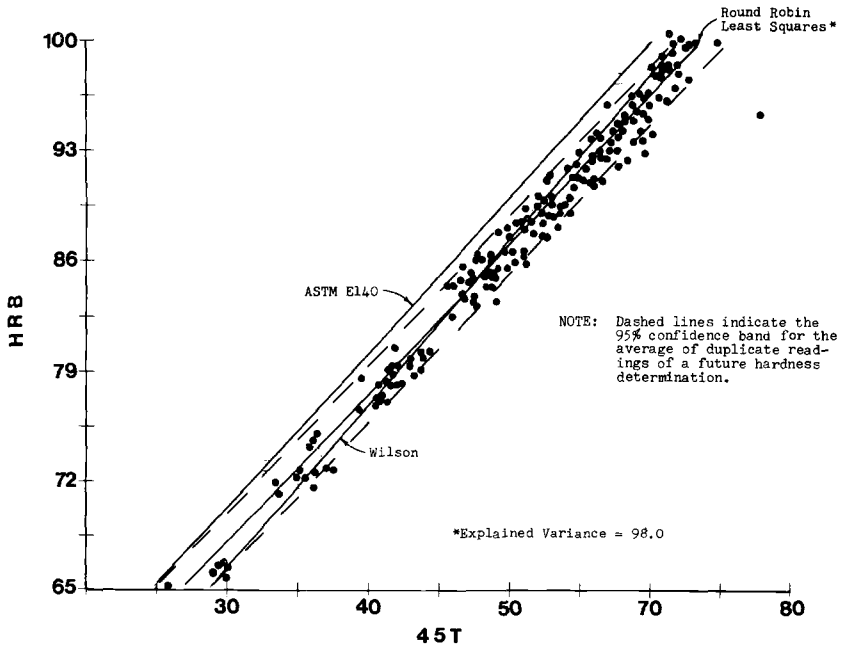


FIG. 7—Round robin test results 45T to Rockwell B.

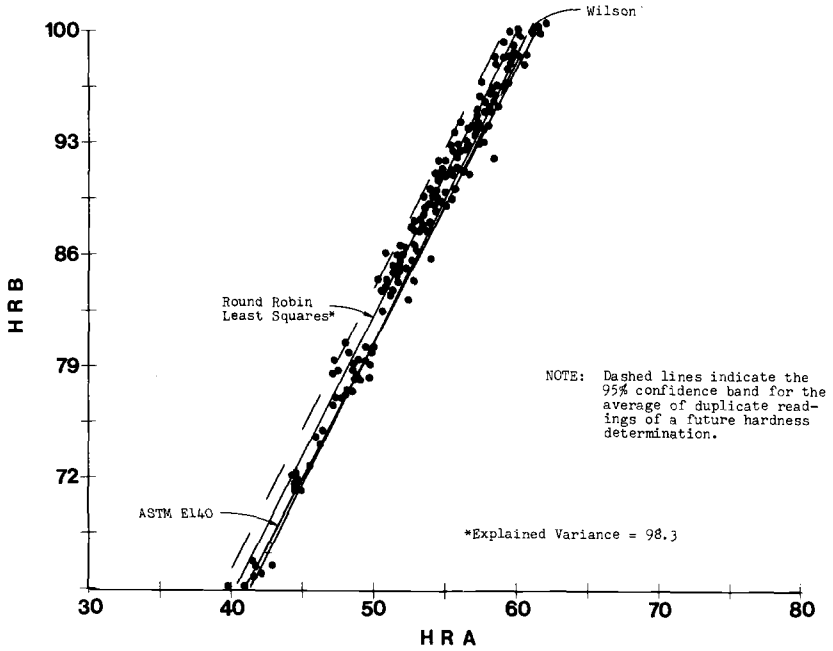


FIG. 8—Round robin test results Rockwell A to Rockwell B.

will fall within this band. The Wilson conversion line and the ASTM Method E 140 line are also shown on each plot.

In each case, the Wilson conversion line represents the round robin data better than does the ASTM Method E 140 austenitic conversion, as expected. For the conversions from Rockwell 30T, 45T, and A to Rockwell B, the Wilson line falls within the 95 percent confidence band through the entire range from Rockwell B65 to Rockwell B100. In the case of the conversion from Rockwell 15T to Rockwell B, the Wilson line falls within the 95 percent confidence band only for hardnesses of Rockwell B80 and above.

Tables 1-4 present the conversion equations to Rockwell B from the Rockwell 15T, 30T, 45T, and A scales, respectively. Each table contains

TABLE 1—Rockwell 15T to Rockwell B hardness conversion equations.

Equation	Source	Standard Deviation <sup>a</sup>
$HRB = 2.725599 (15T) - 152.8762$	round robin data	2.10
$HRB = 3.100855 (15T) - 188.5761$	Wilson Chart	3.59
$HRB = 2.700805 (15T) - 147.2251$	ASTM Method E 140 (austenitic)	4.06

<sup>a</sup> Standard deviation calculated for the round robin data from the indicated equation.

TABLE 2—Rockwell 30T to Rockwell B hardness conversion equations.

Equation	Source	Standard Deviation <sup>a</sup>
$HRB = 1.424263 (30T) - 18.15879$	round robin data	1.71
$HRB = 1.556488 (30T) - 28.65048$	Wilson Chart	2.03
$HRB = 1.436132 (30T) - 15.51974$	ASTM Method E 140 (austenitic)	3.93

<sup>a</sup> Standard deviation calculated for the round robin data from the indicated equation.

TABLE 3—Rockwell 45T to Rockwell B hardness conversion equations.

Equation	Source	Standard Deviation <sup>a</sup>
$HRB = 0.949634 (45T) + 30.19974$	round robin data	1.30
$HRB = 1.046618 (45T) + 24.60585$	Wilson Chart	1.61
$HRB = 0.985327 (45T) + 30.82865$	ASTM Method E 140 (austenitic)	3.10

<sup>a</sup> Standard deviation calculated for the round robin data from the indicated equation.

TABLE 4—Rockwell A to Rockwell B hardness conversion equations.

Equation	Source	Standard Deviation <sup>a</sup>
$HRB = 1.770906 (HRA) - 6.26374$	round robin data	1.20
$HRB = 1.798527 (HRA) - 9.55136$	Wilson Chart	2.20
$HRB = 1.712181 (HRA) - 5.22965$	ASTM Method E 140 (austenitic)	2.42

<sup>a</sup> Standard deviation calculated for the round robin data from the indicated equation.

the least squares equations obtained from (a) the round robin results from all six laboratories, (b) a computer plot of the conversion data presented in Wilson Chart No. 52, and (c) the 1966 round robin to determine the austenitic conversions which are now found in ASTM Method E 140, Table 7. The standard deviations given result from comparing the round robin data obtained in this program to each of these three lines, as indicated. For each conversion, the data fit is best, obviously, for the least squares data line, followed by the Wilson line, and finally the ASTM Method E 140 line.

## Conclusions

Since conversion of hardness values from one scale to another is approximate, conversions should only be used when it is impossible to test the material using the desired scale. The major source of conversion error is

the difference in strain hardening characteristics of different steels. For example, although an annealed and a cold reduced steel may have identical hardness when tested on one of the superficial scales, the higher strain hardening capacity of the annealed material may result in a significantly higher hardness reading for this material when the greater load of the Rockwell B scale is applied.

Since hardness conversions are approximate, the Wilson Chart appears to be satisfactory for converting from Rockwell A, 30T, and 45T to Rockwell B in the hardness range from Rockwell B65 to 100. In the case of the Rockwell 15T scale, the difference between the round robin least squares line and the Wilson conversion line is significantly greater. The standard deviations presented in Table 1 indicate (a) greater data scatter on this scale in the round robin testing and (b) a less satisfactory correlation between the round robin data and the Wilson conversion line than was found for the other three scales (Tables 2-4). The very light load used in testing on the 15T scale results in an increased sensitivity to surface condition and greater data scatter. Hardness conversion involving the 15T scale is therefore even less accurate than hardness conversion in general and should be done with caution and a full understanding of the dangers involved. Conversion of Rockwell 15T results below 86 (about HRB 80) is not recommended.

The goals of this round robin program were to determine (a) which of the two common conversions does a better job for ferritic stainless steels and (b) whether a different conversion might exist which would fit these materials significantly better than either of the two commonly used ones. The latter question cannot be answered at present due to a lack of information concerning the establishment of the Wilson Chart. Since information such as materials included, number of specimens, standard deviation, etc., cannot be determined for the Wilson Chart, evaluation of the relative significance of our round robin conversions and those included in the Wilson Chart would require quite a comprehensive test program. Since all conversions are approximate and their use should not be encouraged, it is doubtful whether such a program would be presently justifiable.

### Subsequent ASTM Actions

As a result of work completed in this round robin program, a joint task group was formed under ASTM Subcommittees A-01.13 and E-28.06 to recommend changes in the hardness conversion tables included in ASTM Method and Definitions for Mechanical Testing of Steel Products (A 370-75a) and Method E 140. In early 1974, this task group issued its final report.<sup>5</sup> Briefly, the recommendations of the task group are to: (a) include hardness

<sup>5</sup> Heberling, T. G., "Recommendations of Task Group on Hardness Conversion," report to R. H. Colin, chairman, ASTM Subcommittee E-28.06, and G. E. Selby, chairman, ASTM Subcommittee A-01.13, 20 Feb. 1974.

conversion tables for soft steels (down to HRB 30) in ASTM Method E 140, (b) bring ASTM Methods A 370 and E 140 hardness conversion tables into agreement, and (c) arrange the hardness conversion tables of ASTM Method E 140 in a more logical order and format. The conversions recommended for ferritic steels (including ferritic stainless steels) were derived from the Wilson Chart, based on the information obtained in this test program. The proposed changes are presently being balloted by the sponsoring committees and subcommittees. If approved by these groups and by the Society, the changes will be incorporated into the 1976 Book of ASTM Standards.

### *Acknowledgments*

The author is grateful to the following participants in the round robin program for their participation and helpful suggestions: C. H. Brown, Cyclops Corporation; A. G. Cook, Allegheny Ludlum Steel Corporation; A. DeBellis, American Chain and Cable Company; J. M. Holt, United States Steel Corporation; and S. E. Tyson, Carpenter Technology Corporation. Special thanks also go to E. S. Harris of Armco Steel Corporation for his valuable assistance in statistical analysis of the results of the program and to R. L. Lewis for typing the manuscript.

## Static Mean Stress and Cyclic Yield Strength

---

**REFERENCE:** Weissmann, G. F. and Davis, J. A., III, "Static Mean Stress and Cyclic Yield Strength," *Recent Developments in Mechanical Testing, ASTM STP 608*, American Society for Testing and Materials, 1976, pp. 55-66.

**ABSTRACT:** The cyclic yield strength of metals depends on the cyclic plastic deformation, the static mean stress, the number of cycles, and the frequency. For a number of different alloys, the cyclic yield strength in bending was determined as a function of the plastic deformation and the mean stress. The application of a static stress always caused a reduction of the cyclic yield strength. The magnitude of the reduction depends on the type of material investigated. The results are discussed with respect to possible spring applications.

**KEY WORDS:** mechanical tests, stresses, mechanical properties, yield strength, plastic deformation

The WT-bend tester provides a convenient tool for the determination of small offset yield stresses of thin flat-spring materials subjected to reversed bending [1,2].<sup>3</sup> Instead of measuring deviation from linearity as is done in the conventional tension tests [ASTM Definition of Terms Relating to Methods of Mechanical Testing (E 6-66 (1973))], it uses energy dissipation as a yield criterion. The equivalent yield stresses between 0.002 and 0.012 percent offsets are readily determined [3]. For many applications, metals are not subjected to reversed bending alone, but cycled about various static stresses resulting from the application of static bending moments. The apparatus has been modified to allow the application of such bending moments and to measure the resulting offset yield stresses.

### WT-Bend Tester

The WT-bend tester uses energy dissipation as the yield criterion and is applicable for the characterization of flat springs and flat-spring materials. The apparatus has been described previously [1,2], and it suffices here to repeat the general principles and the modifications made in order to apply

<sup>1</sup> Supervisor, Mechanics of Materials, Bell Laboratories, Murray Hill, N. J. 07974.

<sup>2</sup> Student, Prairie View University, Prairie View, Tex. 77445.

<sup>3</sup> The italic numbers in brackets refer to the list of references appended to this paper.

a static bending moment. A photograph of the modified apparatus is shown in Fig. 1. The schematic sketch in Fig. 2 will be used to explain the apparatus. For reversed bending, Specimen A is clamped on one end to the Table T and the other end to attachment Part P. Table T is supported by bearings and held by solenoid S1 in a fixed position. Attachment Part P is set in motion when Specimen A is subjected to bending. When it reaches the amplitude of rotation  $\Phi_a$ , an optical switch O1 triggers solenoid S2 and releases solenoid S1. This causes a small rotation  $\Delta\Phi$  of Table T. This position is shown in Fig. 2 where the dotted lines represent the rotation of Table T after attachment Part P has obtained the amplitude of rotation  $\Phi_a$ . Since the operation of the solenoids is fast compared to the oscillation

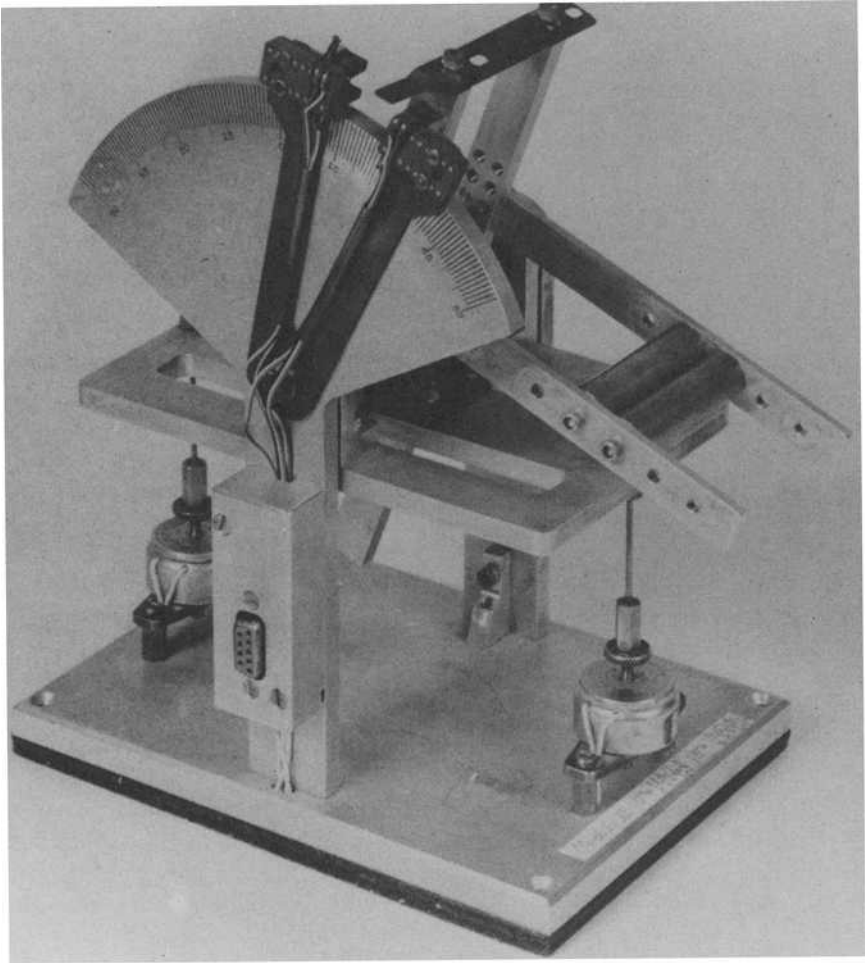


FIG. 1—*Modified bend tester.*

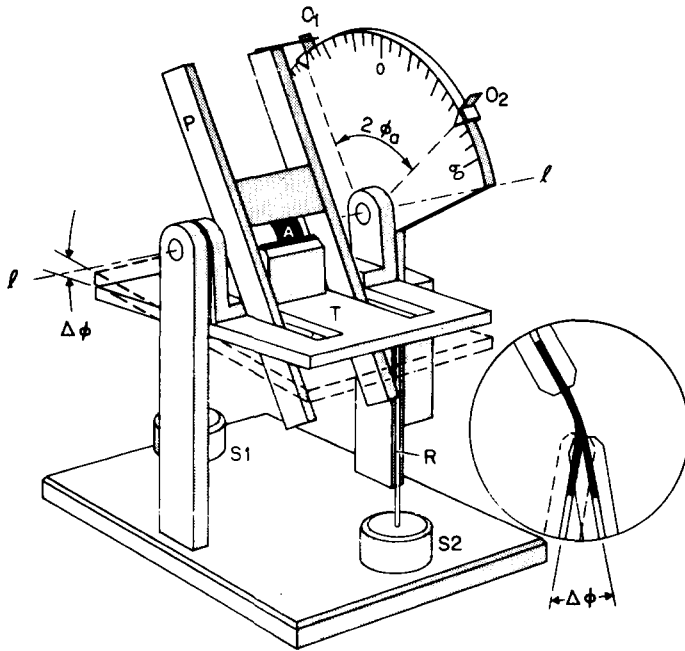
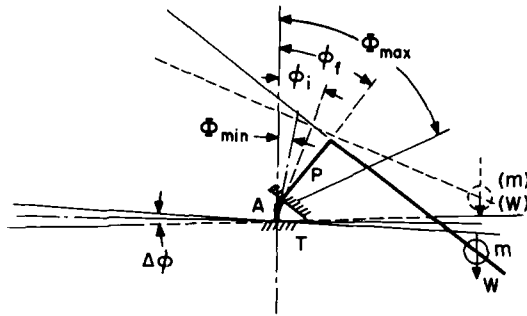


FIG. 2—Schematic drawing of WT-bend tester.

of attachment Part P, Specimen A is subjected to an almost instantaneous decrease of its radius of curvature, as shown in the insert of Fig. 2. This change of the radius of curvature of the specimen causes an increase of the strain energy. The process is reversed when the attachment part reaches the amplitude of rotation in the opposite direction. Provisions have been made for moving the optical switches O1 and O2 automatically to the position of the amplitude of rotation of the attachment part. After a number of cycles, the apparatus reaches its steady-state condition. The apparatus is modified, as shown in Fig. 3, by the application of an eccentric weight  $W$  to attachment Part P which causes an initial static rotation of Specimen A to an angle  $\Phi_i$ . (The maximum fiber stresses of the specimen due to the angle  $\Phi_i$  are always smaller than the 0.01 percent offset yield strength.) An additional manual rotation of the attachment part starts the oscillation and the operation of the bend tester. When the rotation reaches a maximum angle  $\Phi_{max}$ , Table T will rotate instantaneously counter-clockwise about a fixed angle  $\Delta\Phi$  and remain in the dotted position until the minimum angle  $\Phi_{min}$  is reached, which causes a reversal of the angle  $\Delta\Phi$  of Table T. Again, after a number of oscillations, the attachment part obtains a steady-state condition. When the oscillation is discontinued, the attachment part stops at a final angle  $\Phi_f$  which is always greater or equal to the initial angle  $\Phi_i$ . The bending moment  $M$  acting on the center of



- A** = SPECIMEN  
**P** = ATTACHMENT PART  
**T** = TABLE  
**W** = WEIGHT  
 $\Delta\phi$  = ROTATION OF TABLE  
 $\phi_i$  = INITIAL ROTATION  
 $\phi_f$  = FINAL ROTATION  
 $\Phi_{\max}$  = MAXIMUM ROTATION  
 $\Phi_{\min}$  = MINIMUM ROTATION  
 $\phi_a = \frac{1}{2} (\Phi_{\max} - \Phi_{\min})$  = AMPLITUDE OF ROTATION  
 $\bar{\phi} = \frac{1}{2} (\Phi_{\max} + \Phi_{\min})$  = AVERAGE ROTATION

FIG. 3—Schematic of modified WT-bend tester.

Specimen A is readily calculated from the known eccentric weight  $W$  and the angle  $\phi_f$ .

The amplitude of rotation  $\Phi_a$  is defined as

$$\Phi_a = \frac{1}{2} (\Phi_{\max} - \Phi_{\min}) \quad (1)$$

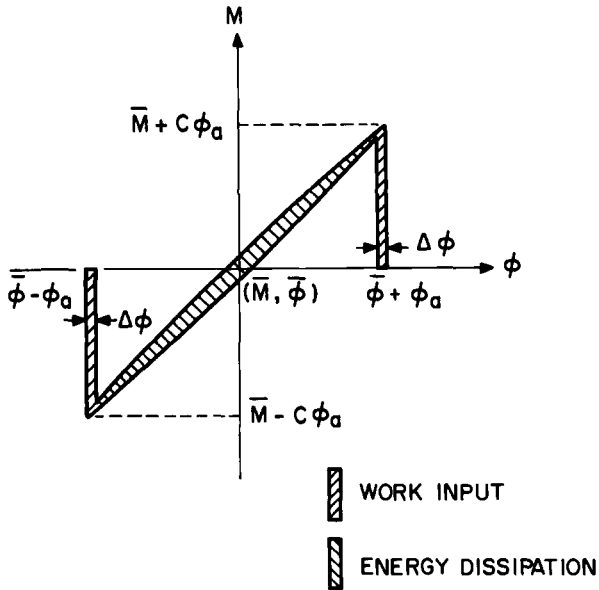
and the average rotation  $\bar{\Phi}$  becomes

$$\bar{\Phi} = \frac{1}{2} (\Phi_{\max} + \Phi_{\min}) \quad (2)$$

Figure 4 shows the moment rotation relationship of an oscillating specimen in the WT-bend tester. For a one degree-of-freedom oscillating system, the spring constant  $C$  of the specimen becomes

$$C = J\omega^2 \quad (3)$$

where  $J$  is the mass-moment of inertia of attachment Part P with respect to the center of Specimen A, and  $\omega$  is the angular frequency.



WORK ADDED = DISSIPATED ENERGY

FIG. 4—Work input and energy dissipation of specimen in modified WT-bend tester.

During the steady-state condition of a vibrating system, the dissipated energy  $W$  per cycle must be equal to the work added per cycle. In Fig. 4, the dissipated energy is represented by the hysteresis loop and the work added by  $2C\Phi_a\Delta\Phi$ . It follows

$$W = 2C\Phi_a\Delta\Phi = 2J\omega^2\Phi_a\Delta\Phi \quad (3)$$

Figure 5 finally shows the moment-rotation response of a specimen subjected to both reversed bending ( $\bar{M} = 0$ ) and an additionally applied static moment ( $\bar{M} = \text{constant}$ ). The final rotation  $\bar{\Phi}$  due to the moment  $\bar{M}$  is shown.  $\Phi_0$  represents the cyclic amplitude of rotation for reversed bending and  $\Phi_a$ , the cyclic amplitude for a static moment  $\bar{M}$ .

The amplitude of rotation  $\Phi_a$  in Eq 3 is considered to be a function of the following parameters

$$\Phi_a = \Phi_a(\Delta\Phi, \bar{\Phi}, n, \omega) \quad (4)$$

$n$  represents the number of cycles and indicates cyclic softening and fatigue failure. For most metals, the dependence on the angular frequency  $\omega$  or on the strain rate is small and can be neglected. This is particularly true for stresses above the onset of plastic deformation at low and intermediate frequencies (0.5 to 200 Hz) [4]. However, for many plastics and rubbers, the frequency or the strain rate is important and must be considered. The same applies for most metals at very low stresses.

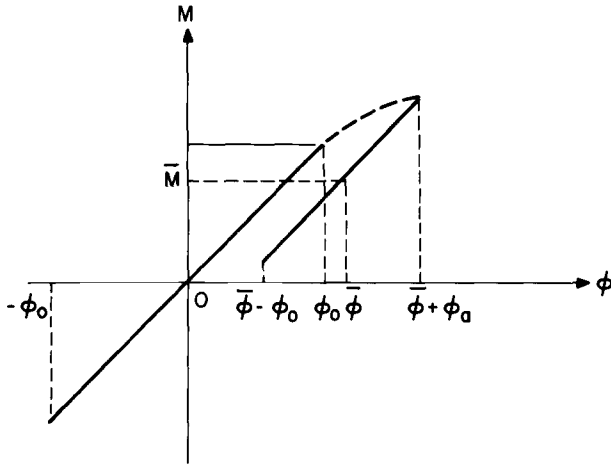


FIG. 5—Reversed bending and effect of static moment.

Expressing the rotations in terms of the maximum fiber strains of a specimen with rectangular cross-sectional area subjected to uniform bending one obtains

$$\Delta\epsilon = \frac{h}{2l} \Delta\Phi; \quad \epsilon_a = \frac{h}{2l} \Phi_a; \quad \bar{\epsilon} = \frac{h}{2l} \bar{\Phi} \quad (5)$$

where

- $\Delta\epsilon$  = maximum strain at the outside fiber due to the table rotation  $\Delta\Phi$ ,
- $\epsilon_a$  = outside fiber strain caused by the amplitude of rotation  $\Phi_a$ ,
- $\bar{\epsilon}$  = outside fiber strain due to the average rotation  $\bar{\Phi}$ ,
- $h$  = thickness,
- $b$  = width, and
- $l$  = nominal length of the specimen.

The corresponding stresses are

$$\bar{\sigma} = \frac{6\bar{M}}{bh^2}; \quad \sigma_a = \frac{6J\omega^2}{bh^2} \Phi_a \quad (6)$$

where

- $\bar{\sigma}$  = maximum fiber stress due to the static moment  $\bar{M}$  and
- $\sigma_a$  = maximum fiber stress due to the amplitude of rotation  $\Phi_a$ .

It has been shown previously that the “design stress”  $\sigma_1$  is closely related to the offset yield strength for an offset  $\Delta\epsilon$  and can be expressed approximately as [1]

$$\sigma_1 = 0.87\sigma_a \quad (7)$$

The coefficient 0.87 accounts for the stress gradient in a specimen of rectangular cross section and is based on the validity of Lazan's law which states that the energy dissipation is an exponential function of the stress or strain amplitude. The error introduced by this approximation is generally less than 3 percent [1], and the corresponding design strain becomes

$$\epsilon_1 = 0.87\epsilon_a \quad (8)$$

From Eqs 4, 5, and 7, there follows for the design stress of metals

$$\sigma_1 = \sigma_1(\Delta\epsilon, \bar{\epsilon}, n) = 0.87 \frac{6J\omega^2}{bh^2} \Phi_a \quad (9)$$

Finally, the maximum value of the design stress becomes

$$\sigma_{\max} = \bar{\sigma} + \sigma_1 \quad (10)$$

and the corresponding strain is accordingly

$$\epsilon_{\max} = \bar{\epsilon} + \epsilon_1 \quad (11)$$

### Test Results

A number of alloys used or intended for spring applications have been evaluated by means of the modified WT-bend tester. They are listed in Table 1, together with their temper, heat treatment, rolling direction, and modulus of elasticity. The specimen had a nominal thickness of 0.25 mm, a width of 12 mm, and a length of about 40 mm.

Equation 9 was used to calculate the design stress  $\sigma_1$ . The case of reversed bending with  $\bar{\epsilon} = 0$  is shown in Fig. 6. The design stress  $\sigma_1$  is determined

TABLE 1—Materials tested.

No.	Material	Temper (Reduction)	Heat Treatment	Direction	Modulus of Elasticity, GN/m <sup>2</sup>
A	carbon steel		C 1095 <sup>a</sup>	rolling	200 to 207
BL	copper-beryllium CA-172	½ hard (21%)	3 h at 302°C	rolling	130
BT	copper-beryllium CA-172	½ hard (21%)	3 h at 302°C	transverse	131
CL	phosphor bronze CA-510	textured (97.3%)	as rolled	rolling	110
CT	phosphor bronze CA-510	textured (97.3%)	as rolled	transverse	132

<sup>a</sup> C1095: normalized at 1650°F, reheated to 1475°F, quenched in oil, tempered at 400 to 1300°F.

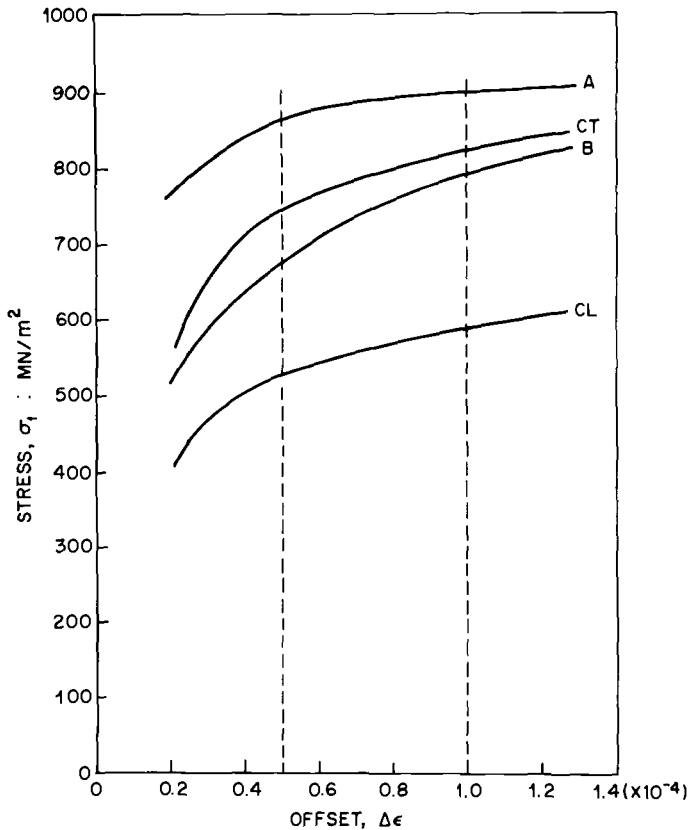


FIG. 6—Design stress versus offset.

for increasing values of the offset  $\Delta\epsilon$ .  $\Delta\epsilon$  was varied from 0.00002 to 0.00012 in steps of 0.00002. The values shown in Fig. 6 represent the averages of at least three readings. The spread of the data was always smaller than  $\pm 30$  MN/m<sup>2</sup>. The number of cycles  $n$  applied at each offset  $\Delta\epsilon$  was smaller than 200 and caused no significant reduction of the design stress  $\sigma_1$  for the materials listed in Table 1. The effect of an increasing and decreasing offset  $\Delta\epsilon$  and of cyclic softening has been investigated previously [3]. The significance of the stress sensitivity limit was also discussed [3-5].

The effect of a static moment  $\bar{M}$  on the design stress  $\sigma_1$  was investigated next. The static moments caused initial rotations  $\Phi_i$ . These moments caused maximum fiber stresses below the 0.01 percent offset yield strength. Subsequent cycling increased the angle of rotation to  $\Phi_f$ . In all cases, the final angle  $\Phi_f$  was identical to the average angle  $\bar{\Phi}$  which corresponded to a mean outside fiber strain  $\bar{\epsilon}$ .

Figure 7 shows the effect of a mean outside fiber strain  $\bar{\epsilon}$  on the design stress  $\sigma_1$  for a constant offset  $\Delta\epsilon = 0.00005$ . Again, a minimum of three specimens was used to establish these curves. The spread of the data was less than  $\pm 30$  MN/m<sup>2</sup>. In all cases, the final static outside fiber strain  $\bar{\epsilon}$  caused a reduction of the design stress  $\sigma_1$ . However, different materials showed a remarkably different behavior. Material B, the heat-treated one half hard copper beryllium, showed a much smaller reduction of the design stress  $\sigma_1$  with an increase of the final mean strain  $\bar{\epsilon}$  than any of the other materials tested. It should be noted that the cyclic design strain  $\epsilon_1$  alternates about an average final mean strain  $\bar{\epsilon}$ . The design stress  $\sigma_1$  for an offset  $\Delta\epsilon = 0.00005$  represents a value above the stress sensitivity limit [4] and may be considered to be an upper bound of this value. It is often assumed that the stress sensitivity limit is identical to the fatigue limit [3-5]. The fatigue limit shall be defined as the stress which the specimen can sustain for more than  $10^8$  cycles. Therefore, the design stress shown in Fig. 7

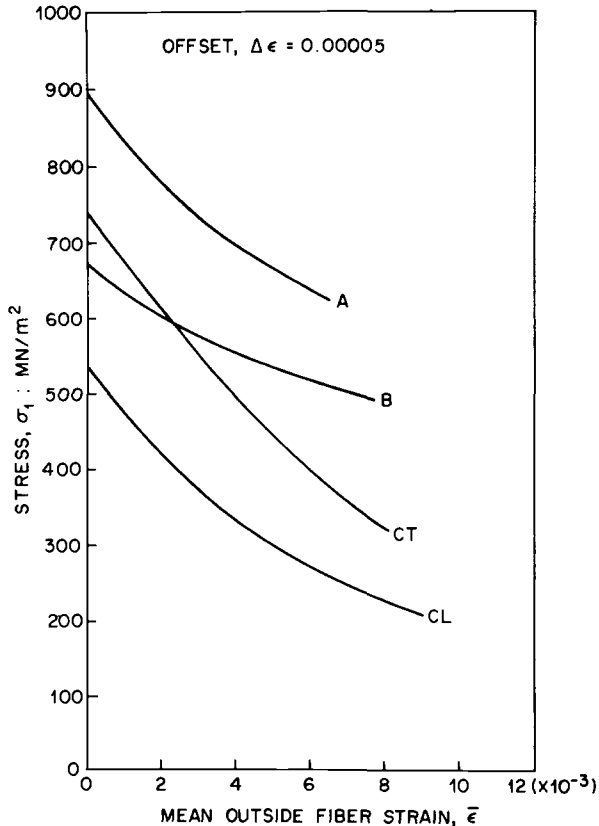


FIG. 7—Design stress versus mean outside fiber strain.

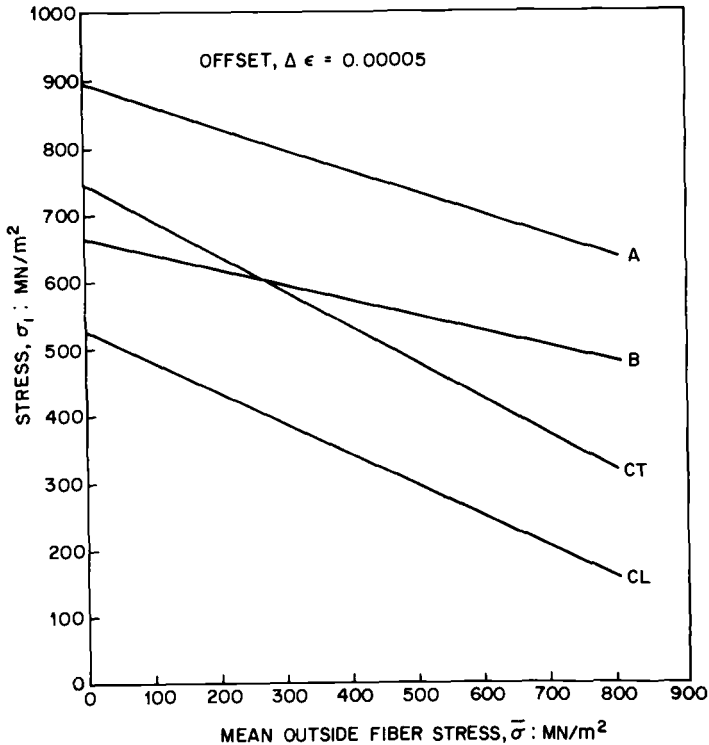


FIG. 8—Design stress versus mean outside fiber stress.

should be an upper bound and a good indication of the change of the fatigue limit as a function of the mean outside fiber strain.

In Fig. 8, the design stress  $\sigma_1$  is shown as a function of the mean outside fiber stress  $\bar{\sigma}$  for the same constant offset  $\Delta\epsilon = 0.00005$ . The dependence of the design stress  $\sigma_1$  on the mean outside fiber stress  $\bar{\sigma}$  is similar to that shown in Fig. 7. However, the design stress  $\sigma_1$  shows a linear decrease with an increase of the mean stress  $\bar{\sigma}$ . A similar linear effect of the fatigue limit was observed by G. Sines and J. L. Waisman [6] who also proposed a theoretical model to explain this phenomenon. Their results support the assumption that the design stress  $\sigma_1$  with an offset  $\Delta\epsilon = 0.00005$  is greater than the fatigue limit and is a good indication of the change of the fatigue limit as a function of the mean stress  $\bar{\sigma}$ .

Finally, the mean outside fiber stress  $\bar{\sigma}$  as a function of the mean outside fiber strain  $\epsilon$  has been determined from Figs. 7 and 8 or Eqs 5 and 6 and are shown by the dotted lines in Fig. 9. In addition, the maximum stress  $\sigma_{\max}$  versus the maximum strain  $\epsilon_{\max}$  have been determined using Eqs 10 and 11 and are represented by the solid lines in Fig. 8. It is interesting to note that Materials B and CT show nearly identical curves even though

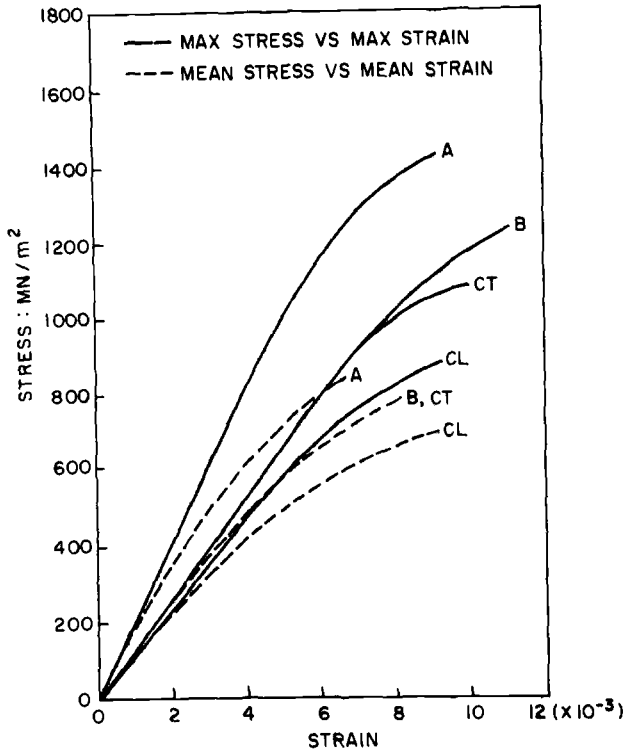


FIG. 9—Maximum stress versus maximum strain curve.

the range of the design stress  $\sigma_1$  and the proportional fatigue limit differ significantly.

### Summary and Conclusions

The effect of a mean stress on the cyclic plastic deformation was investigated for a number of spring materials. The results can be summarized as follows.

1. A material subjected to static stresses will exhibit the expected initial deformations.
2. An additional cyclic stress (design stress) applied to the material will increase the mean deformation.
3. The design stress is an alternating stress with a specified constant offset or plastic deformation.
4. The design stress decreases with an increasing static mean stress or mean final deformation.
5. The fatigue strength is expected to be proportional to the design stress.

The WT-bend tester not only determines the offset yield strength or the design stress in bending as a function of the offset or plastic deformation, and the number of cycles for repeated loading, but is readily modified to study the effect of a static stress distribution on the cyclic behavior of materials.

### References

- [1] Weissmann, G. F., *Journal of Testing and Evaluation*, Vol. 1, No. 2, 1973, pp. 133-138.
- [2] Weissmann, G. F. and Wonsiewicz, B. C., *Journal of Engineering for Industry, Transactions*, American Society of Mechanical Engineers, Vol. 96, Series B, No. 3, 1974, pp. 839-844.
- [3] Weissmann, G. F., *Experimental Mechanics*, Vol. 15, No. 3, March 1975, pp. 96-101.
- [4] Lazan, B. J., *Damping of Materials and Members in Structural Mechanics*, Pergamon Press, London, 1968, Chapters 5 and 6.
- [5] Adams, R. D., *Journal of Sound and Vibration*, Vol. 32, No. 2, 1972, pp. 199-216.
- [6] Sines, G. and Waisman, J. L., *Metal Fatigue*, McGraw-Hill, New York, 1959, p. 145.

## Use and Reproducibility of a Gage to Measure the Lateral Expansion of Charpy V-Notch Impact Specimens<sup>2</sup>

---

**REFERENCE:** Holt, J. M., "Use and Reproducibility of a Gage to Measure the Lateral Expansion of Charpy V-Notch Impact Specimens," *Recent Developments in Mechanical Testing, ASTM STP 608*, American Society for Testing and Materials, 1976, pp. 67-90.

**ABSTRACT:** Because the lateral expansion that occurs on the compression side of the Charpy V-notch specimen, directly opposite the notch, appears to be a direct measure of notch ductility and appears to be independent of strength variation and of chemical composition, its use as a notch-ductility criterion is increasing. During the years that U. S. Steel Corporation has been measuring lateral expansion, a gage was developed for measuring this value rapidly. This paper describes the gage and the method for using it and presents the results of a test program conducted on standard specimens of A36 and ASTM 514 Type F steels to determine the accuracy and reproducibility of lateral-expansion measurements made with this gage. Measurements were made at several U. S. Steel Corporation plants that produce or use plates to ensure that plant personnel are able to obtain the same values as those obtained at a research laboratory, within an allowable tolerance.

The results of the test program may be summarized as follows: (1) The accuracy of the measurements was the same as the accuracy of the dial indicator that was integral with the gage; for the standard 1-mil gage, this accuracy is  $\pm 2$  mils (1 mil = 0.001 in.). (2) The reproducibility of measurements made with the standard gage was about the same as the accuracy, that is,  $\pm 2$  mils. (3) Prior experience in using the gage is not necessary to obtain this degree of reproducibility. (4) Plant personnel can obtain values that are in agreement with those obtained at a research laboratory. (5) Measurements made with micrometers were accurate and were generally reproducible to the same degree as the gage; however, considerably greater care is required in making micrometer measurements, and, for this reason, the use of the dial gage is recommended over the use of micrometers.

Improved precision can be obtained by replacing the standard 1-mil dial indicator with a 1/10-mil (0.0001 in.) dial indicator at modest additional cost.

**KEY WORDS:** mechanical tests, Charpy impact tests, measurement, mechanical properties

<sup>1</sup> Senior research engineer, U. S. Steel Corp., Monroeville, Pa. 15146.

<sup>2</sup> It is understood that the material in this paper is intended for general information only and should not be used in relation to any specific application without independent examination and verification of its applicability and suitability by professionally qualified personnel. Those making use thereof or relying thereon assume all risk and liability rising from such use or reliance.

Charpy V-notch (CVN) transition temperatures at a constant energy-absorption level (such as 15 ft · lb or 20.4 J) do not provide a reliable measure of susceptibility to brittle fracture for steels of different strengths, deoxidation practices, and thicknesses.<sup>3</sup> This should not be unexpected, since energy absorption is a function of (a) the strength of the steel, which controls the force required to deform the specimen, and (b) the ductility of the steel, which determines the distance through which the force acts prior to fracture of the specimen. Since loss of notch toughness is usually due to loss of ductility, a criterion that evaluates notch ductility instead of notch toughness (absorption energy) should be a better measure of the service properties of structural steels.

Various investigators, beginning with Gross and Stout, have proposed measuring the expansion that occurs on the compression side of the CVN specimen directly opposite the notch (that is, lateral expansion) or measuring the contraction that occurs at the root of the notch (lateral contraction). Gross and Stout's systematic study<sup>4</sup> of the variation in notch-ductility measurements with strength and chemical composition indicated that lateral expansion is a good measure of notch ductility over wide ranges of strengths and chemical compositions and led to further studies and interest in the method. In 1968, lateral expansion was included in the ASTM Standards (ASTM Methods and Definition for Mechanical Testing of Steel Products (A 370-68)) as a method of determining ductile-to-brittle transition temperatures. Because personnel at U. S. Steel Corporation research laboratories were among the first to measure and report lateral-expansion values on a routine basis, they aided in the preparation of the test method for lateral expansion described in the ASTM specification.

The present paper describes the device which was developed at U. S. Steel Corporation research laboratories to measure lateral expansion and which is shown in ASTM Method A 370-72 and gives the results of a test program conducted to determine the accuracy and reproducibility of lateral-expansion measurements. The testing program was conducted by using different measuring devices (gages) of the same general design and was performed by personnel at U. S. Steel Corporation research laboratories and at six U. S. Steel Corporation plants. For comparison, measurements were also made with micrometers by research personnel.

### The Lateral-Expansion Gage

Since lateral expansion is the expansion in width of the compression surface of a CVN impact specimen (dimension A in Fig. 1), a quick and

<sup>3</sup> Gross, J. H. in *Impact Testing of Metals*, ASTM STP 466, American Society for Testing and Materials, 1970, pp. 21-52.

<sup>4</sup> Gross, J. H. and Stout, R. D., *The Welding Journal*, Research Supplement, Vol. 37, No. 4, April 1958, pp. 151s-159s.

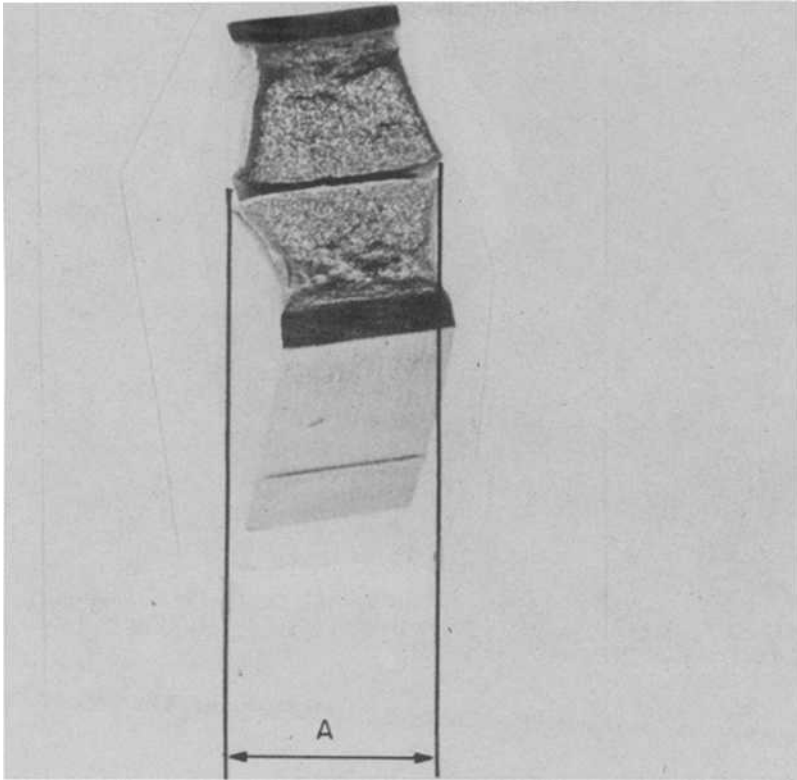


FIG. 1—Halves of broken Charpy V-notch impact specimen joined for the measurement of lateral expansion, dimension *A*.

accurate method for measuring this value is required. At first, regular micrometers were used. The width of the compression surface opposite the notch was measured prior to testing; after testing, the broken halves were fitted together, and this section was remeasured. The difference between the final measurement and the original measurement was the lateral expansion. Later, a trigger-actuated, spring-loaded dial indicator was substituted for the micrometers. Subsequently, the gage device described in the present paper was developed at U. S. Steel Corporation research laboratories for measuring lateral expansion. A photograph of the lateral-expansion gage is shown in Fig. 2, and working drawings of the gage are included in ASTM Method A 370-75a. Two companies are selling gages manufactured to these drawings.

As can be seen in Fig. 2, the device consists of a dial indicator with 0.001-in. (0.025-mm) dial divisions and a flat contact surface. The dial indicator is mounted on top of a stop which, in turn, is attached to a base

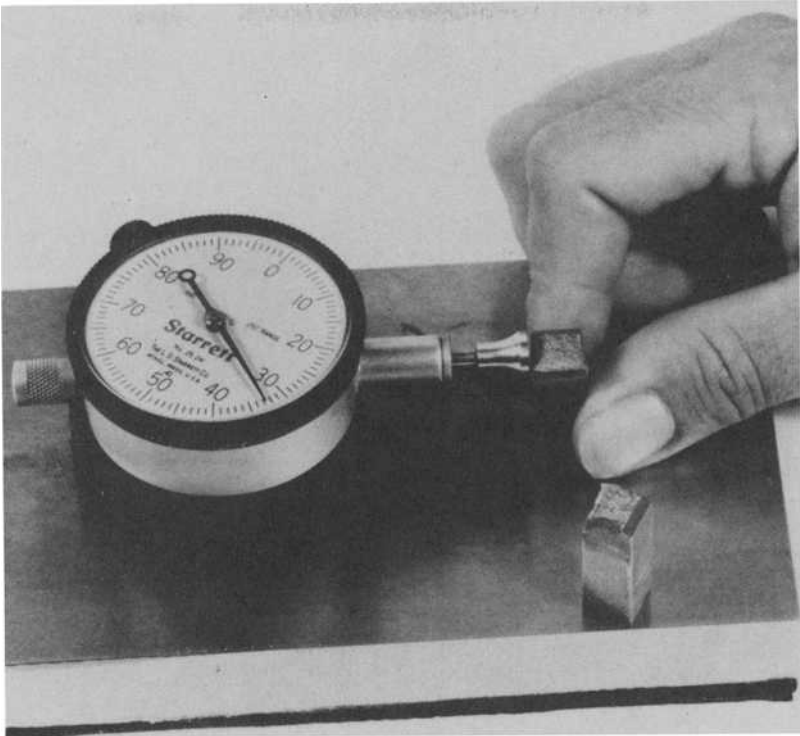


FIG. 2—Lateral-expansion gage for Charpy V-notch impact specimens.

plate. Before using the device, a flat surface is positioned against the stop, causing the contact surface of the dial indicator to move. The adjustable bezel of the indicator is then set to indicate zero, thus zeroing the gage. (It is essential that the plane of the contact surface be the same as that of the stop. This requirement can be checked by positioning a tested half specimen at several locations and measuring the lateral expansion, as described next. If the surfaces are coplanar, the readings will be identical.) When the protrusions of the broken specimen are pressed against the contact surface and the body of the specimen is pressed against the stop, the amount of protrusion is indicated directly on the dial indicator.

The lateral expansion that occurs during the fracturing of a CVN specimen is determined with the gage, as follows. Since expansion occurs on each side of the compression surface of both halves of the specimen, there are four protrusions to be measured, shown as *A*, *B*, *C*, and *D* in Fig. 3. Protrusions *A* and *B* form the expansion that occurs on one side of the specimen, and *C* and *D* form the expansion on the other side. Protrusions *A* and *B* are separately measured by first placing one of the specimen halves against the stop so that the protrusion causes the dial indicator to indicate

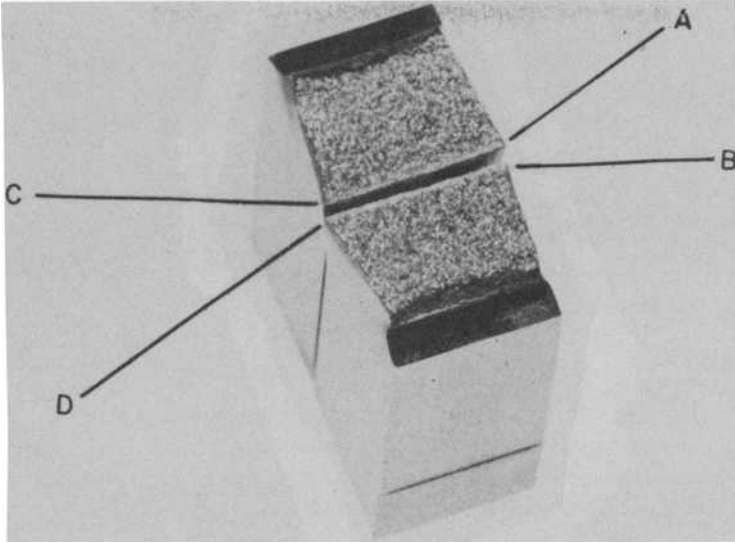


FIG. 3—Broken Charpy V-notch impact specimen showing protrusions on compression face.

a value, as shown in Fig. 2; the other half is then similarly measured. The process is repeated for the other pair of protrusions, *C* and *D*. The lateral expansion is the sum of the larger value measured for the first pair and the larger value measured for the second pair. With practice, both halves—one held in each hand—may be measured concurrently; the larger protrusion of each half is automatically determined, and the lateral expansion is the sum of these two measurements. Lateral expansion is usually expressed in mils (1 mil = 0.001 in. = 0.025 mm).

Before any measurements are made, the sides perpendicular to the notch must be checked to ensure that no burrs were formed during impact testing that might touch the contact surfaces of the stop. If such burrs exist, they must be removed (by rubbing on emery cloth, for example), making sure that the protrusions that are to be measured are not rubbed during the removal of the burr. The fracture surface of the specimen halves must be examined to ascertain that the protrusions were not damaged by contacting the testing-machine anvil or mounting surface during the impact test. If such damage exists to either half, the sample should not be measured, since this damage may cause erroneous readings.

## Materials and Experimental Work

### *Specimens Measured*

For this investigation, two sets of standard-size CVN specimens were machined for use as standard specimens. One set of specimens was machined

from a 1/2-in.-thick (12.7-mm) plate of ASTM A36 steel, and the other set was machined from a 1/2-in.-thick plate of USS "T-1" constructional alloy steel (ASTM A517 Grade F steel). These specimens are hereafter referred to as the A specimens and the T specimens, respectively. The chemical composition and tensile properties determined for these plates were typical for these two grades (Table 1). The CVN tests were performed on the specimens in accordance with ASTM Method A 370-72 over temperature ranges sufficient to develop complete transition-temperature curves (Table 1).

### *Reproducibility Tests at Research*

There are two major sources of errors in measuring lateral-expansion values: those attributable to the dial indicator, which affect accuracy; and those attributable to the operator, which affect reproducibility. Two studies were made at U. S. Steel Corporation research laboratories to isolate these sources of errors, as described next.

A total of five lateral-expansion gages was used to obtain 40 sets of readings on each of the two sets of specimens. Three gages were equipped with the standard dial indicator with 0.001-in. (0.025-mm) divisions, the fourth gage was equipped with a dial indicator with 0.0005-in. (0.013-mm) divisions, and the fifth gage was equipped with a dial indicator with 0.0001-in. (0.0025-mm) divisions. These gages are hereafter referred to as the standard, the 1/2-mil, and the 1/10-mil gages, respectively. The reason for using the special gages is that the error allowed in dial indicators manufactured to the American Gage Design (AGD) specifications is  $\pm 1$  dial division over the full measuring range of the indicator except for the 1/10-mil indicator, for which the allowed error is  $\pm 1$  division for the first 2 1/2 revolutions and  $\pm 3$  divisions thereafter. Since lateral-expansion measurements involve two measurements to determine a single value, the error in any value reported could be as much as twice that allowed—that is, 2 mils for the standard gage, 1 mil for the 1/2-mil gage, 0.2 mil for the 1/10-mil gage in its initial range, and 0.6 mil for the 1/10-mil gage in the remaining portion. The error in any dial indicator is believed by the manufacturers to be generally repeatable.

The error due to the operator was investigated by having technicians measure the two sets of specimens a minimum of seven times on the five aforementioned gages. Fourteen research technicians and five technicians at the various plants made a total of 45 sets of measurements with the five research gages. The technicians were classified as experienced if they had made lateral-expansions measurements on a regular basis during the past year; semiexperienced if they had made this measurement on a regular basis, but not within the past year; and inexperienced if they had not made this measurement before this study. The technicians were not told how

TABLE 1—Composition and mechanical properties of materials tested.

Chemical Composition—%																						
Steel	Analysis	Specimen Code	C	Mn	P	S	Si	Cu	Cr	Mo	V	B	Ni									
ASTM A36	Check	A	0.24	1.19	0.009	0.034	0.040	ND <sup>a</sup>	ND	ND	ND	ND	ND									
USS "T-1"	Ladle	T	0.17	0.88	0.011	0.016	0.22	0.28	0.52	0.45	0.04	0.003	0.84									
(ASTM A517 Grade F)																						
Tensile Properties (Average of Two Tests)																						
Specimen Code	Yield Point, ksi		Yield Strength (0.2% Offset), ksi		Tensile Strength, ksi		Elongation, % in 2 in.		Reduction of Area, %													
	Upper	Lower	Lower	Upper	Lower	Upper	Lower	Upper	Lower	Upper												
A	47.2	44.0	ND	ND	78.0	78.0	30.5	30.5	66.9	66.9												
T	ND	ND	114.0	114.0	124.0	124.0	18.8	18.8	66.2	66.2												
Charpy V-Notch Properties																						
A Specimens																						
1	3	4	5	6	7	8	9	10	11	12	13	14	15	17	18	19	20	21	22	23	24	
Temperature, °F	200	50	200	75	50	0	125	75	100	175	-25	25	-50	150	0	-25	25	175	125	100	-50	150
Ft · lb	91	46	91	80	39	11	74	81	54	87	9	30	6	95	16	11	13	106	100	76	6.5	106
Shear, %	100	45	100	70	45	20	85	65	65	98	15	30	10	95	20	15	30	100	95	65	10	100
T Specimens																						
1	2	3	4	7	9	10	12	13	14	15	16	17	18	19	20	21	22	23	24			
Temperature, °F	25	-75	-100	75	-50	75	125	0	125	-100	-25	-75	-50	50	-25	125	0	-100	75	50		
Ft · lb	46	16.5	13	52	23	55	54	34	54	11	26	16.5	21	45	34	42	41	13	52	48		
Shear, %	85 <sup>b</sup>	30	20	100	40	100	100	65	100	25	50	30	40	85	55	75	70	30	100	90		

NOTE—Conversion factors are: 1 ksi = 6.895 MN/m<sup>2</sup>; 1 in. = 25.4 mm; C = 5/9 (F - 32); and 1 ft · lb = 1.36 J.

<sup>a</sup> ND = not determined.

<sup>b</sup> Specimen fissured upon testing; shear value difficult to rate.

their readings corresponded with those of other technicians until after they had measured all the specimens.

Since technicians with varying amounts of prior experience made the same measurements with the same gages, a measure of the skill level required to obtain valid lateral-expansion measurements was obtained.

#### *Other Measurements at Research*

In addition to the measurements made with the lateral-expansion gages, three of the technicians measured the lateral expansion by using hand-held micrometers, and two machinists measured the expansion by using a shadowgraph. For the micrometer measurements, the specimens were firmly clamped in a steel-faced bench-style vise, and a standard outside-micrometer caliper, with a ratchet stop and 0.001-in. divisions, was used. The maximum error permitted for this type of micrometer is 0.0001 in. (1/10 mil) over its entire travel of 1 in. (25.4 mm); according to the manufacturer, the error is approximately proportional to the travel and generally about one half of the permitted error. For the shadowgraph measurements, the specimens halves were individually placed against a stop on a contour-measuring projector, and the length of the shadow (at  $\times 50$  magnification) of the protrusions was measured by using the 0.0001-in.-division micrometer of the projector.

#### *Reproducibility Tests at the Plants*

The primary purpose of the measurements made within U. S. Steel Corporation plants was to ascertain that plant personnel could obtain results that agreed with those obtained by research personnel within an allowable experimental error. To accomplish this, the standard CVN specimens were taken to five plants that customarily make lateral-expansion measurements and to one plant that expects to be required to make these measurements in the near future. Plant 1 uses a gage of their own design that is completely different from the gage described here. Two plants, Plants 3 and 6, use gages that they made from the original research drawings. Plants 2 and 5 have purchased gages made commercially from the research drawings by an outside source. Plant 4 did not have a gage at the time of these tests and used a research gage. At facilities where more than one technician made the readings, the technicians were not told how their readings corresponded with those obtained by others until after they had measured all the specimens. At Plant 1, one complete set of measurements was made by four experienced technicians, each of whom measured approximately one quarter of the specimens. At Plant 4, two technicians, both of whom were inexperienced, measured the specimens as a joint effort.

## Results and Discussion

### *Reproducibility Tests at Research*

The results of the individual lateral-expansion measurements made with the five different gages by research personnel are shown in Table 2 for the A specimens and in Table 3 for the T specimens. The tables also show, for each specimen, the value that was obtained most often by the individual gages (or the average if two or more values were obtained equally often)<sup>5</sup>; this value is hereafter referred to as the best value. The best values obtained with the various gages are summarized in Table 4.

The 1/10-mil gage was positioned on the stop so that approximately 3 mils of travel were required to zero the gage; thus, according to the AGD specifications, expansion values of approximately 44 mils or less can be accurately measured to  $\pm 0.2$  mil (twice the tolerance and the range), and expansion values greater than approximately 44 mils can be accurately measured to  $\pm 0.6$  mil. The 1/2-mil gage is accurate to  $\pm 1.0$  mil over its entire range, and the standard (1-mil) gages are accurate to  $\pm 2.0$  mils over their entire ranges.

Because of the greater accuracy and reproducibility of the 1/10-mil gage, the best values obtained by using this gage are hereafter considered to be the most nearly correct values. The 1/10-mil best values were subtracted from the best values obtained by use of the other gages, and the resulting differences are given in Table 5. As can be seen, the extremes in the amount of the difference for the individual gages were approximately twice the AGD specification for allowable error of the dial indicators; for the reasons discussed previously, these differences are not unreasonable. The manufacturers' contention that errors in dial indicators tend to be reproducible and generally consistent was also borne out; that is, the range of the amount of difference was also usually about 2 dial divisions. Thus, the accuracy of measuring lateral expansion appears to be about  $\pm 2$  dial divisions or  $\pm 2$  mils when the standard gage is used.

The difference between the highest value and lowest value measured for each specimen by each gage was also determined. These differences are shown in Table 6; the frequency with which these difference values occur is shown at the bottom of the table. From Table 6, it can be seen that the amount of scatter in the values obtained for the individual specimens is dependent on whether the 1/10-mil, the 1/2-mil, or the standard (1-mil) gage is used. The frequency tabulation indicates that the reproducibility (that is, the likelihood of the same successive readings) is dependent on the sensitivity of the dial indicator. It should be kept in mind that this difference value is highly dependent on the existence of extreme values. For example,

<sup>5</sup> This averaging technique was not followed in several instances—for example, for Specimen T-23 measured with the 1/10-mil gage, and for several of the micrometer readings.

TABLE 2—Summary of lateral-expansion values (in mils) measured at research for specimens as ASTM A36 steel (A specimens).

Technician Code	Degree of Experience	Specimen Number																							
		1	2	3	4	5	6	7	8	9	10	11	12	13	14	15	17	18	19	20	21	22	23	24	
		1/10-MIL GAGE—GAGE No. 5																							
A	E <sup>a</sup>	67.9	42.9	67.5	65.8	37.5	12.1	62.5	65.8	46.5	69.1	6.7	29.4	5.7	71.0	17.3	9.1	14.3	78.1	77.3	64.0	4.4	76.7		
B	E	68.2	42.5	67.7	65.9	38.0	12.2	62.3	65.9	46.7	68.2	7.1	28.7	5.4	70.9	17.3	9.4	14.4	78.4	77.0	63.9	4.6	76.8		
P	E	67.25	43.3	67.7	66.1	37.9	12.4	62.2	65.5	46.8	69.0	7.0	28.8	5.8	70.8	17.3	9.3	14.2	78.1	77.2	63.9	4.4	77.0		
G	E	67.9	42.9	67.4	65.8	37.5	12.0	62.4	65.6	46.4	68.8	6.7	29.4	5.8	71.0	17.3	9.1	14.3	78.0	77.2	64.1	4.4	76.8		
H	E	67.9	42.8	67.5	65.8	37.7	12.1	62.6	65.8	46.5	68.8	6.7	29.6	5.7	71.1	17.3	9.3	14.2	78.1	77.3	63.9	4.4	76.8		
K	E	67.8	42.8	67.4	65.7	37.6	12.0	62.5	65.6	46.5	68.7	6.7	29.4	5.7	71.1	17.2	9.2	14.1	78.2	77.3	64.0	4.5	76.7		
I	E	67.9	42.8	67.4	65.8	37.3	12.0	62.3	65.8	46.5	68.7	6.7	29.4	5.8	71.1	17.3	9.2	14.0	78.1	77.3	63.9	4.6	76.8		
J	S	68.0	43.0	67.2	65.8	37.8	12.1	62.6	65.4	46.5	68.8	6.8	29.4	5.8	70.9	17.3	9.3	14.2	77.9	77.3	64.0	4.4	76.6		
Best value		67.9	42.8	67.4	65.8	37.5	12.05	62.55	65.8	46.5	68.8	6.7	29.4	5.8	71.1	17.3	9.3	14.2	78.1	77.3	63.9	4.4	76.8		
		1/2-MIL GAGE—GAGE No. 4																							
A	E	68.5	43	68.5	67	38	12	63	67	47	69.5	7	30	6	72	17.5	9.5	15	79	78	64.5	5	77.5		
B	E	68.5	43	68.5	66.5	37.5	12.5	63.5	67	47	69	7	28.5	5	70.5	17.5	9.5	14	79	78	65.5	5	77.5		
H	E	68.5	43	68	66.5	37.5	12	63	66	46.5	69.5	7	29	6	71.5	17	9	14	78.5	77.5	64.5	4.5	77		
I	E	68.5	43	68	67	38	12.5	63	66.5	47	69.5	7	29.5	6.5	71.5	17.5	10.5	14.5	78.5	76.5	65	5	77.5		
K	E	68.25	43	67.75	66.25	37.5	12	62.75	67	46.75	69	7	29.25	6	71.25	17.25	9.5	14.25	78.5	77.5	64.5	4.5	77.25		
P	E	68	42.5	67.5	66	37	11.5	62.5	66	46	69	6.5	29	5	71	17	9	14	78	77	64	4.5	76.5		
Best value		68.5	43	68	67	38	12.5	63.5	66.5	47	69.5	6.5	30	6.5	71.5	17.5	9.5	14.5	78.5	78	64.5	5	77.5		
		STANDARD GAGE—GAGE No. 1																							
A	E	68	43	67	66	38	13.5	63	67	46	68.5	8	30	6	70	18	10	15	78	77	63.5	5.5	76.5		
D	E	67	42	67	65	38	13	62	65	46	68	8	30	5.5	69	17	9.5	14	77	74	62	4.5	75		
F	E	68	43	67	66	37	13.5	63	67	46.5	69	8	29	6.5	70	18	10.5	15	78	77	64	5.5	76		
P	E	68	43	67.5	65.5	38.5	13	63.5	66.5	46.5	69	8	30	7	70.5	17.5	10	15	78	76.5	64	5	75.5		
R	I	67	43	67	66.5	38	13	62	66	46	69	8	30	6	68.5	18	10	15	78	77	63	4.5	75.5		
A	E	67	42	66	65	37	12	62	65	46	68	6.5	29	6	70	17	9	13	77	76	63.5	4.5	76		
B	E	66	42	65	64	36	12	61	65	46	66	6.5	28	6	69	16	9	13	76	76	63	4	74		
I	E	68	42	67	65.5	37	12	62	65.5	46	68.5	7.5	29.5	6	70	16.5	9	14	78	76	64	5	76		
J	E	67	41.5	66.5	65	36	12.5	61	65	45.5	68	6	28.5	5	70	15.5	9	13	76.5	76	63	4.5	75		
Best value		67.5	42.5	67	65	37.5	12.5	62	65	46	68.5	8	30	6	70	18	9	15	78	76	63.5	4.5	76		

STANDARD GAGE—GAGE No. 2

A	E	67.5	42	67	65	36.5	11	62	65	46	68	5.5	28	4.5	70	16	8	13	77	76	63	3	77
B	E	67	41	67	64	37	11	61	65	46	67	6	28	4	70	16	9	13	77	76	63	4	76
I	E	66.5	42	66.5	65	36.5	10.5	61	65	45	67.5	5.5	28	4	70	15.5	7	13	77	76	62.5	3.5	75.5
M	I	67	41.5	66.5	65	37	10.5	61	65	45	67.5	5	28	4	70.5	15.5	7.5	13	76.5	74	62	2.5	74.5
P	E	66.5	41.5	66.5	65	37	11	62.5	65	45	67.5	5	28	5	70.5	16	8	13	77	74.5	62.5	3	75.5
H	E	66.5	41	66.5	65	36.5	10.5	61	65	45	67	5.5	28	3.5	70	15.5	7	13	77	75	62.5	3	75.5
B	E	67	41	66	64	36	10	61	63	45	67	5	28	3.5	70	15.5	7	13	77	76	62	3	75
E	E	67	41	67	65	36	10	61	63.5	44	66	5.5	28	4	69	16	7	13	76	75	62	3.5	77
Best value		67	41	66.5	65	36.75	10.75	61	65	45	67.25	5.5	28	4	70	15.75	7	13	77	76	62.25	3	75.5

STANDARD GAGE—GAGE No. 3

I	E	68.5	44	68.5	67	39	13.5	64	68	47	70	8	31	6	72	18	10	15	79	78	64.5	5	77.5
A	E	70	44	69	68	40	14	65	69	48	70	8	31	7	72	18.5	11	16	80	79	65	5.5	78.5
J	S	69	44	68.5	67.5	39	13.5	64	67	47	70	7	30.5	6	72.5	18.5	10	15.5	80	79	65	5	78
D	E	69	44	68	67	38	12	63	67	47	70	7	30	5	72	17	10	14	79	78	65	4.5	77.5
C	I	68.5	43.5	68.5	67	38	12.5	63	67	47.5	70	7.5	30	5.5	72.5	17.5	10	14	79	78	65	4.5	77.5
A	E	69	43.5	68	67	38	12	63	67	47	70	7	30	6	72	17.5	9	14	79	78	65	4.5	77.5
B	E	69	43	69	66	38	12	63	67	48	69	6	30	5	72	17	9	14	80	78	65	3	78
I	E	68	42.5	67.5	66	37.5	11.5	63	66	46	69	6	29.5	5	70.5	16.5	8.5	13.5	78	77	63.5	4	76.5
Best value		69	44	68.5	67	38	12	63	67	47	70	7	30	5.5	72	17.25	10	14	79	78	65	4.5	77.5

MICROMETERS

A	E	66.5	42.5	66.5	68	39.5	13.5	63.5	67	47	70	8	31	6	72	18	11	15.5	76.5	79	64	5	77
J	S	69	42.5	67	66.5	38	13	62.5	65	47	69.5	7	30	6	71	18.5	9.5	14.5	78	76	64	4.5	77
D	E	70.5	42.5	67.5	70	38.5	12.5	62.5	66	47	70	8	30	6	71	17.5	10	14	77.5	78	64	4	77
Best value		69.75 <sup>b</sup>	42.5	67 <sup>b</sup>	67.25 <sup>b</sup>	38.25 <sup>b</sup>	13 <sup>b</sup>	62.5	66 <sup>b</sup>	47	70	8	30	6	71	18 <sup>b</sup>	9.75 <sup>b</sup>	14.25 <sup>b</sup>	77.75 <sup>b</sup>	78.5 <sup>b</sup>	64	4.5 <sup>b</sup>	77

NOTE—1 mil = 0.025 mm.

<sup>a</sup> E, S, and I stand for experienced, semiexperienced, and inexperienced, respectively.

<sup>b</sup> See text.

TABLE 3—Summary of lateral-expansion values (in mils) measured at research for specimens of USS "T-1" steel (ASTM A517 Grade F) (T specimens).

Technician	Degree of Expert-ence	Specimen Number																					
		1	2	3	4	7	9	10	12	13	14	15	16	17	18	19	20	21	22	23	24		
1/10-MIL GAGE—GAGE No. 5																							
A	E <sup>a</sup>	34.2	10.7	7.6	40.1	15.7	42.8	45.9	24.5	45.2	6.1	19.0	10.2	13.9	35.5	24.0	32.0	30.9	5.5	39.6	37.5		
B	E	34.1	10.8	7.5	40.5	16.0	43.1	46.4	25.1	45.4	6.0	19.0	10.4	13.9	35.9	24.3	32.2	31.5	5.7	39.5	38.0		
P	E	34.0	10.7	7.5	40.5	15.6	42.6	45.9	24.6	44.8	6.0	18.8	10.0	13.8	35.3	23.6	31.8	30.9	5.6	39.4	37.7		
G	E	34.3	10.9	7.6	40.1	15.7	42.9	45.8	24.4	45.0	6.2	19.0	10.1	14.0	35.5	23.8	31.9	31.1	5.5	39.4	37.6		
H	E	34.2	10.7	7.7	40.3	15.7	42.7	46.0	24.5	45.2	6.2	19.0	10.2	13.9	35.5	24.0	32.0	31.1	5.6	39.5	37.6		
K	E	34.1	10.7	7.5	40.2	15.6	42.8	45.4	24.5	44.4	6.2	18.9	10.1	14.0	35.4	24.0	30.9	30.9	5.6	38.8	37.5		
I	E	34.2	10.7	7.6	40.2	15.7	42.7	45.5	24.4	44.2	5.9	18.9	10.1	13.9	35.7	24.1	32.0	30.7	5.7	39.0	37.6		
J	S	34.0	10.8	7.7	40.2	15.7	42.8	45.4	24.4	44.3	6.2	19.0	10.1	13.9	35.5	24.0	31.8	31.0	5.6	38.8	37.5		
Best value		34.2	10.7	7.55	40.15	15.7	42.8	45.9 <sup>b</sup>	24.45	45.2	6.2	19.0	10.1	13.9	35.5	24.0	32.0	30.9	5.6	39.45	37.55		
1/2-MIL GAGE—GAGE No. 4																							
A	E	34.5	11	8	40.5	16	43	46.5	25	46	7	19	10.5	14	35.5	24.5	32.5	31	6	39.5	37.5		
B	E	34.5	11	8	40.5	15.5	43	46.5	25	46.5	7	19	10.5	13.5	35	25	33	31	6	39	37		
E	E	34	10	7	40	15.5	42.5	46	24	45.5	6	17	10	13.5	35	23.5	31.5	31	5.5	40	37.5		
H	E	34.5	11	8	40.5	16	43	46.5	25	46	7	19	10.5	14	36	24.5	32	31	6	40	38		
I	E	34	11	7.75	40	15.75	42.75	46.25	24.75	45.25	6	19	10.25	13.75	35.25	24	32	31	5.5	39.5	37.25		
K	E	33.5	10	7	39.5	15	42.5	45.5	24	45	6	18.5	10	13.5	35	24	31.5	30.5	5.5	39	37		
P	E	34.5	11	8	40.5	16	43	46.5	25.5	45.5	7	19.5	10.5	14.5	35.5	24.5	32	31.5	6	40	38		
Best value		34.5	11	8	40.5	16	43	46.5	25	45.75	7	19	10.5	13.5	35	24.5	32	31	6	40	37.25		
STANDARD GAGE—GAGE No. 1																							
A	E	34	11	8.5	40.5	16	43	46.5	25	45	7	19	10.5	14	35.5	25	32	31	6.5	40	38		
D	E	33	11	7.5	39	15.5	42	45	24.5	45	6	18	10.5	13	34	23.5	31.5	28	5.5	38	36		
F	E	35	11	8	41	16	44	47	26	47	7	20	11	14	37	26	34	31	6	39.5	38		
P	E	34	11.5	8	40.5	15.5	42.5	45.5	25	46	6.5	19.5	10.5	14	35.5	25	33	31	6	39.5	38		
R	I	33.5	12	8	40	17	44	47	26	47	7	20	11	14	37	26	34	30.5	6	39.5	37.5		
A	E	33.5	11	8	39	15.5	42.5	45.5	24.5	45	7	19	11	14	35	24	31	30.5	6	39.5	36.5		
B	E	33	11	8	39	15	41	45	24	45	6	18	11	13	34	23	31	29	5	38	36		
I	E	33.5	10.5	8	40	16	42.5	46	25	45	6.5	19	11	14	35	24	32	30	5.5	39	37		
J	E	33	9.5	7	39.5	15	42	45	24.5	44	5.5	18.5	9.5	13	34	23.5	31	30	5	39	36.5		
Best value		33.25	11	8	39	15.75	42.5	45	25	45	6.25	19	10.5	14	35	24	32	30.5	6	39.5	36		

STANDARD GAGE—GAGE No. 2

A	E 33	9	6	39	14.5	41.5	45	22.5	44.5	5	18	9	13	34.5	23	31	30	4.5	38.5	36.5
B	E 32	9	7	38	15	42	45	23	43	5	17	9	13	33	22	31	29	4	38	36
I	E 33	9	5.5	39	14	41.5	45	22.5	43.5	4.5	17	8.5	12.5	34	22	31	30	3	38	36
M	I 33	9	5.5	37	14	41	43.5	22.5	43.5	4.5	17	8.5	12	33.5	22.5	30.5	29.5	3.5	38	36.5
P	E 33	9	6	39	14.5	41.5	45	22.5 <sup>a</sup>	43.5	4.5	17.5	8.5	12	34	22.5	31	29.5 <sup>a</sup>	4	38	36
H	E 33-	9	6-	39	14	41	44.5	22.5	43 <sup>+</sup>	4.5	17	8.5	12 <sup>+</sup>	34	22	30	29	4-	37.5	36.5
B	E 32	9	5	39	14	42	43	22	42	5	17	8.5	11.5	33	22	30.5	28	3.5	37	36
B	E 33	9	6.5	39	14	41	44	22.5	43	5	17	9	12.5	33	22.5	30.5	29.5	4	37	36
Best value	E 33	9	6	39	14	41.25	45	22.5	43.25	4.75	17	8.5	12	33.5	22	31	29.5	4	38	36

STANDARD GAGE—GAGE No. 3

I	E 35	11.5	8	41.5	16.5	44	47	26	46.5	6.5	20	10.5	14.5	37	25.5	33	32	5.5	40.5	38.5
A	E 35	12	8.5	41.5	17	...	...	26	...	...	20.5	11	15	37	26.5	34	32	6.5	41	39.5
J	S 35	11.5	8.5	41.5	17	44	47.5	26	46.5	6.5	20	10.5	13.5	36.5	26	34	32	5.5	40.5	39
D	E 35	11	8	41	16	44	47	25.5	46	7	19	11	14	36.5	24	33	31.5	5	40	38
C	I 34	11	8	41	16	43.5	47	25.5	47	6	19	11	14.5	36.5	24.5	33	32	5.5	40.5	38
A	E 35	11	8	41	16	43	47	25	45.5	6.5	19.5	10.5	14	36.5	24.5	33	32	5.5	40.5	38
B	E 32	11	6	41	15	44	46	25	46	6	19	10	13	36	23	32	31	...	40	38
I	E 34	10	7	39.5	15	42.5	45.5	24.5	45	5.5	18.5	10	13.5	35.5	23.5	32	30.5	5	39.5	38
Best value	E 35	11	8	41	16	44	47	26	46.25	6.5	19	10.75	14	36.5	24.5	33	32	5.5	40.5	38

MICROMETERS

A	E	34.5	12	9	41	16	43.5	45	26	44	6	19	11	14	36	25	30	30	6.5	40	36
J	S	34.5	11	7.5	40.5	16.5	43	46.5	25	46	5.5	19.5	10	14.5	35.5	24.5	32.5	31	5.5	40.5	37
D	E	34.5	11	8	41	16.5	43	47	26	46	5.5	19	11	14	36	24	34	30	5.5	40	38
Best value	E	34.5	11	7.75 <sup>b</sup>	41	16.5	43	46.75 <sup>b</sup>	26	46	5.5	19	11	14	36	24.5 <sup>b</sup>	33.25 <sup>b</sup>	30	5.5	40	37 <sup>b</sup>

NOTE—1 mil = 0.025 mm.

<sup>a</sup> E, S, and I stand for experienced, semiexperienced, and inexperienced, respectively.

<sup>b</sup> See text.

TABLE 4—Summary of best values (in mils) obtained at research.

Gage Used	Specimen Number																							
	1	2	3	4	5	6	7	8	9	10	11	12	13	14	15	16	17	18	19	20	21	22	23	24
A SPECIMENS																								
1/10-mil gage, Gage 5	67.9	...	42.8	67.4	65.8	37.5	12.05	62.55	65.8	46.5	68.8	6.7	29.4	5.8	71.1	...	17.3	9.3	14.2	78.1	77.3	63.9	4.4	76.8
1/2-mil gage, Gage 4	68.5	...	43	68	67	37.75	12.25	63	67	47	69.5	7	29.5	6	71.5	...	17.5	9.5	14	78.5	78	64.5	5	77.5
Standard (1- mil) gage, Gage 1	67.5	...	42.5	67	65	37.5	12.5	62	65	46	68.5	8	30	6	70	...	18	9	15	78	76	63.5	4.5	76
Standard (1- mil) gage, Gage 2	67	...	41	66.5	65	36.75	10.75	61	65	45	67.25	5.5	28	4	70	...	15.75	7	13	77	76	62.25	3	75.5
Standard (1- mil) gage, Gage 3	69	...	44	68.5	67	38	12	63	67	47	70	7	30	5.5	72	...	17.25	10	14	79	78	65	4.5	77.5
Micrometers	69.75 <sup>a</sup>	...	42.5	67 <sup>a</sup>	67.25 <sup>a</sup>	38.25 <sup>a</sup>	13 <sup>a</sup>	62.5	66 <sup>a</sup>	47	70	8	30	6	71	...	18 <sup>a</sup>	9.75 <sup>a</sup>	14.25 <sup>a</sup>	77.75 <sup>a</sup>	78.5 <sup>a</sup>	64	4.5 <sup>a</sup>	77

T SPECIMENS

1/10-mil gage, Gage 5	34.2	10.7	7.55	40.15	...	15.7	...	42.8	45.9	...	24.45	45.2	6.2	19.0	10.1	13.9	35.5	24.0	32.0	30.9	5.6	39.45	37.55
1/2-mil gage, Gage 4	34.5	11	8	40.5	...	16	...	43	46.5	...	25	45.75	7	19	10.5	13.5	35	24.5	32	31	6	40	37.25
Standard (1- mil) gage, Gage 1	33.25	11	8	39	...	15.75	...	42.5	45	...	25	45	6.25	19	10.5	14	35	24	32	30.5	6	39.5	36
Standard (1- mil) gage, Gage 2	33	9	6	39	...	14	...	41.25	45	...	22.5	43.25	4.75	17	8.5	12	33.5	22	31	29.5	4	38	36
Standard (1- mil) gage, Gage 3	35	11	8	41	...	16	...	44	47	...	26	46.25	6.5	19	10.75	14	36.5	24.5	33	32	5.5	40.5	38
Micrometers	34.5	11	7.75 <sup>a</sup>	41	...	16.5	...	43	46.75 <sup>a</sup>	...	26	46	5.5	19	11	14	36	24.5 <sup>a</sup>	33.25	30	5.5	40	37 <sup>a</sup>

NOTE—1 mil = 0.024 mm.

<sup>a</sup> See text.

TABLE 5—Difference between best value obtained at research for various gages and best value obtained for 1/10-mil gage.<sup>a</sup>

Specimen No.	A Specimens					T Specimens					
	Best Value for 1/10-Mil Gage	Difference Between Best Values				Best Value for 1/10-Mil Gage	Mi-crometers	Difference Between Best Values			Mi-crometers
		4 <sup>b</sup>	1 <sup>c</sup>	2 <sup>c</sup>	3 <sup>c</sup>			4 <sup>b</sup>	1 <sup>c</sup>	2 <sup>c</sup>	
1	67.9	0.6	-0.4	-0.9	1.1	1.85	0.3	-0.95	-1.2	0.8	0.3
2	...	...	...	...	...	...	0.3	0.3	-1.7	0.3	0.3
3	42.8	0.2	-0.3	-1.8	1.2	-0.3	0.45	0.45	-1.55	0.45	0.2
4	67.4	0.6	-0.4	-0.9	1.1	-0.4	0.35	-1.15	-1.15	0.85	0.85
5	65.8	1.2	-0.8	-0.8	1.2	-1.45	...	...	...	...	...
6	37.5	0.25	0.0	-0.8	0.5	0.75	...	...	...	...	...
7	12.05	0.2	0.45	-1.3	-0.05	0.95	0.3	0.05	-1.7	0.3	0.8
8	62.55	0.5	-0.5	-1.6	0.6	-0.05	...	...	...	...	...
9	65.8	1.2	-0.8	-0.8	1.2	0.2	0.2	-0.3	-1.6	1.2	0.2
10	46.5	0.5	-0.5	-1.5	0.5	0.5	0.6	-0.9	-0.9	1.2	0.85
11	68.8	0.7	-0.3	-1.6	1.2	1.2	...	...	...	...	...
12	6.7	0.3	1.3	-1.2	0.3	1.3	0.55	0.55	-1.95	1.55	1.55

13	29.4	0.1	0.6	-1.4	0.6	0.6	45.2	0.55	0.2	-1.95	0.95	0.8
14	5.8	0.2	0.2	-1.8	-0.3	0.2	6.2	0.8	0.05	-1.55	0.3	-0.7
15	71.1	0.4	-1.1	-1.1	0.9	-0.1	19.0	0.0	0.0	-2.0	0.0	0.0
16	...	...	...	...	...	...	10.1	0.4	0.4	-1.6	0.65	0.9
17	17.3	0.2	0.7	-1.6	-0.05	0.7	13.9	-0.4	0.1	-1.9	0.1	0.1
18	9.3	0.2	-0.3	-2.3	0.7	0.45	35.5	-0.5	-0.5	-2.0	1.0	0.5
19	14.2	-0.2	0.8	-1.2	-0.2	0.05	24.0	-0.5	0.0	-2.0	0.5	0.5
20	78.1	0.4	0.1	-1.1	0.9	-0.35	32.0	0.0	0.0	-1.0	1.0	1.25
21	77.3	0.7	-1.3	-1.3	0.7	1.2	30.9	0.1	-0.4	-1.4	1.1	-0.9
22	63.9	0.6	-0.4	-1.7	1.1	0.1	5.6	0.4	0.4	-1.6	-0.1	-0.1
23	4.4	0.6	-0.1	-1.4	0.1	0.1	39.45	0.55	0.05	-1.45	1.05	0.55
24	76.8	0.7	-0.8	-1.3	0.7	0.2	37.55	-0.3	-1.55	-1.55	0.45	-0.55
Extreme difference		-0.2	-1.3	-2.3	-0.3	-0.4		-0.5	-1.55	-2.0	-0.1	-0.9
		+1.2	+1.3	-0.8	+1.2	+1.85		+0.8	+0.55	-0.9	+1.55	+1.55
Range of difference:		1.4	2.6	1.5	1.5	2.25		1.3	2.10	1.1	1.65	2.45

NOTE—1 mil = 0.025 mm.

<sup>a</sup> All values are given in mils.

<sup>b</sup> 1/2-mil gage.

<sup>c</sup> Standard 1-mil gages.

TABLE 6—Difference<sup>a</sup> between highest value and lowest value measured at research.

Specimen No.	A Specimens					T Specimens					Mi-crometers
	Gage No. <sup>b</sup>					Gage No. <sup>b</sup>					
	5	4	1	2	3	5	4	1	2	3	
1	1.0	0.5	2	1	2	0.3	1	2	1	3	0
2	...	...	...	...	...	0.2	1	2.5	0	2	1
3	0.8	1	1.5	1	1.5	0.2	1	1.5	2	2.5	1.5
4	0.5	1	2.5	1	1.5	0.4	1	2	2	2	0.5
5	0.4	1	2.5	1	2	...	...	...	...	...	...
6	0.7	1	2.5	1	2.5	...	...	...	...	...	...
7	0.4	1	1.5	1	2.5	0.4	1	2	1	2	0.5
8	0.4	1	2.5	1.5	2	...	...	...	...	...	...
9	0.5	1	2	2	3	0.5	0.5	1.5	1	1.5	0.5
10	0.4	1	1	2	2	1.0	1	1	2	2	2
11	0.9	0.5	3	2	1	...	...	...	...	...	...
12	0.4	0.5	2	1	2	0.6	1.5	1	1	1.5	1
13	0.9	1.5	2	0	1.5	1.2	1.5	1	2.5	2	2
14	0.4	1.5	2	1.5	2	0.3	1	1.5	0.5	1.5	0.5
15	0.3	1.5	2	1.5	2	0.2	2.5	2	1	2	0.5
16	...	...	...	...	...	0.4	0.5	1.5	0.5	1	1
17	0.2	0.5	2.5	0.5	2	0.2	1	1	1.5	2	0.5
18	0.3	1.5	1.5	2	2.5	0.6	1	1.5	1.5	1.5	0.5
19	0.4	1	2	0	2.5	0.7	1.5	2.5	1	3.5	1
20	0.5	1	2	1	2	0.4	1.5	2	1	2	4
21	0.3	1.5	3	2	2	0.8	1	3	2	1.5	1
22	0.2	1.5	2	1	1.5	0.2	0.5	1.5	1.5	1.5	1
23	0.2	0.5	1.5	1.5	2.5	0.8	1	2	1.5	1.5	0.5
24	0.4	1	2.5	2.5	2	0.5	1	2	0.5	1.5	2



Technician B, using the 1/10-mil gage, read specimen A-11 (Table 2) considerably lower than any of the other seven people. If this one value was eliminated, the difference between the highest and lowest value for this specimen (with the 1/10-mil gage) would be 0.4 rather than 0.9 mil. Thus, the reproducibility of measuring lateral expansion appears to be about  $\pm 2$  dial divisions or  $\pm 2$  mils when the standard gage is used. Since the values obtained by Technicians C, M, and R, who were inexperienced, were similar to those obtained by experienced technicians, prior experience with this gage does not appear to be a factor in obtaining reproducible results.

#### *Other Measurements at Research*

The values obtained by use of micrometers are also given in Tables 2-6. Best values were derived as before except when three different values were obtained for the same specimen; in the latter instance, the best value is the average of the two most similar readings and is noted with an asterisk. Note in Table 5 that the range of difference between the micrometer best value and the best values for the 1/10-mil gage was greater than corresponding range of difference obtained with each of the expansion gages. The greater range of difference for the micrometer readings is probably due to the difficulty of ensuring that the micrometer did not twist during the measurement.

The readings obtained with the shadowgraph were quite erratic and hence are not tabulated. In using the shadowgraph, it was difficult to obtain a zero reading and to adjust the shadow to maximum sharpness.

#### *Reproducibility Tests at the Plants*

The results of the lateral-expansion measurements made by plant personnel on the A and T specimens are shown in Table 7. The best values obtained by research personnel with the 1/10-mil gage are shown, along with the best value obtained by research with Gage 3, since many of the plant personnel used the latter gage. For this reason, the data in these tables are arranged according to the gages used rather than by the plant at which the tests were made.

It can be seen from Table 7 that plant personnel obtained essentially the same lateral-expansion values as did research personnel when using the same gage. The best values obtained by the two groups of technicians were usually the same and differed by not more than 1 mil except for specimen A-7, for which the difference was 2 mils. The range of values obtained by the plant personnel was within the range obtained by research personnel. The divergent values obtained by Plant 1 personnel are believed to be due to the inherent difficulties in zeroing their gage and in using a rounded contact surface on the dial-indicator stem. The scatter in the values obtained

with the other gages appears to be similar to the scatter obtained by research personnel in measurements made with the three standard gages.

The values obtained by Plant 4 personnel support the previous statement regarding prior experience.

### *Sources of Error in Measurements*

In the use of the gage described in this paper, erroneous values can occur for several reasons. Probably the foremost and least obvious is that the contact surface of the dial gage may not be flat or may not be parallel to the plane of the stop. If the contact surface is not flat or parallel, the protrusions will project against an inclined plane, and, thus, the values obtained are dependent on where the protrusions contact the plane. The error occurs twice and is related to the sine of the angle formed by the plane of the stop and the contact surface—measurements made with a nonparallel contact surface are lower than the correct values.

This type of difficulty can be detected by comparing the expansion values obtained from a single protrusion place so that it contacts the dial-gage contact point at four locations, 90 deg ( $\pi/2$  rad) apart around the periphery and at the center. If the gage is aligned properly, all the readings will be identical. An alternative method is to place the protrusion at opposite sides of the contact surface to check horizontal alignment and then place a flat edge against the stop and contact surface while holding the gage toward a bright light. If light can be seen at the top or bottom of the contact surface, then the gage is not aligned vertically. Several of the gages checked during this program were found to be out of alignment. Another source of error is malfunction of the dial indicator due to dirt or mechanical wear.

In addition, the operator can obtain erroneous values if he does not make certain that the specimen is in firm contact with the stop. Erroneous values can also be obtained if the operator grips the specimen above or slightly below where it contacts the stop, since gripping high tends to cause the specimen to rotate about the top leg of the stop. During the course of this investigation, it was observed that many plant technicians have a tendency to hold both halves of the tested specimen in one hand, which causes the two halves to contact one another. If the two halves are in contact, it was postulated that the deformation of the hinge on the compression surfaces might prevent the individual halves from contacting the stop properly. Therefore, specimen T-9 was machined so as to locate the notch much closer to the midlength of the specimen than required by ASTM and was tested at a high temperature to ensure a large amount of deformation during fracture. On the basis of a limited number of observations, this postulation does not appear to be well founded; however, it is still recommended that the halves do not touch one another during measurement.

TABLE 7—Summary of lateral-expansion

Plant	Technician Code	Gage Identification	Specimen No.							
			1	2	3	4	5	6	7	8
A SPECIMENS										
Laboratory	best value	1/10-mil gage	67.9	...	42.8	67.4	65.8	37.5	12.05	62.55
Laboratory	best value	Laboratory 3	69	...	44	68.5	67	38	12	63
Plant 5	3	Laboratory 3	68	...	43	69	67	39	14	64
Plant 4	... <sup>a</sup>	Laboratory 3	70	...	44	69	67	39	14	63
Plant 3	A	Laboratory 3	69	...	44	69	67	38	14	64
Plant 3	B	Laboratory 3	70	...	45	70	69	39	14	65
Plant 2	A	Laboratory 3	68	...	43	69	66	38	12	63
Plant	best value	Laboratory 3	69	...	43.5	69	67	39	14	63.5
Plant 5	1	ML 70	68	...	44	68	66	40	14	71
Plant 5	2	ML 70	66	...	44	69	67	40	15	64
Plant 6	1	Plant 6—No. 1	67	...	44	67	65.5	38	13	63
Plant 1	... <sup>a</sup>	Plant 1—No. 1	72	...	44	72	70	31	11	66
Plant 2	A	Plant 2—No. 1	67	...	42	66	65	36	10	61
Plant 2	B	Plant 2—No. 1	65	...	42	66	63	36	10	56
T SPECIMENS										
Laboratory	best value	1/10-mil gage	34.2	10.7	7.55	40.15	...	...	15.7	...
Laboratory	best value	Laboratory 3	35	11	8	41	...	...	16	...
Plant 5	3	Laboratory 3	34	11	8	41	...	...	16	...
Plant 4	... <sup>a</sup>	Laboratory 3	35	11	7	41.5	...	...	16	...
Plant 3	A	Laboratory 3	35	11	8	41	...	...	17	...
Plant 3	B	Laboratory 3	36	12	8	42	...	...	17	...
Plant 2	A	Laboratory 3	35	11	8	41	...	...	17	...
Plant	best value	Laboratory 3	35	11	8	41	...	...	17	...
Plant 5	1	ML 70	34	13	8	42	...	...	17	...
Plant 5	2	ML 70	36	14	10	43.5	...	...	19	...
Plant 6	1	Plant 6—No. 1	34	11	8	41	...	...	15	...
Plant 1	... <sup>a</sup>	Plant 1—No. 1	33	11	8	42	...	...	19	...
Plant 2	A	Plant 2—No. 2	33	9	6	39	...	...	15	...
Plant 2	B	Plant 2—No. 1	31	10	10	39	...	...	14	...

NOTE—1 mil = 0.025 mm.

<sup>a</sup> See text.

It was suggested by one of the plant technicians that the surface roughness of the 10 by 10-mm ends of the CVN specimen influences the measurements. Therefore, specimen T-14 was remachined (by using a dull milling cutter) so that the surface finish on these ends was about 500 rms rather than the normal finish of about 63 rms and was tested at a low temperature so that little expansion would occur, and minor variations might be more noticeable. As can be seen in Table 6, the difference values between the highest and lowest measurements were in the middle of the frequency distribution for each of the five research gages.

### Summary and Conclusions

A gage was designed and built at U. S. Steel Corporation research laboratories to rapidly and accurately measure the lateral expansion of

values (in mils) measured in the plants.

Specimen No.															
9	10	11	12	13	14	15	16	17	18	19	20	21	22	23	24
A SPECIMENS															
65.8	46.5	68.8	6.7	29.4	5.8	71.1	...	17.3	9.3	14.2	78.1	77.3	63.9	4.4	76.8
67	47	70	7	30	5.5	72	...	17.25	10	14	79	78	65	4.5	77.5
68	47	70	8	30	5	72	...	17	10	15	79	77	64	4	77
67	47	70	8	31	6	72	...	18	11	15	80	78	65	5	77
67	48	70	8	30	5	73	...	18	10	15	80	78	65	5	78
68	48	71	8	31	6	73	...	18	10	15	80	79	66	5	79
67	48	70	8	30	6	72	...	18	9	15	80	78	65	5	78
67	48	70	8	30	6	72	...	18	10	15	80	78	65	5	77.5
66	48	68	9	34	7	71	...	19	14	15	78	76	64	7	77
68	49	71	10	32	8	72	...	20	13	17	80	76.5	66.5	7	77.5
67	46	69	7	30	6	71	...	18	9.5	15	78	78	64	5	76
70	50	65	10	29	7	80	...	20	12	16	78	86	60	6	80
65	46	67	6	28	4	70	...	16	8	13	76	76	63	3	75
63	44	66	5	28	4	68	...	16	9	11	74	74	63	3	74
T SPECIMENS															
42.8	45.9	...	24.45	45.2	6.2	19.0	10.1	13.9	35.5	24.0	32.0	30.9	5.6	39.45	37.55
44	47	...	26	46.25	6.5	19	10.75	14	36.5	24.5	33	32	5.5	40.5	38
...	...	...	25	...	...	19	10	14	36	25	33	31	5	40	38
...	...	...	25	...	...	19	10	13.5	36	25.5	33	32	5.5	41	38
...	47	...	25	46	...	20	10	15	37	25	33	32	6	40	38
...	48	...	26	47	...	21	11	15	37	26	34	32	6	41	39
44	47	...	25	47	7	19	11	14	36	24	33	32	6	40	38
44	47	...	25	47	7	19	10	14.5	36	25	33	32	6	40	38
...	...	...	25	...	...	20	12	15	37	26	34	32	6	41	39
...	...	...	28	...	...	21	12.5	15	39	27	35	33.5	8	42.5	40
...	...	...	24.5	...	...	19	11	14	35	24.5	32.5	31.5	6	40	38
...	...	...	24	...	...	20	12	17	35	27	35	31	7	40	37
42	45	...	23	44	5	17	9	13	34	23	31	29	4	39	36
41	47	...	23	44	5	18	11	13	33	22	31	30	4	39	37

CVN impact specimens. Drawings for this gage are included in ASTM Method A 370-72, and gages based on these drawings have been commercialized by two companies. The present paper describes the gage and the method of using it.

The paper also gives the results of an extensive investigation made to determine the accuracy and reproducibility of measurements made with this type of gage. For this investigation, numerous lateral-expansion measurements were made by U. S. Steel Corporation research and plant personnel on CVN specimens of ASTM A36 and USS "T-1" (ASTM A517 Grade F) steels that had been tested over temperature ranges sufficient to develop complete transition-temperature curves. Additional measurements were made with machinists' outside-micrometer calipers.

The conclusions reached may be summarized as follows:

1. The accuracy of dial indicators used to perform the actual measurement is  $\pm 1$  dial division. For the dial indicator used on the standard gage,

the accuracy is 1 mil (1 mil = 0.001 in. = 0.025 mm). Since two measurements are made to determine the lateral expansion, the accuracy of the gage with the standard dial indicator is  $\pm 2$  mils. For this reason, two additional dial indicators were obtained and used in the study; one indicator had dial divisions of 1/2 mil, and the second had dial divisions of 1/10 mil. The values obtained with the 1/10-mil dial indicator, referred to as the 1/10-mil gage, were considered to be the most nearly correct values.

2. The reproducibility of the gages, with any dial indicator, appears to be approximately the same,  $\pm 2$  dial divisions. Reproducibility is a measure of the ability to obtain the same expansion value two or more times for the same specimen.

3. Prior operating experience with this gage does not appear to be a factor in obtaining reproducible results.

4. Lateral expansion measured with micrometers appears to be accurate to about  $\pm 2$  mils when compared with the values obtained with the 1/10-mil gage, even though the micrometers are more accurate.

5. Lateral expansion measured with micrometers appears to be generally reproducible to about  $\pm 1$  mil. However, considerable care is required to obtain this reproducibility, and, for this reason, the use of micrometers to measure lateral expansion is *not* recommended.

6. Plant personnel are capable of measuring lateral expansion with the same degree of reproducibility as are research personnel when using the type of gage described here.

7. Specimen preparation does not appear to affect the ability to measure lateral expansion. Although specimen preparation can have a great effect on the amount of expansion that occurs, it appears that this amount can be measured within the aforementioned limits.

The accuracy and reproducibility of lateral-expansion measurements are functions of the least reading of the dial indicator. These qualities can be therefore improved at a modest additional cost by replacing the standard 1-mil indicator with a 1/10-mil indicator. The accuracy and reproducibility would be expected to improve from the  $\pm 2$  mils obtained with the standard indicator to about  $\pm 0.2$  mil with the 1/10-mil indicator. There are no problems in retrofitting existing gages built to the drawings shown in ASTM Method A 370-72. Since material specifications are being written to arbitrary amounts of lateral expansion (for example, 15 mils), the improved precision should prevent the unnecessary rejection of material.

M. J. Manjoine<sup>1</sup>

## Determination of Plastic or Creep Strains by Grids

---

**REFERENCE:** Manjoine, M. J., "Determination of Plastic or Creep Strains by Grids," *Recent Developments in Mechanical Testing, ASTM STP 608*, American Society for Testing and Materials, 1976, pp. 91-105.

**ABSTRACT:** A method of determining permanent strains by pre- and post-measurements of a grid of reference points or lines on a test specimen, a component, or a model under test is described. The characteristics of the grid at elevated temperature and some of the limitations are presented.

The grid of points or lines is generated by a photographic and electrodeposition process. The determinations of the deformations can be accomplished by direct measurements of the model or photographs of the deformed grid. Measurements of grid lines after extended periods at elevated temperature gave reliable strain distributions.

**KEY WORDS:** mechanical tests, high temperature tests, strain measurement, crack propagation, strain concentration, deformations

The study of the flow and fracture characteristics of materials in a given geometry and for a given loading at elevated temperature often requires a detailed mapping of the strain distribution for the purposes of (a) determining the areas of highest strain or site of fracture initiation, (b) comparing with the strain distribution obtained from computer programs using specific constitutive relationships for material behavior, and (c) validating damage criteria for fracture initiation and propagation.

A reliable method for accomplishing these purposes is the strain-grid technique which enables the determination of surface strains over a large area from room temperature measurements before and after a loading period.

Many methods of applying and reading grids have been devised, and some of these have been reviewed by Parks.<sup>2</sup> The methods of applying the grids include printing, etching, scribing, embossing, and embedding.

<sup>1</sup> Research consultant, Mechanics Department, Westinghouse Research Laboratories, Pittsburgh, Pa. 15235.

<sup>2</sup> Parks, V. C., *Experimental Mechanics*, Vol. 9, No. 7, 1969, pp. 27N-33N.

Readings are taken directly on the specimen or from a photograph or replica by instruments which include calipers, comparators or microscopes with traveling heads, and movable crosshairs or graduated reticles.

The method described in this paper is applicable over a wide temperature range, and considerable experience has been obtained at 1100°F (593°C) for a stainless steel. Most of these methods apply lines or dots of a low melting material and are, therefore, restricted in temperature. Butler<sup>3</sup> has employed scribing and the Hickson replica technique to study the local strain distribution at a hole in an aluminum alloy at a temperature of 200°C. Durelli and Buitrago<sup>4</sup> investigated the same configuration using moiré strain analysis at 1100°F (593°C) for a stainless steel and utilized etched lines which were filled with an oxide to provide contrast.

When the grid method is utilized at elevated temperature, two major problems are encountered: (a) the retention of the grid lines during the oxidation of the surface and (b) the maintenance of contrast so that the measurements or reproduction of the grid can be made. These problems, the factors effecting the accuracy of the measurements, and some applications will be discussed.

## Procedure

### *Grid Selection*

The grid selected for the test described here was a square grid of lines of 30 divisions/in. and a distance between lines of 1/30 in. (0.847 mm). The master grid was prepared by photographic reduction to one third of a square grid of lines spaced 0.1 in. (2.54 mm) apart in each direction within  $\pm 0.0005$  in. (0.0127 mm) and within  $\pm 0.0005$  in. over 10 in. Every tenth line is accented, and alternate blocks of 10 by 10 divisions are numbered. Polyester film was selected for the master because of its stability in ambient temperature and humidity and its ability to conform to flat or cylindrical specimens.

### *Oxidation Characteristics of the Specimen Surface*

The printed grid can be distorted or separated from the surface when the surface oxidizes in the air atmosphere usually used in an elevated tempera-

<sup>3</sup> Butler, S., Paper C152, *Proceedings*, International Conference on Creep and Fatigue in Elevated Temperature Applications, Institution of Mechanical Engineers, London, 1973-1974.

<sup>4</sup> Durelli, A. J. and Buitrago, J., "Residual Strains in a Stainless Steel Plate with a Circular Hole Subjected to Reverse Loading at Elevated Temperature," Publication G00088, American Society of Mechanical Engineers, June 1975.

ture test. Through a study of the oxidation characteristics of the specimen material, a feasible substrate can be usually developed for the desired time of testing for a given temperature. For the stainless steel used in the tests reported here, no substrate was employed for the 1100°F (593°C) exposure.

### *Surface Finishing for Grid Retention*

The pretreatment just described can be a part of the grid retention scheme during the processing. The polished surfaces of the stainless steel specimens described here were treated by a light vapor blast to retain the photographic emulsion during the printing and cleaning.

### *Providing Contrast for Readability*

At elevated temperature, the emulsion will dissolve; therefore, the grid must be etched into the surface or a plating must be applied to the surface. A negative master was employed in the contact printing of the lines, and the spaces between the lines were plated with gold. The diffusion of the gold plating and the difference between the oxidation rates of the plated and unplated areas provide contrast, and the slight plating thickness enhances this contrast. To prevent significant alteration of the test specimen, the plating thickness was usually less than 0.01 mm.

### *Measuring the Grid*

The measurements or photographing of the grid were usually performed at no load and room temperature before and after loading. In a creep test, the measurements were made at different periods during the long-time loading.

Several methods of measurements were employed. The virgin specimen with grid lines was measured in both directions by a microscope mounted on a traveling head. Readings on the virgin specimen were made for every ten divisions in each direction and over the full gage section. The least count of the comparator was 0.00005 in. (0.00127 mm), so that a change of one count equals a strain of 0.00167 percent for 90 divisions, 0.015 percent for 10 divisions, and 0.15 percent for 1 division. The ability to set the cross hairs at the precise edge of the grid line intersection varies with investigators. Reproducibility of a reading improved with experience but degraded with eye fatigue. The reproducibility of the measurement of an interval for the grid on the specimen was usually about ten times the least count, but, by taking multiple readings, the average could be reproduced within 0.00015 in. (0.0038 mm).

### *Recording the Grid*

A permanent record of the grid lines were made both before and after a loading period by a photograph. A bellows camera was fixed at a focal distance to give a one-to-one reproduction. A 203 mm, f7.7 lens set at f32 was employed. The camera was carefully positioned in distance and height, and the image and object planes were maintained parallel and in focus. A circular fluorescent light was mounted around the lens so that a direct uniform lighting was obtained. At least three photographs were made at each recording using (a) an instant photo paper, (b) a high contrast film, and (c) a high contrast glass plate.

Each specimen is provided with a dummy on the right and left of the test section. The dummy is of the same material as the specimen and has its grid processed at the same setup as the test section. The dummy is unloaded during the test but is held in specimen plane by clips throughout the testing and photographing. The measurements of the dummy grid become a known scale and allow accounting for reproduction and magnification changes. A specimen with dummies is shown in Fig. 1.

As the test progresses at elevated temperature, the differences in oxidation can alter the width of the grid lines. This has only a secondary effect on the distance between lines, but it increases the difficulty in setting the cross hairs of the microscope on the edge of a line. Therefore, an increase in error can be encountered with time of test.

In areas where the strain gradient is large, it is necessary to measure successive grid intervals. The photographs can be enlarged to reduce the strain value of the least count. When resolution is marginal, a cellulose nitrate tape replica can be made of the grid at no load and room temperature. The replica can also be enlarged photographically for measurement. Such an enlargement is illustrated by Fig. 2 which is a portion of a central hole in a plate specimen with a high strain gradient and a propagated crack.

### *Analysis of Readings*

Because of the large number of readings and the desirability of plotting the strain distribution, the readings are prepared for computer analysis. The readings from the undeformed or virgin sample or from its photograph are recorded or stored in the computer or both for comparison with the deformed readings to calculate the strains.

A data reduction package has been developed by Dhalla<sup>5</sup> to plot the virgin grid, the subsequent distortion, and the strain distribution.

<sup>5</sup> Dhalla, A. K., "Strain-Grid Reduction Scheme," "Validation of High Temperature Design Methods and Criteria," WARD-HT-3045-8, Quarterly Report, Westinghouse Advanced Reactor Division, U. S. Energy Research and Development Administration, Oak Ridge, Tenn., 30 Nov. 1974.

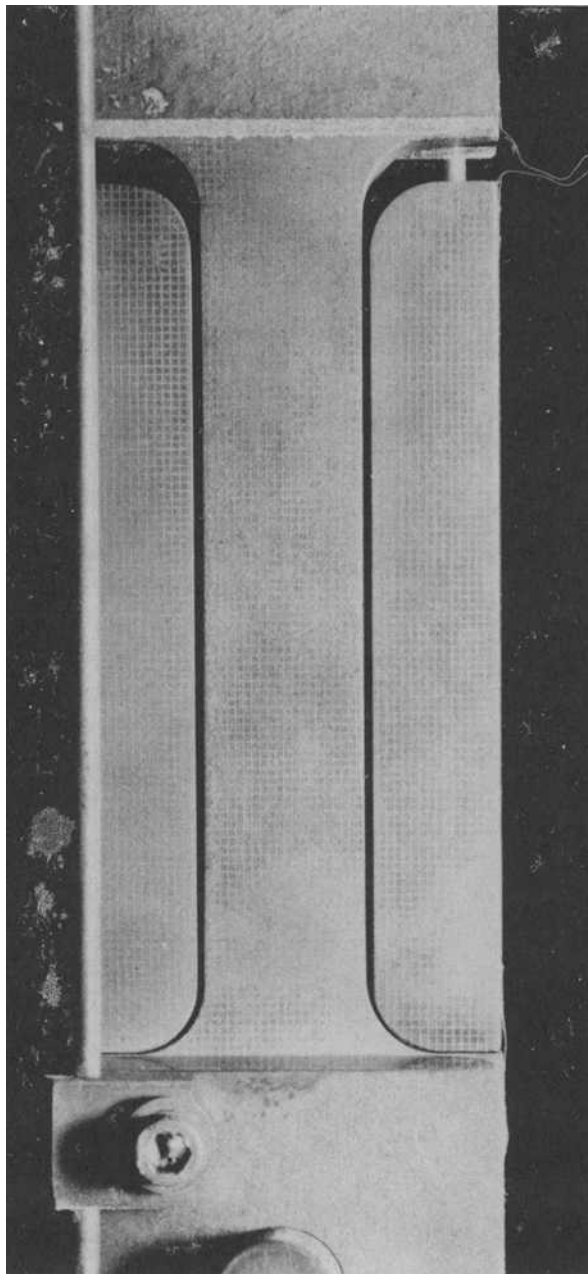


FIG. 1—Grid of Specimen A1 after 303 h at 1100°F.



FIG. 2—Enlargement of replica at area of high-strain gradient.

## Experimental Work

### *Plane-Stress Test*

The mechanical properties of materials are usually investigated by using the uniaxial tension test under plane stress of a specimen with a uniform gage section. The strain is assumed to be constant over a gage length which is a portion of the gage section. Often, when a furnace or environmental chamber surrounds the specimen, it is more convenient to measure the displacements of the heads of the specimen (extension beyond the uniform gage section) and to calculate the strains of the gage section. The strain distribution along the length of the specimen, however, is influenced by the geometry of the gage section and that of the heads. The measurements from a grid on a plane-stress specimen allow the establishment of an "effective gage length"<sup>6</sup> (according to ASTM Recommended Practice for Conducting Creep, Creep-Rupture, and Stress-Rupture Tests of Metallic Materials (E 139-70) to correlate the strain measured from the motion of the heads with the uniform strain at the midlength of the specimen.

The axial strain measurements over ten divisions along the length of the plane stress specimen, A1, Fig. 1, are plotted in Fig. 3. The average strains are given for the middle 1 in. and 2 in. and those for the uniform 3-in. section and for the extensometer which measured from the heads.

After the fracture of specimen A1 at 1826 h, the final strains were measured from the grid lines in both the length and width directions and by the change in dimensions (using a micrometer) for the width and thickness. The strain distributions at fracture are plotted in Fig. 4.

### *Tests with a Degree of Plane Strain*

The larger section at the heads restricts the strain into the uniform section. This constraint can be modified by the geometry of the heads and that of the gage section. Specimen B2, Fig. 5, had the same uniform length as Specimen A1, but the width was five times larger. The heads of the specimen were constrained in the width direction but not in the thickness direction. Therefore, for this specimen with a width-to-thickness ratio of ten and a uniform width to length ratio of one to one, the degree of plane strain will vary from a maximum at the head to a minimum at the mid-length of the uniform section. The strain-grid technique allows (a) a measure of the strain distribution over the entire specimen, (b) an evaluation of the effect of the constraints, and (c) the strain at the point of crack initiation (Fig. 5). This figure also illustrates the readability of a photograph after 9139 h at 1100°F.

<sup>6</sup> Manjoine, M. J., *Transactions, American Society for Mechanical Engineers*, Vol. 67, 1945, p. 115.

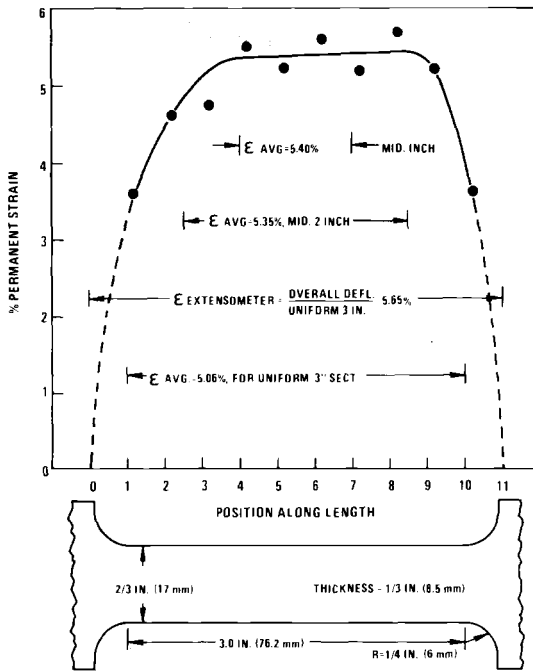


FIG. 3—Axial strain distribution of Specimen A1 at 303 h from grid measurements.

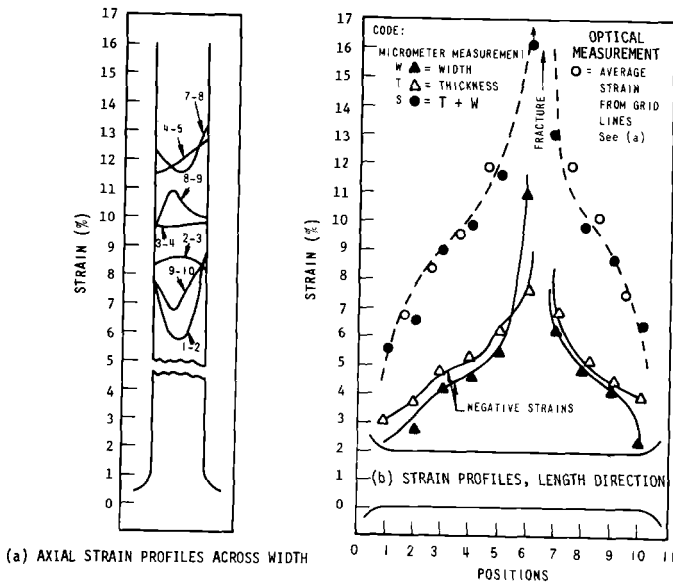


FIG. 4—Strain distributions of Specimen A1 at fracture.

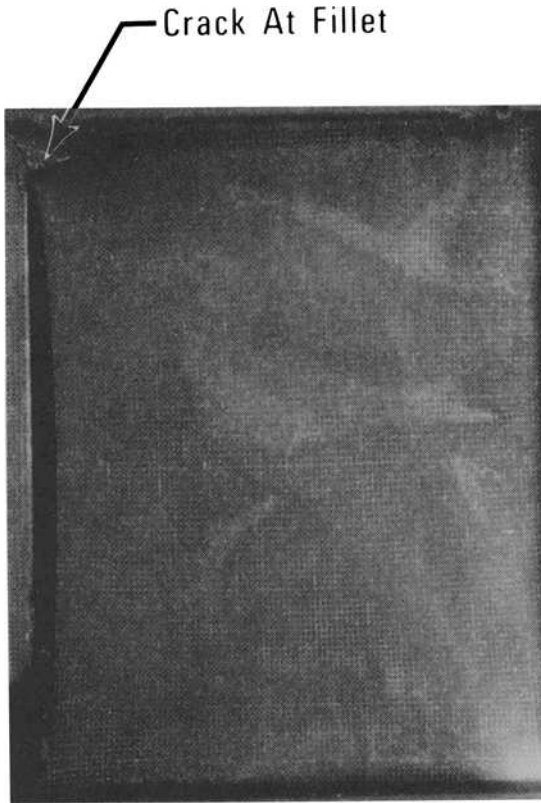
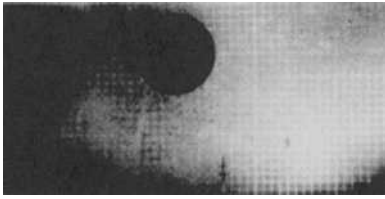
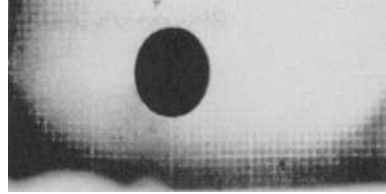


FIG. 5—Grid of Specimen B2 after 9139 h at 1100°F.

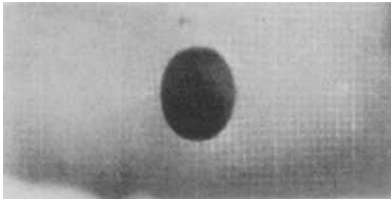
The grid can also be photographed at temperature and load. A series of photographs of a plate with a central hole are shown in Fig. 6 for a creep test at 21 ksi (144.8 MPa) net section stress and 1100°F. The crack extension with respect to the hole or grid can be measured, as well as the local strain near the crack tip through the deformation of the grid. These photographs were taken through a port in the furnace by a firmly positioned camera (Fig. 7). A press camera with a 135-mm lens and a +6 closeup lens was employed. The light was projected through the port which was opened only during photographing. The crack growth, as measured by the sum of the crack lengths on each side of the hole, is plotted in Fig. 8. The overall deflection for the 3-in. uniform section and the strain away from the hole, as measured by a weldable strain gage, are also shown in Fig. 8. These will be used in future comparisons with the grid measurements and results from an elastic-plastic-creep analysis.



a. No Load



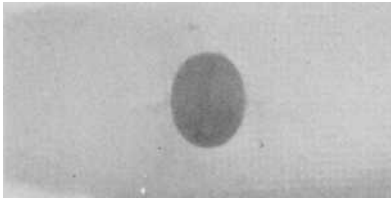
b. Loaded To 21 KSI



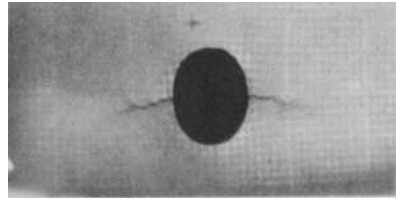
c.  $t = 310$  Hours (Estimated Crack Initiated At 285 Hours)



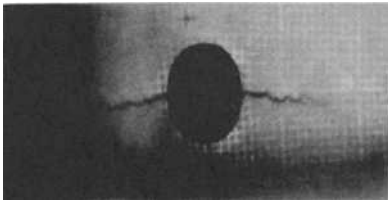
d.  $t = 334$  Hours



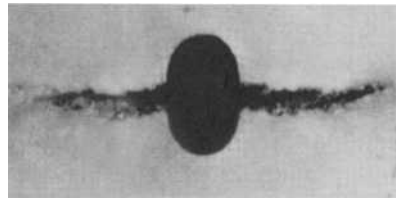
e.  $t = 342$  Hours



f.  $t = 368$  Hours



g.  $t = 390$  Hours



h.  $t = 397$  Hours Final

FIG. 6—Grid and crack patterns at a central hole in a plate during rupture test at 1100°F.

### Discussion

The two dummies are machined to fit the contour of the test specimen. The grid lines are printed by positioning the master grid over all parts. When a photograph such as Fig. 1 is made, a direct comparison of the deformations can be made between the unloaded dummies and the specimen for any magnifications.

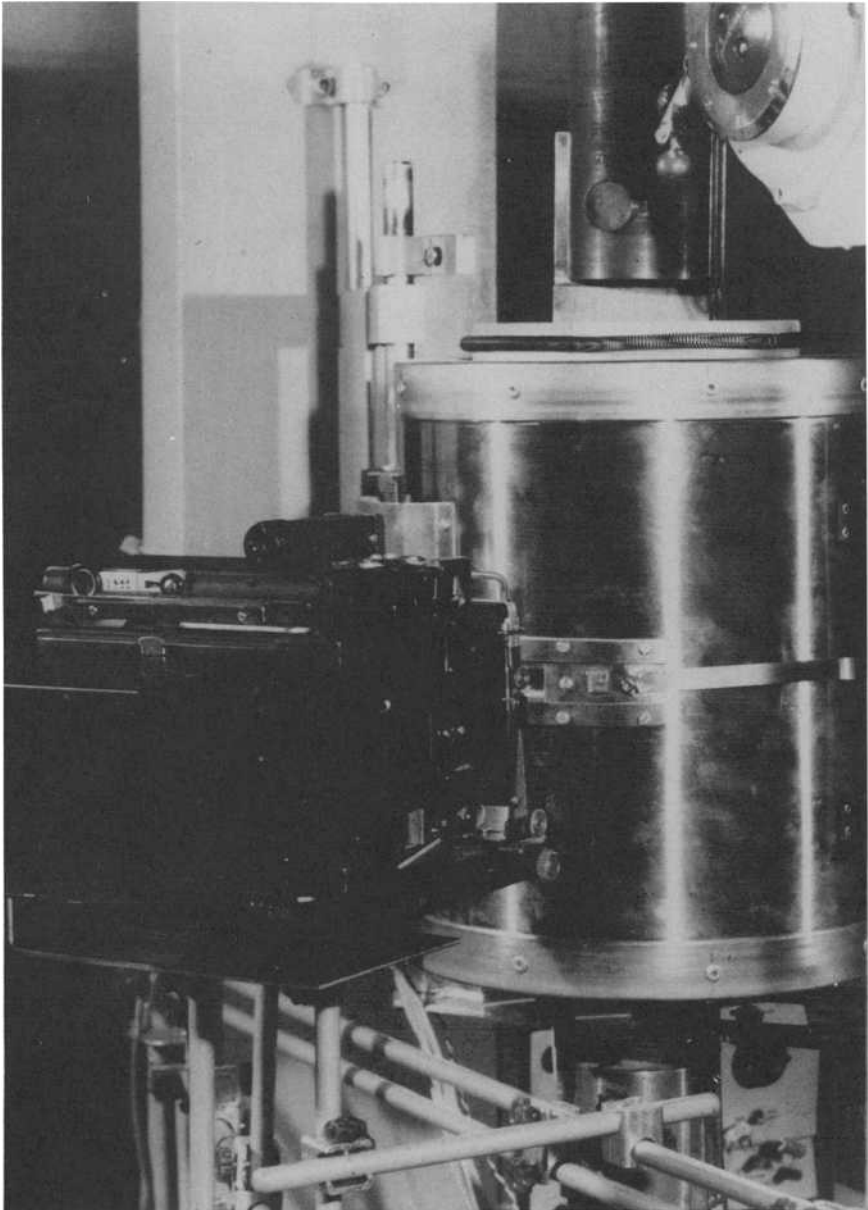


FIG. 7—Camera fixed for sequence photographs through furnace port.

# CREEP-RUPTURE OF T304 STAINLESS STEEL AT 1100°F AND 21,000 PSI NET SECTION STRESS

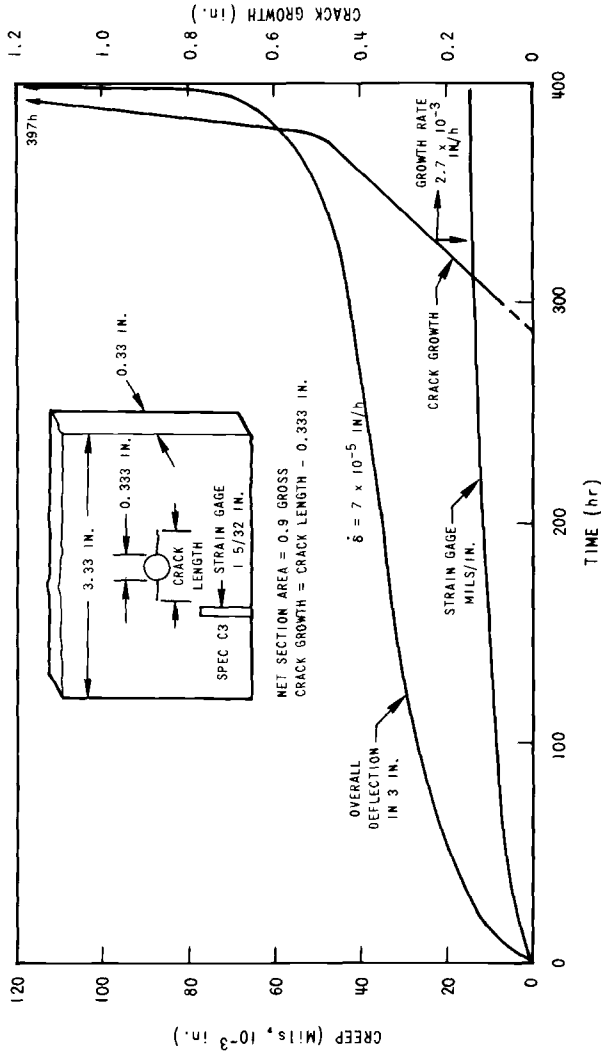


FIG. 8—Crack growth and creep curves for specimen C3.

The strain profiles in Fig. 3 show (a) a nearly uniform strain area about the middle half of the uniform gage section, (b) a reduction in strain up to the ends of the uniform section, and (c) a sharp reduction in strain in the fillet and at the heads. The average strain for the middle inch is 5.40 percent. That for the middle 2 in. is only slightly smaller at 5.35 percent, but that for the uniform 3-in. section is only 5.06 percent. Because of the strain in the fillet and heads, the strain as measured by the overall extensometer using the 3-in. gage length is 5.65 percent, which is slightly larger than the uniform strain at 5.40 percent. From the grid measurements, the effective gage length for the extensometer<sup>6</sup> is calculated to be 3.14 in. (79.7 mm). ASTM Method E 139-70 proposes a way of calculating an effective gage length. Using this method, the effective gage length is 3.17 in. (80.5 mm) which is only 1 percent different. The measurements in the uniform strain area show a deviation from the mean of 0.15 percent strain. The strain readings were made consecutively by a technician with little experience so that, if the first interval is read low, the next will be high. In a uniform strain region, better accuracy can be obtained by averaging an even number of consecutive readings. After fracture of Specimen A1 in 1826 h, the grid was measured in the axial direction at five positions across the width. The axial strain gradient across the width is plotted in Fig. 4a; the individual curves are coded with the axial position interval numbers. Thus, Curve 1-2 is the average axial strain in the interval between positions 1 and 2 of the specimen contour shown in Fig. 4b. At this position, the original stress concentration resulted in a strain concentration at the fillets. However, with plastic flow, the constraint of the heads causes a reduction in strain relative to the middle of the gage section. Curve 9-10 is the same relative position at the other end of the gage section and reflects a difference similar to that found at 303 h (Fig. 3).

In Fig. 4b, a comparison is made between the strain measurements from the grid and the micrometer measurements of the fractured specimen. Since the volume is essentially constant, the axial strain can be calculated as the sum of strains in the width and thickness directions with a change in sign. For this plane-stress Specimen A1 with a width to thickness of 2 to 1, the average strain in the thickness direction is only slightly higher than that in the width direction. From a comparison of open and closed circles of Fig. 4b, it can be seen that good agreement was obtained with the grid strains. Near the fracture area, the grid gives slightly higher strains since some cracking occurs, resulting in an effective increase in volume.

At fracture, there is no uniformly strained section. However, by a comparison of Figs. 3 and 4b and a review of the creep-rupture data, the strain was nearly uniform near the middle 2 in. up to the transition from second to third stage creep (8.3 percent permanent strain at 1260 h). After the transition, the highest strained middle volume begins to neck and causes a high strain gradient near the fracture. The elongation strain calculated

from the overall deflection and the effective gage length is 11.5 percent. It can be seen from Fig. 4 that only two small volumes of the specimen near the fracture have this magnitude of strain, while the strain is larger for the middle inch, and smaller for the uniform inch near each head. Elongation values, therefore, are less useful in describing material ductility than the uniform strain at the instability of local necking.

The grid method enables the determination of the area of maximum damage during a loading period. Since fracture is a process of initiation and propagation, the strains in the area of crack initiation and propagation can be evaluated by a sequence of measurements. For Specimen B2 shown in Fig. 5, the area of crack initiation was at the fillet where there was a strain concentration. The average creep strain of Specimen B2 at 9139 h (Fig. 5) was 14 percent. Even after this long time exposure at 1100°F, the grid lines are readable over a large percentage of the area. The contrast for the direct lighting used is influenced by the surface oxides and discolorations. Indirect lighting improves the contrast and was useful for direct measurements on the specimens.

In Fig. 6, a sequence of pictures was taken throughout the test to determine the strain at crack initiation and the rate of crack growth. The grid here serves a dual purpose. The strains at the point of initiation can be evaluated, as well as those along the crack propagation path. The crack propagation distances can also be measured with reference to the deformed grid.

When a test is interrupted and cooled to room temperature, a replica can be made of the surface at an area of high strain gradient or crack initiation (Fig. 2). A replica is also made of the dummy by the same technique so that any distortion of the replica tape is accounted for. The replica can be enlarged, along with that of the dummy, to improve the accuracy of measurements. The tape used for Fig. 2 was 1 in. (25.4 mm) wide.

## Conclusion

A technique has been developed which allows the use of the grid method of strain measurements at elevated temperatures. The grid is placed on the surface of a specimen or component under test by a process utilizing a photographic emulsion and printing combined with etching and plating. Measurements of grid spacings are made before and after a loading period. These can be made on the specimen itself or from reproductions by photography or replicas.

Reliable strain distribution and crack growth measurements have been achieved over most of the surface for periods of over 9000 h at a temperature of 1100°F (593°C) for a stainless steel.

*Acknowledgments*

The development of the grid technique described here was a cooperative effort by the Mechanics, Physical and Inorganic Chemistry, and Electronic Services Departments of the Westinghouse Research Laboratories. The tests and strain analyses were sponsored by the U. S. Energy Research and Development Administration under Contract AT(11-1)-3045. The support and assistance of all parties are gratefully acknowledged.

## Stress Relaxation in Bending

---

**REFERENCE:** Parikh, P. and Shapiro, E., "Stress Relaxation in Bending," *Recent Developments in Mechanical Testing, ASTM STP 608*, American Society for Testing and Materials, 1976, pp. 106–117.

**ABSTRACT:** This paper describes a technique for stress relaxation measurement in bending at ambient and elevated temperatures. This technique utilizes a double-triangle-shaped specimen which is loaded at three points. The load remaining in the specimen at any time during the test is determined using a lift-off technique. This technique satisfies ASTM Recommended Practice for Stress-Relaxation Tests for Materials and Structures (E 328–75). The use of an analytical expression for extrapolation of short-time data to predict behavior at long times is also presented. Data of two copper alloys, phosphor bronze and nickel silver, are extrapolated to estimate the stress relaxation at 100 000 h.

**KEY WORDS:** mechanical tests, stresses, bending stress, mechanical properties, copper alloys, contact pressure, phosphor bronzes, copper nickel zinc alloys, stress relaxation tests

Copper base alloys are widely used in the electronic connector applications [1,2].<sup>2</sup> These connectors are most often designed as flexural springs, and electrical contact is maintained by the action of the bending stresses that are developed. A high, stable contact pressure assures a reliable contact and thus is an important performance criterion for electronic connectors [3]. In order to determine time dependence of contact pressure of a connector, stress relaxation properties of the material in the bending mode should be known. This paper describes a simple technique of determining stress relaxation properties of strip materials in the bending mode at ambient and elevated temperatures. An analytical expression for extrapolation of short-time data to predict stress remaining at long time is presented. While specific examples are cited for copper alloys, the measurement technique is broadly applicable.

### Test Procedure

This three-point bending stress relaxation test utilizes a double-triangle-shaped specimen, Fig. 1. The load is applied at the specimen center via a

<sup>1</sup> Engineering specialist and supervisor, respectively, Mechanical Metallurgy Group, Olin Metals Research Laboratory, New Haven, Conn. 06504.

<sup>2</sup> The italic numbers in brackets refer to the list of references appended to this paper.

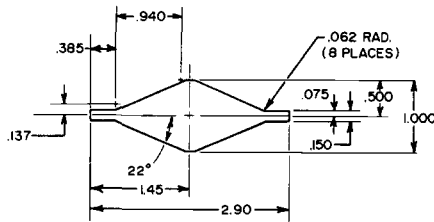


FIG. 1—Specimen design. Dimensions in inches. Multiply inch by  $2.54 \times 10^{-2}$  to obtain meter.

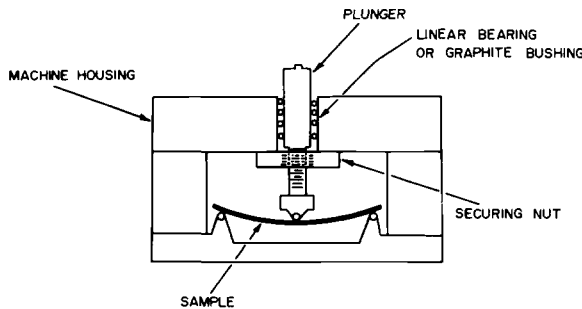


FIG. 2—Schematic diagram of stress relaxation testing jig.

plunger, while the specimen is held at both ends. Figure 2 shows a schematic of the testing jig. The overall length of the device is about 6 in., and the height is about 4 in. Friction between the machine housing and the plunger is virtually eliminated with the use of linear bearings or graphite bushings.

The initial load corresponding to the desired initial applied stress is calculated using elastic flexure formula (Appendix I). This load is applied to the plunger by a universal testing machine operating in a compressive mode and is measured with a load cell. A loading rate of 0.1 in./min was used in all tests. When the desired load is reached, the securing nut is tightened, locking the loading plunger in place for the duration of the test. This assures a constant specimen curvature (initial strain) at all times. Because the actual initial load will depend on how securely the lock nut is fastened, the exact initial load is determined by making a measurement of load remaining in the specimen within 1 min of when the lock nut was fastened. This exact value is used as the initial load, and the stress relaxation test begins (zero time) at this point.

The load (stress) remaining in the specimen at any time during the test is determined using a lift-off technique and makes use of the enormous difference between the machine stiffness and the specimen stiffness [4]. The testing jig is reloaded, and the load versus time (plunger displacement) is continuously recorded, Fig. 3. The initial linear plot of load versus time corresponds to the stiffness of the testing jig. When the applied load just

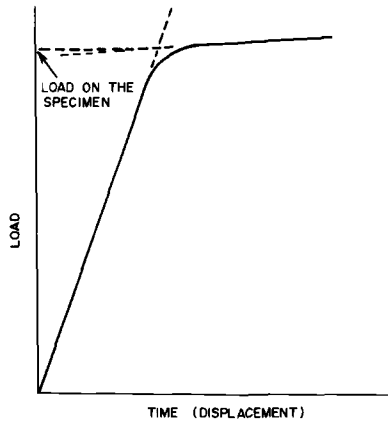


FIG. 3—Load versus time (displacement) curve.

exceeds the load on the sample, the securing nut will move slightly away from the top housing plate. This causes a sharp break in the load-displacement curve as shown in Fig. 3. Beyond this break point, the load-displacement curve reflects the stiffness of the specimen. The additional specimen displacement introduced by the measurement technique is less than 1 percent of the initial displacement. The load (stress) remaining in the specimen is determined by the intersection technique shown in Fig. 3. The load was measured to an accuracy of 0.2 lb. The amount of stress relaxation is the difference between the applied stress and the stress remaining.

For elevated temperature tests after setting the initial load at ambient, the jig is put into the furnace and allowed to come to temperature. After a fixed time period (we use 1 h), an initial reading of load (stress) remaining after elevated temperature exposure is taken at room temperature. This reading serves as the zero time for the elevated temperature tests. All subsequent measurements of stress relaxation are made at room temperature after exposing the specimen at elevated temperature for a time interval.

The test equipment, specimen preparation, and the testing procedure just described are in accord with ASTM Recommended Practice for Stress-Relaxation Tests for Materials and Structures (E 328-75). Appendix II describes the limitation due to material thickness on length to width ( $L/b$ ) ratio of the specimen for preventing the occurrence of curvature in the width direction. The criterion described in Appendix II is general and is applicable to any type of specimen deformed in bending.

In order to characterize the initial test condition, measurement of the maximum deflection of the specimen is required. Maximum deflection is used to determine the radius of curvature, since the double-triangle-shaped specimen deforms with cylindrical curvature. Assuming that the neutral

radius is in the center of the beam, the nominal outer fiber strain,  $\epsilon$ , is given by  $\epsilon = t/(2R + t)$ , where  $R$  is the radius of curvature, and  $t$  is the thickness. According to Section 32.12 of ASTM Method E 328, Part C, this strain value can be used to determine the equivalent tensile stress on loading from the stress-strain curve. Equivalent tensile stress on loading is defined as the stress corresponding to the outer fiber strain on the tensile stress-strain curve. Alternatively, stress may be reported as the product of strain and modulus of elasticity and defined as the nominal elastic stress on loading according to Section 32.11 of ASTM Method E 328.

## Results and Discussion

The room temperature tensile properties of phosphor bronze (CA 510) and nickel silver (CA 762) used in this investigation are recorded in Table 1. The phosphor bronze is in the spring temper, and the nickel silver is in the extra hard temper. The bend stress relaxation results of CA 510 and CA 762 at two temperatures are shown in Figs. 4 and 5, respectively. The stresses in the figures are calculated using elastic flexure formula. A summary of initial stress and stress remaining at 1000 h calculated using the elastic flexure formula is given in Table 2. Measurements required to describe the initial test condition are listed in Table 3. The stress values reported in this

TABLE 1—Room temperature tensile properties of CA 510 and CA 762 parallel to the rolling direction.

	Young's Modulus $\times 10^6$ psi ( $\times 10^8$ MN/m <sup>2</sup> )	0.2% Yield Strength, ksi (MN/m <sup>2</sup> )	Ultimate Tensile Strength, ksi (MN/m <sup>2</sup> )	Elongation in 2 in., %
CA 510	16.3 (112.39)	110 (758)	111 (765)	2.6
CA 762	18.3 (126.18)	105 (724)	107 (738)	2.3

TABLE 2—Stress relaxation data for CA 510 and CA 762 parallel to the rolling direction.

	Test Temperature, °C	Initial Stress, ksi (MN/m <sup>2</sup> )	Stress Remaining at 1000 h, ksi (MN/m <sup>2</sup> )
CA 510	RT <sup>a</sup>	97 (669)	92 (634)
	105	95/90 <sup>b</sup> (655/621)	72 (496)
CA 762	RT	84 (579)	83 (572)
	105	83/81 <sup>b</sup> (572/559)	73 (503)

<sup>a</sup> RT = room temperature.

<sup>b</sup> Stress remaining after 1-h exposure at 105°C, that is, zero time stress.

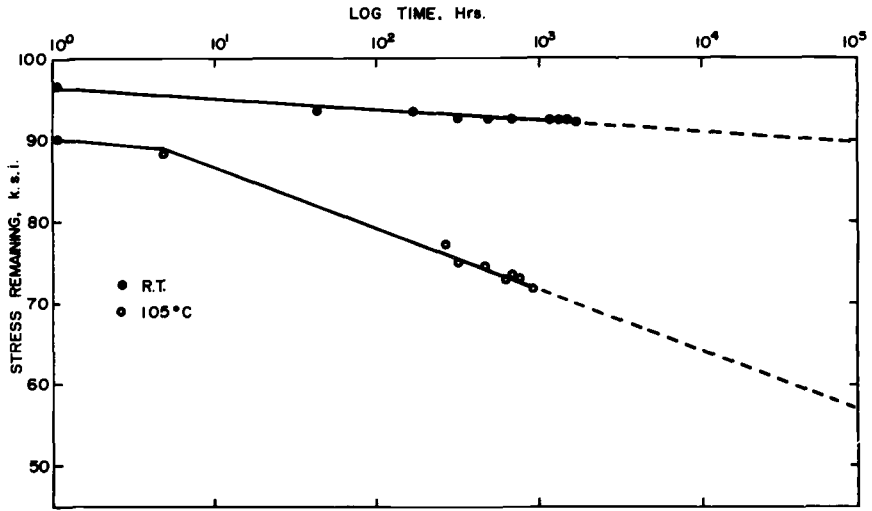


FIG. 4—Stress remaining versus time for CA 510. Multiply ksi by 6.895 to obtain MN/m<sup>2</sup>.

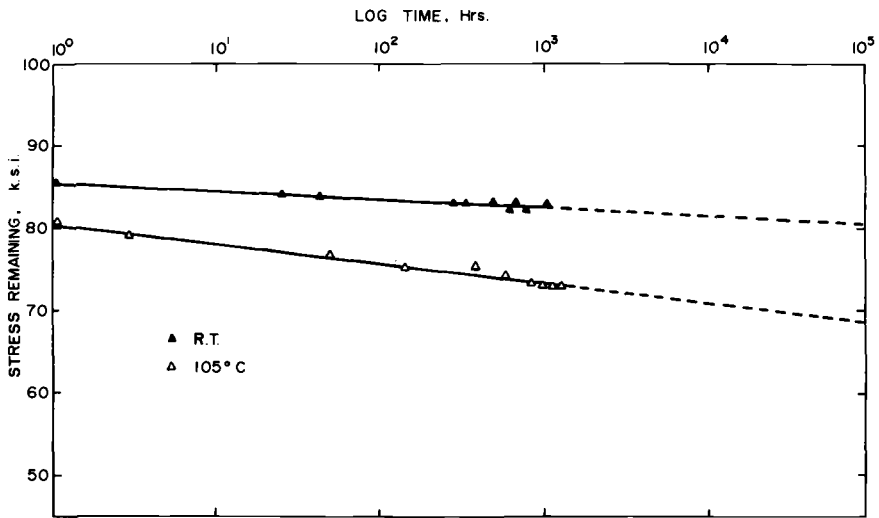


FIG. 5—Stress remaining versus time for CA 762. Multiply ksi by 6.895 to obtain MN/m<sup>2</sup>.

paper are not corrected for the change in the line of action of force at the point of contact due to deflection. This correction can be made from the deflection and specimen dimensions data reported in Table 3.

Estimate of stress remaining at long time is valuable for alloy selection. In developing the formulation for extrapolation, we have adopted the view that the time dependence of stress remaining can be described by the

TABLE 3—Specimen dimension and deflection data for CA 510 and CA 762.

Alloy	Test Temperature, °C	Dimensions, in. ( $10^{-2} \times$ m)			Thickness ( $t$ )	Initial Deflection, in. ( $10^{-2} \times$ m)	Radius of Curvature, in. ( $10^{-2} \times$ m)
		Length ( $L$ )	Width ( $b$ )				
CA 510	RT <sup>a</sup> 105	2.534 (6.436)	0.967 (2.456)	0.042 (0.107)	0.259 (0.658)	3.23 (8.20)	
		2.518 (6.396)	0.967 (2.456)	0.042 (0.107)	0.217 (0.551)	3.76 (9.55)	
CA 762	RT 105	2.506 (6.365)	0.965 (2.451)	0.040 (0.102)	0.202 (0.513)	3.99 (10.14)	
		2.555 (6.490)	0.978 (2.484)	0.040 (0.102)	0.173 (0.439)	4.80 (12.19)	

<sup>a</sup> RT = room temperature.

following formulae commonly employed for kinetic problems of this type [5]; see Appendix III for details

$$\sigma_t = - \frac{k}{1 - n} (t + a)^{(1-n)} + X \quad \text{for } n \neq 1 \quad (1a)$$

or

$$\sigma_t = -k \log (t + a) + X \quad \text{for } n = 1 \quad (1b)$$

where  $\sigma_t$  is the stress remaining at any time,  $t$ ; and  $k, n, a$ , and  $X$  are constants independent of time but dependent on initial stress and temperature.

Figure 6 shows schematically the stress remaining versus time curves for different values of  $n$ . One to two thousand hours of data are generally adequate to define the curves of Type b and c by Eqs. 1b and 1a, respectively. However, for the curve of Type a, where the stress remaining is decreasing quite rapidly, data for times longer than 2000 h would be required for a more reliable estimate of long-time behavior.

The procedure of estimating stress remaining at longer times using equations 1a and 1b is described in Appendix IV.

This extrapolation technique was used to estimate stress remaining at 100 000 h for CA 510 and CA 762. The estimated values are listed in Table 4. In the literature, long-time results for the same tempers of CA 510 and CA 762 are not available. However, Fox [6,7] has performed tests up to about 20 000 h on some conditions of CA 510 in strip and wire form. Based on his data, stress remaining at 100 000 h is estimated for spring temper and compared with the extrapolated values in Table 4. The agreement between the two values is quite reasonable.

**Conclusions**

A three-point bending stress relaxation device employing a lift-off measurement technique and a double-triangle-shaped specimen has been

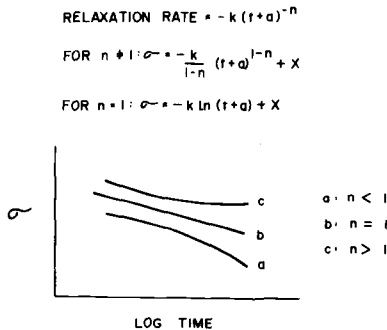


FIG. 6—Schematic stress remaining versus time for different values of  $n$ .

TABLE 4—Stress remaining at 100 000 h for CA 510 and CA 762.

Alloy	Test Temperature, °C	Initial Stress, ksi, (MN/m <sup>2</sup> )	Extrapolated Stress Remaining at 100 000 h, ksi (MN/m <sup>2</sup> )	Stress Remaining at 100 000 h Based on Fox's Data, ksi (MN/m <sup>2</sup> )
CA 510	RT <sup>a</sup>	97 (669)	89 (614)	88 (607)
	105	95 (496)	58 (400)	62 (428)
CA 762	RT	84 (572)	80 (552)	...
	105	83 (503)	68 (469)	...

<sup>a</sup> RT = room temperature.

developed. This technique is simple, economical, and is amenable to ambient and elevated temperature testing. This technique and device satisfy the requirements of the ASTM Method E 328, Part C.

Analytical expressions for extrapolation of short-time data to predict stress remaining at long times are given. Extrapolated values of CA 510 are found to be in agreement with long-time test data.

### Acknowledgment

Dr. C. M. Tyler, Jr., originally designed this three-point test, and J. Hoyt, Jr., developed it in its present form. W. Bailey performed the stress relaxation measurements.

## APPENDIX I

### Calculation of Load for the Three-Point Stress Relaxation Test

The following equation derived from elastic flexure formula is used to calculate load or stress remaining

$$P = \frac{4\sigma bt^2}{6L}$$

where

- $P$  = load (lb),
- $\sigma$  = stress (psi),
- $b$  = width (in.),
- $t$  = thickness (in.), and
- $L$  = length (in.).

The width and length are defined as shown in Fig. 7.

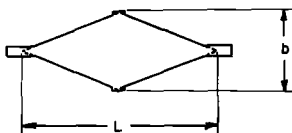


FIG. 7—Schematic specimen diagram.

## APPENDIX II

### Limitation on $L/b$ Ratio of the Specimen Due to Material Thickness

According to Timoshenko and Goodier [8], the following formula gives the deformation in the width direction of a beam bent with a moment  $M$ . The deformation in the width direction results in an anticlastic surface

$$Y_{\max} = \pm \frac{b}{2} \left( 1 - \frac{\nu t}{2R} \right) \quad (2)$$

where

- $b$  = specimen width,
- $\nu$  = Poisson's ratio,
- $t$  = specimen thickness,
- $R$  = radius of curvature of the beam due to moment  $M$ , and
- $Y_{\max}$  = displacement of the outer fiber in the width direction.

In order to determine the limitation on  $L/b$  that prevents anticlastic surface, we assume that  $Y_{\max}$  can be  $+0.99 b/2$  or  $1.01 b/2$ , that is, only 1 percent deformation in the width direction is allowed. Since  $1/R = M/EI$ ,  $I = bt^3/12$ , and  $M = PL/4$ , Eq 2 becomes

$$Y_{\max} = \pm \frac{b}{2} \left( 1 - \frac{3\nu PL}{2Ebt^2} \right) \quad (3)$$

Let us apply Eq 3 to the following two examples.

1. Let  $P = 10$  lb,  $\nu = 0.5$ ,  $E = 15 \times 10^6$  psi, and  $t = 0.01$  in. Applying the restriction of 1 percent stated previously we obtain

$$\frac{L}{b} \leq 2$$

2. Let  $P = 50$  lb,  $\nu = 0.5$ ,  $E = 15 \times 10^6$  psi, and  $t = 0.1$  in. Applying the restriction of 1 percent just stated, we obtain

$$\frac{L}{b} \leq 40$$

## APPENDIX III

### Stress Relaxation Extrapolation

Time dependence of stress relaxation rate can be described as follows

$$\text{stress relaxation rate} = -k(t + a)^{-n}$$

where  $k$ ,  $a$ , and  $n$  are constants independent of time but dependent on the initial stress and temperature. Equations of this form are used to describe the kinetics of recovery. Analogous to other kinetic processes, the relaxation rate is highest initially, and it decreases with increasing time. The rate of decrease in the relaxation rate depends upon the value of  $n$ .

The driving force for stress relaxation in a cold-worked material is due to the unstable, high-energy dislocation substructure developed as a result of cold work. During stress relaxation, the substructure rearranges into a more stable, low-energy configuration. As the substructure transforms from high-energy to low-energy arrays, the driving force decreases, and the stress relaxation rate decreases. This behavior is analogous to what happens in the material during recovery. Accordingly, the time dependence of stress relaxation rate can be described by the previous expression. Integration of this expression gives Eqs 1a or 1b, depending upon the value of  $n$ .

## APPENDIX IV

### Procedure for Extrapolation of Stress Relaxation Data

In Eqs 1a and 1b, the constant  $a$  accounts for the short time transient in the stress relaxation behavior. In general, transients occur within the first 100 h. For example, in Fig. 4, the datum point at 1 h is on the transient portion of the curve. Therefore, in order to simplify the procedure described next to determine the constants  $X$ ,  $n$ , and  $k$ , the constant  $a$  in Eqs 1a and 1b can be neglected if data for times exceeding 100 h are used.

For Eq 1a, the following expressions may be used to calculate  $X$ ,  $n$ , and  $k$  from the relaxation data, that is, the stress remaining versus time curve

$$X = \frac{\sigma_2^2 - \sigma_1\sigma_3}{2\sigma_2 - \sigma_1 - \sigma_3} \quad (4)$$

$$n = 1 - \log \frac{\sigma_1 - \sigma_2}{\sigma_2 - \sigma_3} \frac{1}{\log J} \quad (5)$$

and

$$k = - \frac{(\sigma_1 - X)(1 - n)}{t_1^{(1-n)}} \quad (6)$$

where  $\sigma_1$ ,  $\sigma_2$ , and  $\sigma_3$  are stresses at times  $t_1$ ,  $t_2$ , and  $t_3$ , respectively. Times  $t_1$ ,  $t_2$ , and  $t_3$  are selected such that  $t_1/t_2 = t_2/t_3 = J$ .

Equations 4, 5, and 6 are derived as follows. Equation 1a can be written as

$$\frac{(\sigma - X)(1 - n)}{-k} = t^{(1-n)} \tag{7}$$

Let  $t_1, t_2,$  and  $t_3$  be such that  $t_1/t_2 = t_2/t_3 = J$ . At  $t_1, t_2,$  and  $t_3$ , Eq 7 becomes

$$\frac{(\sigma_1 - X)(1 - n)}{-k} = t_1^{(1-n)} \tag{8}$$

$$\frac{(\sigma_2 - X)(1 - n)}{-k} = t_2^{(1-n)} \tag{9}$$

$$\frac{(\sigma_3 - X)(1 - n)}{-k} = t_3^{(1-n)} \tag{10}$$

Divide Eq 8 by Eq 9 and Eq 9 by Eq 10 to obtain

$$\frac{\sigma_1 - X}{\sigma_2 - X} = \left(\frac{t_1}{t_2}\right)^{(1-n)} \tag{11}$$

and

$$\frac{\sigma_2 - X}{\sigma_3 - X} = \left(\frac{t_2}{t_3}\right)^{(1-n)} \tag{12}$$

Since  $t_1/t_2 = t_2/t_3$

$$\frac{\sigma_1 - X}{\sigma_2 - X} = \frac{\sigma_2 - X}{\sigma_3 - X} \tag{13}$$

Solve for  $X$  in Eq 13 to obtain

$$X = \frac{\sigma_2^2 - \sigma_1\sigma_3}{2\sigma_2 - \sigma_1 - \sigma_3}$$

Substituting for  $X$  in Eq 11

$$\frac{\sigma_1 - \frac{\sigma_2^2 - \sigma_1\sigma_3}{2\sigma_2 - \sigma_1 - \sigma_3}}{\sigma_2 - \frac{\sigma_2^2 - \sigma_1\sigma_3}{2\sigma_2 - \sigma_1 - \sigma_3}} = \left(\frac{t_1}{t_2}\right)^{(1-n)} = J^{(1-n)} \tag{14}$$

Simplifying, Eq 14 becomes

$$\frac{\sigma_1 - \sigma_2}{\sigma_2 - \sigma_3} = J^{(1-n)} \tag{15}$$

Solving for  $n$  in Eq 15 to obtain

$$n = 1 - \log \frac{\sigma_1 - \sigma_2}{\sigma_2 - \sigma_3} \frac{1}{\log J}$$

Knowing  $X$  and  $n, k$  can be determined from any of the Eqs 8-10.

To show the application of Eq 1a, the following sample calculation for stress relaxation test data for copper wire [9] is done next. The top curve (initial stress = 25 000 psi) in Fig. 12 is used (figure number refers to figure in source just cited). The shape of this curve corresponds to the shape of the curve for  $n < 1$  in Fig. 6.

The following stress values were determined from the curve in Fig. 12 of Ref 9.

<u>Elapsed Time, h</u>	<u>Residual Stress, psi</u>
1	23 460
10	21 440
100	18 846
1 000	15 770
10 000	12 300
42 000	10 000

Since  $100/1000 = 1000/10\ 000 = 0.1$ , stresses corresponding to these three time periods were used to obtain  $X = 42\ 860$ ,  $n = 0.948$ , and  $k = 983$  with Eqs 4, 5, and 6.

Equation 1a becomes

$$\sigma = - \frac{983}{0.052} \times t^{0.052} + 42\ 860$$

Using this equation, the following stresses were calculated.

<u>Elapsed Time, h</u>	<u>Calculated Stress, psi</u>
1	23 956
10	21 551
100	18 841
1 000	15 786
10 000	12 342
42 000	9 978

The agreement between the calculated stress at 42 000 h, which was not used to calculate the constants, and the measured stress value at 42 000 h is quite good.

For Eq 1b,  $\sigma$  (stress remaining) versus  $\log t$  will be a straight line which can be extrapolated graphically to any desired time.

### References

- [1] Schlabach, T. D., *Transactions on Parts, Hybrids, and Packaging*, Institute of Electrical and Electronics Engineers, Vol. PHP-9, No. 4, Dec. 1973, p. 237.
- [2] Butt, S. H., "Choice of New Copper Alloys for Use in Miniaturization of Electrical and Electronic Terminals and Connectors," Technical Report No. W71-12.2, American Society for Metals, 1971.
- [3] Parikh, P., Shapiro, E., and Crane, J., "Mechanical Metallurgy of Copper Base Alloy Electronic Connectors," *Proceedings, 7th Annual Connector Symposium*, Electronic Study Group, Inc., Cherry Hill, N. J., Oct., 1974.
- [4] Manjoine, M. J., *Journal of Materials*, Vol. 6, No. 2, June 1971, pp. 253-264.
- [5] Honeycombe, R. W. K., "The Plastic Deformation of Metals," St. Martin Press, New York, 1968, pp. 284, 352.
- [6] Fox, A., *Journal of Materials*, Vol. 6, No. 2, 1971, pp. 422-435.
- [7] Fox, A., "Stress Relaxation and Fatigue of Small Diameter Wires Used for Miniature Springs," Technical Report 69-WA/Met. 2, American Society of Mechanical Engineers, 1969.
- [8] Timoshenko, S. P. and Goodier, J. N., *Theory of Elasticity*, 3rd ed., McGraw-Hill, New York, p. 287.
- [9] Gohn, G. R. and Fox, A., *Materials Research and Standards*, Vol. 1, No. 12, Dec. 1961, Fig. 12, p. 964.

A. K. Schmieder<sup>1</sup> and R. S. Robinson<sup>1</sup>

## Comparison of Manual to Automatic Unloading During Relaxation Tests

---

**REFERENCE:** Schmieder, A. K. and Robinson, R. S., "Comparison of Manual to Automatic Unloading During Relaxation Tests," *Recent Developments in Mechanical Testing, ASTM STP 608*, American Society for Testing and Materials, 1976, pp. 118-133.

**ABSTRACT:** Relaxation tests are commonly made using the two following procedures: first by using a special machine, load is removed automatically in many small steps as the strain tends to increase. In the second procedure, a creep machine is used, and the load is reduced manually whenever the strain reaches a certain limit. In this case, the number of stress steps down is relatively small. One of a pair of specimens was tested by each method for several materials and the relaxation curves compared. They were found to be in good agreement when the magnitude of the stress step down is chosen in a particular manner. The factors involved in this choice are discussed in detail. The incremental creep curves obtained at each stress level of the manual test are compared with the normal creep curves at constant load. The previously reported disagreement between the results of these two methods of relaxation testing are discussed, and an explanation is offered.

**KEY WORDS:** mechanical tests, stress relaxation tests, unloading, strains, creep tests, extensometers, stresses

During the tests reported here, the upper limit of strain is never allowed to exceed a predetermined strain limit. The specimen is loaded to reach this limit as quickly as is convenient and then unloaded as frequently as is necessary to avoid exceeding the limit. During the manual tests, one or more weights are lifted from the load pan by hand whenever the indicating extensometer reaches the predetermined strain limit. About ten of these "stress steps down" are made during each test. During the automatic tests, the stress is reduced whenever the pressure between contact points of an extensometer exceeds a preset amount. The change of stress at each reduction is less than 1/5 percent. Hundreds of reductions occur during a normal test.

<sup>1</sup> Manager, Materials Testing Unit, and Supervisor, Creep Testing, respectively, General Electric Co., Schenectady, N. Y. 12345.

The principal objective of the tests reported here was to determine whether the manual method and the automatic method give the same values for remaining stress for the test conditions normally used during the evaluation of bolting materials. To do this, a test was made on each of two similar specimens, one test being a manual relaxation test and the other test an automatic relaxation test. Both were made at the same strain limit and temperature. The tests were repeated later on specimens from another heat of the same material and also on two other materials. Except for the last material tested, both specimens were taken from the same piece of stock.

A secondary objective of this report is to compare creep during the constant force increments of the manual relaxation test to creep during normal creep tests when the force is constant throughout the test.

The technique for manual relaxation testing differs from that for normal creep testing in that a choice of magnitude of the stress steps down must be made. Since there is little information in the published literature on this subject, a separate section is devoted to it.

### **Materials Tested**

Four materials were tested. Two of these had the same specification but were from different heats. Chemical composition, heat treatment, and tension test results (when available) are shown in Table 1. The materials in the order tested are:

1. Modified Crucible 422, 1st set.
2. All weld metal, low ferrite, 347 stainless steel.
3. Modified Crucible 422, 2nd set.
4. AISI 4340.

### **Equipment Used**

The same type machine was used for both manual and automatic relaxation tests. It is of our design, Model CR. The furnace is 33 in. high, 16 in. in diameter, with a 3 in. bore. Three heating zones of resistance wire are wound on the outside of the muffle tube. The top and bottom zones are 5 in. long, and the center zone is 8 in. long. Autotransformers are used to adjust the heat input to each zone manually. To control temperature, the input voltage is switched from its higher level to 85 percent of this level by a thermostat. The input level is chosen so that the voltage is at the higher level 50 percent of the time when line voltage is normal. The laboratory is supplied through constant voltage transformers. Typically, the temperature cycling rate of the furnace is 9 cycles/h with an amplitude of 0.5°F indicated by thermocouples attached to the specimens.

The loading system consists of a 20:1 lever with 5-lb lead weights causing a 1 ksi increase in stress per weight. The specimen is 0.375 in. in diameter

TABLE 1—Properties of materials tested.

Chemical Composition, percent by weight												
Material No.	Description	C	Ni	Cr	Mo	V	W	Mn	Si	P	S	Cb
1	Modified Crucible 422	0.19	0.77	12.8	1.03	0.24	1.15	0.77	0.20	0.020	0.018	...
2	all weld metal, low ferrite, 347	0.09	10.2	19.2	...	...	...	1.96	0.27	0.025	0.012	0.68
3	Modified Crucible 422	0.19	0.66	12.7	1.03	0.30	0.97	0.84	0.47	...	...	...
4	AISI 4340 manual test	0.41	1.78	0.81	0.25	...	...	0.77	0.21	0.006	0.005	...
	automatic test	0.41	1.76	0.80	0.25	...	...	0.73	0.26	0.006	0.005	...
Heat Treatment												
Material No.												
1	1600°F—2 h—furnace cooled; 1900°F—2 h—oil quenched; 1250°F—6 h—air cooled											
2	as welded											
3	1900°F—oil quenched; 1200°F—air cooled											
4	1600°F—2.8 h—air cooled; 1525°F—2.8 h—oil quenched; 1020°F—4 h—air cooled; 970°F—4 h—air cooled											
Tension Test Results												
Material No.	Test Temperature, °F	Tensile Strength, ksi	Yield Strength 0.02% Offset, ksi	Yield Strength 0.2% Offset, ksi	Elongation, %	Reduction in Area, %						
1	70	143.0	106.0	...	16.0	47.8						
1	1300	33.4	...	...	33.0	92.4						
3	70	162.0	110.0	...	16.0	44.0						
3	1300	40.5	...	...	...	...						
4 manual	70	160.0	...	147.0	19.9	61.9						
4 manual	650	139.0	...	117.0	20.5	71.2						
4 automatic	70	157.0	...	144.0	17.8	60.0						
4 automatic	650	138.0	...	112.0	21.5	72.5						

with 0.50-in.-diameter threaded ends. The reduced portion is 7 in. long. The extensometer used during the manual relaxation tests has a rod and tube on each side of the specimen extending from the clamps on the specimen shoulders to an averaging head outside the furnace. The displacement of the rods relative to the tubes is read without further magnification by a dial indicator with 0.0001 in. divisions. Tenths of a division are estimated, giving reading to  $1.4 \times 10^{-6}$  strain. The repeatability of these readings is about  $3 \times 10^{-6}$ .

The extensometer and unloading system used during the automatic relaxation tests has been described previously [1].<sup>2</sup>

The axially of loading of the Type CR machines has been previously reported [2]. The bending strains are within the limits given in ASTM Recommended Practice for Creep, Creep-Rupture, and Stress-Rupture Tests of Metallic Materials (E 139-70).

Tests on the first two materials listed were made in a laboratory where the ambient temperature varied about 15°F daily during the summer and autumn when the tests were made. The other two materials were tested in an air-conditioned laboratory where the ambient temperature ranged over less than 5°F.

### Testing Procedure

Except for loading and unloading techniques, the testing procedure was the same for both the manual and automatic tests. Temperature was measured by three chromel-alumel thermocouples, one attached at each end and one at the center of the reduced portion of the specimen. While the specimen is brought to temperature and equalized, the temperature is recorded and controlled by a suppressed zero instrument having 1 in. of pen motion for each 2°F. The controller is set by a precision potentiometer. After the temperature has stabilized within 1°F of the set point, the thermostat is set to cycle from high to low power within the 1°F range of the furnace cycle. Control is then transferred to the thermostat. The recording is continued for several hours to assure that the mean temperature was not changed during the transfer of control. The specimen is then loaded. The temperature indicated by each of the three thermocouples is read daily during the test. Ambient temperature is read whenever strain is recorded during the manual relaxation tests.

During initial loading and final unloading of the manual tests, a weight was added or removed from the weight pan at 10-s intervals, giving an average rate of loading of 6 ksi/min. The extensometer reading was plotted immediately after each weight change. This plot was used to determine when loading should stop. When the addition of one more weight would

<sup>2</sup> The italic numbers in brackets refer to the list of references appended to this paper.

result in a strain greater than the specified strain limit, loading was stopped and the extensometer watched until the strain limit was reached by creep. Then the first stress step down was made by removing one or more weights. The extensometer was read immediately after the stress step down and at equal intervals thereafter to provide approximately ten readings between each stress step down. When the strain limit was again reached, another stress step down was made. In general, each stress step down was of the same magnitude during any one test. The selection of this magnitude will be discussed in the next section. The relaxation data from the manual test consist of the stress and time immediately before each stress step down. The strain data at each level of stress were plotted versus time to estimate the time for the next stress step down. These curves are called flow rate curves, and the maximum slope is called the flow rate at that stress.

During the automatic relaxation tests, the loading and unloading was at approximately the same rate as during the manual tests, and the same readings were taken. The loading motor was operated manually. At preselected stress levels, the loading was interrupted and the extensometer manually turned to the switching point and the strain read. Control was switched from manual to automatic when the strain limit was reached by creep. Thereafter, the stress was read and time recorded periodically for the remainder of the test.

### **Procedure for Selecting the Magnitude of Stress Step Down**

Other things being equal, uniform stress steps down are used. The magnitude is chosen before the relaxation test is started. This simplifies instruction and reporting and also aids in the analysis of the flow rate data.

Small steps would occur so rapidly during the first part of the test that creep data could not be obtained. A practical limit for manual reading is about one reading of the extensometer every 10 s and a time between the first and second stress step down of at least 1 min. Small steps also increase the cost of the test since more operator attention is required. Another lower limit of step size is the sensitivity of the extensometer. In order for the creep reading at each stress level to be significant, the elastic recovery at each stress step down should be about ten times the least strain change that can be read with the extensometer. Our extensometer readings are repeatable to  $3 \times 10^{-6}$  strain. So a stress step down of 0.5 ksi is the least that can be used, and 1 ksi is the preferred lower limit.

An upper limit for the size of stress step down is set by the desirability of having at least five points on the relaxation curve. This means that, in general, no more than one tenth of the maximum stress is removed during one stress step down. Three ksi is the largest stress step down we use. One or two ksi are used in the majority of tests.

For extrapolation, it is desirable to plot the relaxation data so the test points fall on or near a straight line. To achieve this objective, time is

usually plotted on a logarithmic scale and stress on a uniform or a logarithmic scale. It is customary to choose test conditions so that the plotted points will be spaced approximately uniformly along the curve. When points are uniformly spaced along a log time axis, the accumulated time at any point is obtained by multiplying the accumulated time at the preceding point by a constant. The incremental time between points is then similarly related by the same constant. This constant will be called the incremental time ratio. Two is a convenient and practical value for this constant in manual relaxation testing. Then the incremental time at the next stress is equal to the accumulated time to the step down which established that stress. Therefore, only one stress step down need be made during the night following the first day in test. If the second step down is made after 0.02 h, then the nineteenth will occur at 2624 h, an adequate but not excessive number of test points.

The next question is how to determine before the test starts what size the stress step down should be so that each increment will last twice as long as the preceding one. A guiding value can be readily calculated if creep or rupture tests have been made on the material.

If creep tests are available, log stress versus log time to any specified strain should be plotted to measure the slope of a straight line through the points. For increased accuracy in observing scatter, it is usually desirable to have a log cycle of stress represented by three (four or five) times as much distance as a log cycle of time. Then the observed length of the stress side of the slope triangle should be divided by three (four or five) to obtain the slope that would be observed if the scales were uniform. If only three tests are available and they do not lie near a straight line, the calculation of step down size may not be reliable. If more tests are available, a line may be faired through the data points.

The size of stress step down is solved by Eq 1 which is derived in the appendix

$$s_1 - s_2 = -s_1 n \log_e a \quad (1)$$

where

$s$  = stress,

$a$  = incremental time ratio,

Subscript 1 = stress after first step down,

Subscript 2 = stress after second step down, and

$n$  = minimum slope of the plot of log (stress) versus log (time to a specified strain) from constant force creep tests at the same temperature as the relaxation test.

For the recommended incremental time ratio of 2, Eq 1 becomes

$$s_1 - s_2 = -0.7 s_1 n \quad (2)$$

The chosen value of strain for plotting the constant force creep data has little effect on the slope for most materials. If rupture tests at the temperature of the relaxation test are available and if the elongations are fairly uniform, the slope  $n$  may be measured from a plot of log stress versus log time to rupture [3]. If rupture tests at various temperatures are available and the elongations are fairly uniform, the rupture times may be converted to the equivalent times at the relaxation test temperature using one of the parametric relationships from ASTM Method E 139. Then these equivalent times and stresses are plotted as described previously.

If no creep or rupture data are available on the material, the size of the steps down can be determined immediately from the loading data as follows. Select a loading increment such that 15 to 30 increments will result in a stress equal to the strain limit times the modulus of elasticity at the test temperature. Hold each stress level 1 min and record strain just before and just after each weight is placed on the pan. Tabulate creep strain for each increment. A suitable size step down increment is about one tenth of the difference between the maximum stress attained and the lowest stress at which creep was clearly apparent.

### Results of Tests

The two upper rows of Table 2 show the independent variables of temperature and strain limit. The third row shows the slope of the linear portion of the stress strain curve on loading. The next row shows the maximum stress applied to reach the strain limit. For the three tests at the higher temperatures, the manual tests had a value less than the automatic test by from 0 to 20 percent. The next row shows that this difference increased as the time to the first stress step down. The following rows compare the remaining stress at the last stress step down in the time range of the automatic relaxation test. To avoid subjective interpretation, the automatic test values are taken at the most nearly equal time when the load indicator was read. The difference between the manual test and the automatic test values were +4 to -6 percent for the two short time tests. For the two tests over 2000 h in length, the difference is negligible.

The first section of Table 3 shows the relationship between the creep rate at maximum stress following an increase in force and the value at the same stress following a decrease in stress. The value shown for the increased stress case is the change in strain while the maximum stress was applied divided by the time to first step down (shown in Table 2). The value for decreased stress is obtained by plotting the average creep rates during the constant stress increments versus stress and extrapolating back to maximum stress. The rate following a stress increase is from 1.4 to 12 times that following a stress decrease. The remaining sections of Table 3 give statistics on the magnitude and frequency of the stress steps down.

TABLE 2—Comparison of results from manual and automatic relaxation tests.

Material	347 Weld							
	422				4340			
	Manual		Automatic		Manual		Automatic	
Type of Test	Manual	Automatic	No. 1	No. 2	Manual	Automatic	Manual	Automatic
Temperature, °F	1100	1100	1200	1200	1050	1050	650	650
Strain limit $\times 10^3$	2.0	2.0	2.0	2.0	2.0	2.0	1.5	1.5
Apparent modulus of elasticity, psi $\times 10^{-6}$	18.1	18.2	15.5	14.5	20.4	19.4	27.3	26.0
Maximum stress, ksi	26.0	32.0	29.0	28.6	37.0	38.5	39.0	38.0
Time to first step down, h	0.8	0.02	0.02	0.03	0.03	0.03	1.8	1.8
stress, ksi after	14.0	14.5	18.0	17.2	12.0	12.1	32.5	32.5
time (h)	(183)	(188)	(351)	(329)	(2135)	(2105)	(2879)	(2865)

TABLE 3—Further results from manual relaxation tests.

422 Set 1	347 Weld	422 Set 2	4340
<i>Creep Rate per Hour at Maximum Stress After Increase in Force</i>			
$5.6 \times 10^{-4}$	$37.0 \times 10^{-4}$	$24.0 \times 10^{-3}$	$12.0 \times 10^{-6}$
<i>Creep Rate per Hour at Maximum Stress After a Decrease in Force</i>			
$2.7 \times 10^{-4}$	$3.0 \times 10^{-4}$	$2.4 \times 10^{-3}$	$2.5 \times 10^{-6}$
<i>Total Number of Steps Down</i>			
7	4	12	7
<i>Most Frequent Magnitude of Step Down, ksi</i>			
2	3	2	1
<i>Number of Steps Down at This Step Down Magnitude</i>			
7	3	7	6
<i>Range of Incremental Time Ratios at This Step Down Magnitude</i>			
3.2 to 1.9 <sup>a</sup>	25.7 to 3.9 <sup>a</sup>	3.9 to 2.0 <sup>a</sup>	3.6 to 1.9 <sup>a</sup>
<i>Average of Incremental Time Ratios at This Step Down Magnitude</i>			
2.5	14.8	3.0	2.4

<sup>a</sup> Trend was for a decreasing ratio as the test proceeded.

Figure 1 shows the variation of stress with time for both the manual and automatic relaxation tests. For the manual tests, the stress and time just before each stress step down in the plotted range is shown. The maximum difference is about 6 percent. In general, the difference decreases as the test continues. The manual test stress values which lie about the automatic test curve are about equal in number to those which lie below. The difference between manual and automatic tests is about equal in magnitude to the difference between the two automatic tests on the same material.

Figure 2 shows the variation of strain preceding the last two stress steps down. The shortening of the specimen after a stress step down is typical. Also typical is the increased apparent magnitude of the negative creep as the stress decreases. The maximum creep rate (called the flow rate) at 8 ksi is 1.6 times the average creep rate at the stress (called the average flow rate).

## Discussion

The comparison tests reported here were made to determine whether the two methods gave equivalent results and to determine the strain during the manual test which should be used to characterize the test to make the results of the two methods agree. These tests indicate that the remaining stress at long time is the same for manual and automatic relaxation tests, when the upper strain limits and temperature are the same. This is very convenient but is unexpected both on the basis of published opinion and simple rational

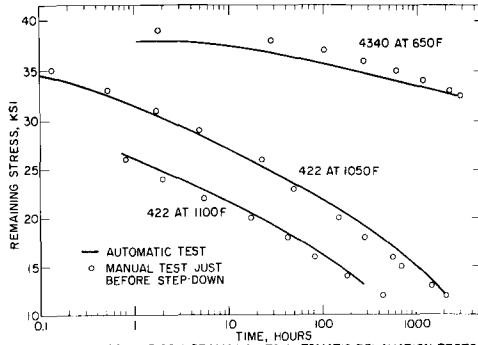


FIGURE 1. COMPARISON OF MANUAL TO AUTOMATIC RELAXATION TESTS

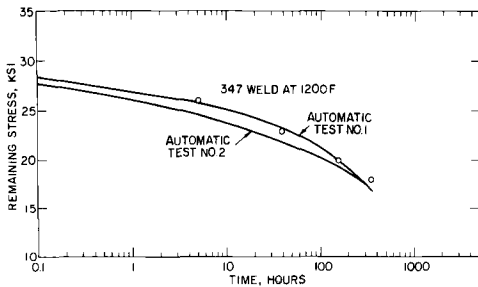


FIGURE 1. COMPARISON OF MANUAL TO AUTOMATIC RELAXATION TESTS (Cont'd)

FIG. 1—Comparison of manual to automatic relaxation tests.

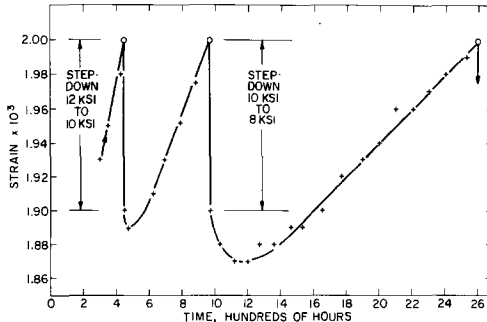


FIGURE 2. FLOW-RATE CURVES FOR CRUCIBLE 422 AT 1100°F

FIG. 2—Flow-rate curves for Crucible 422 at 1100°F.

analysis. Note 7 of ASTM Recommended Practice for Stress-Relaxation Tests for Materials and Structures (E 328-75) says that the manual test may indicate higher design stresses or lower relaxation rates than the automatic test.

As far as we know, the most comprehensive comparison of manual and automatic relaxation tests and creep tests on a single material is that

published by Gohn and Fox [4]. This shows the curves for manual relaxation tests at higher stresses than for automatic relaxation tests. However, the strain limits are not stated and the loading procedure was such that the manual tests must have had higher strain limits. This certainly accounts for some of the difference they report and may account for all of it. Since there is little, if any, experimental evidence that the manual test results in higher stresses than the automatic test when the upper strain limits are the same, it is presumed that the common opinion on this point stems from a rational basis.

One rational basis for expected higher stresses from the manual test is that most of the time the stress is less than would be required for a constant strain limit. Therefore, it is expected that accumulated plastic strain would be less and the remaining stress would be more than if the strain were constant at the limit. This reasoning implies that the incremental creep curves during the manual test follow the usual laws for creep during constant force tests. Figure 2 shows clearly that the usual creep laws do not apply and that a transient shortening action is initiated at each unloading operation. This shortening action is apparently proportionately greater for the smaller steps of the automatic test and compensates for the greater average stress. In any case, it seems clear that any calculation of the effect of step size should be based on a hypothesis which is consistent with the observed negative strain after stress step down.

A closely related but more subtle question is whether an equivalent strain limit should be used to characterize the manual test, the equivalent limit presumably being between the upper and the lower limit of strain during each incremental test. Again, any rational equivalent limit should be based on a hypothesis which is consistent with the observed incremental creep curves. The tests reported here show the manual test curves to consistently lie neither above nor below the automatic test curves when the equivalent strain is assumed to be upper limit. Therefore, there is little justification for attempting to calculate and justify a lower equivalent strain limit.

By analysis based on strain hardening theory, Taira and Suzuki [5] have made a theoretical comparison of the stress step down to the automatic relaxation test. They conclude that the two tests should give similar results, independent of the size of the stress steps, when the upper limit of strain is the same for both. Their theoretical conclusions were confirmed by comparison tests on a low carbon steel at 450°C with 0.0025 strain.

When requested to determine remaining stress after several hundred hours, we have been making manual and automatic relaxation tests in about equal numbers for the last 15 years. This indicates that each method has advantages that make it more suitable under some circumstances. The advantages of manual testing are:

1. Tests can be made with normal creep equipment, thus simplifying the matching of equipment with the creep and relaxation test requests on hand.

2. The stress is known at all times and is controlled by the operator's judgment. This is particularly important during very long time tests, when malfunctions of strain control equipment or intervals of low temperature become more probable and could cause overloading of an automatic test. It makes manual testing the clear-cut choice when ambient temperature fluctuations affect strain indication.

3. Flow-rate curves can be used to estimate the constants of generalized equations for creep and relaxation.

The advantages of automatic testing are:

1. The test is more economical since it normally requires no attention during the night and on weekends.

2. The test conditions are more easily described and conform more closely to the simplest definition of relaxation.

3. The strain is constant throughout the test so no justification is required for reporting a single value as representative of a range.

4. The test can be terminated as planned without consideration of whether a particular stress step down process is complete.

Most of the advantages just listed are self evident. The usefulness of the flow-rate data obtained from the manual tests may not be so. We have found no simple relationship between the flow rate at various stresses as measured during the manual relaxation test and the creep rate during a constant load test. Table 2 shows that the constant load test has a greater creep rate at the same stress and strain.

At the other extreme, the flow rate at a given stress is generally larger than the minimum creep rate at the stress. The simplest approximate relationship that we have observed for most materials is that the flow rate is proportional to the creep rate at the same stress and time since loading. The data of Gohn and Fox [4] on copper at room temperature show more common points between manual relaxation tests and constant load creep tests than any tests we have made. Therefore, their data will be used to demonstrate the just mentioned relationship. Table 4 lists all of the common points of stress and time where the slope of the curves for the constant force tests can be measured with useful accuracy. The stresses for the manual relaxation tests are interpolated from their plot of remaining stress just

TABLE 4—Comparison of creep rates from constant force and manual relaxation tests (from Gohn and Fox [4]).

Manual relaxation, initial stress, ksi	25	20	20	15	20	10
Stress at common point, ksi	12.5	12.5	10	10	8	6
Time at common point, h	4250	1000	10 000	1000	8800	4500
Plastic creep rate, per hour $\times 10^8$						
By manual relaxation test	2	9	0.8	7	0.9	1
By constant force test	7	20	3	12	2	2

before step down versus time. The creep rate is taken as the negative of the rate of change of stress divided by the modulus of elasticity. This method of calculation gives the average flow rate. As has been shown in Fig. 2, the flow rate, which is, by definition, the maximum value during the incremental creep, can be almost twice the average for long-time intervals. Therefore, if the data were available to calculate the flow rate, it would be found to be more nearly equal to the creep rate from constant force tests than the values just reported. The example just cited is typical in that the average flow rate is usually about half of the creep rate at the same stress, temperature, and time since the start of test. At the temperatures of normal industrial use, a 3000-h manual relaxation test will give flow rates near  $10^{-7}/h$ . Therefore, the manual relaxation test can be used to select the stress for a creep test to determine this standard creep strength.

The results reported here will be used as illustrations rather than as a basis for the discussion of accuracy and reproducibility of relaxation test results. The basis is founded on a large number of other tests not reported here. The apparent modulus of elasticity values for one material from Table 2 range over 5 percent. This is a normal range. This is several times greater than the error indicated by the accuracy of the extension measuring instruments or the loading system. We have discovered that bending strains normally found in tension-loaded specimens can result in variations of apparent modulus of this magnitude. On the other hand, occasionally much greater deviations from the expected modulus value occur and indicate excessive bending or inaccurate strain measurement. We believe that apparent modulus should be reported with all creep and relaxation data, not as a material property but as a measure of the accuracy of the system. A recent report of an international, cooperative, creep rupture program [6] also says it seems essential to check the performance of the extensometric device by recording the strain-load curve. With most testing equipment, this means that the loading must be done incrementally and relatively slowly, and the loading rate will vary with different machines and operators. This in turn means that the reported initial stress and zero time are the result of the test method as well as the material. The tests reported here were made at nominally the same loading rate, but still the initial stress (maximum stress) had more variability than any other measured quantity. For this reason, we believe that strain rather than initial stress should be used as the independent variable, and the remaining rather than the relaxed stress should be reported.

The formula for selecting the magnitude of stress step down implies that, for a constant increment ratio, a fixed percentage of the existing load be removed at each stress step down. This would also be required if log remaining stress versus log time were linear. Removing a different amount of weight each time would be awkward and fortunately is usually not necessary for equally spaced points. Almost all of our tests show an increasing

negative slope when plotted with double logarithmic scales. Plotting stress versus log time as in Fig. 1 makes the relaxation curve more linear but still with a slightly increasing negative slope at longer times. Thus, with uniform stress step downs, the test points still tend to be spaced closer together at long times. Because it is more linear and conservative (in that extrapolation shows complete relaxation in finite time), we prefer the stress versus log time plot for almost all materials.

Table 3 shows that most of the tests have magnitudes of stress step down and incremental time ratios in the recommended range. The test on welded 347 is an exception. This test was made 15 years ago before the selection procedure was formalized. Using parameter rupture data, a stress step down of 1.4 ksi is solved by Eq 2 compared to the 3 ksi used. The test was unusually erratic in the variation of the incremental time ratio. The elongation at fracture for six parameter rupture tests ranged from 1.5 to 11.0 percent, indicating an exceptionally inhomogeneous or unstable material. Yet even under these adverse circumstances, the agreement between the manual test and the automatic tests is as good as between duplicate automatic tests.

The first three tests listed are all of the direct comparisons of manual to automatic relaxation tests which we have made. We regarded them as sufficient evidence that the two methods can be used interchangeably. Recently, two heats of AISI 4340 with very similar composition were relaxation tested, one manually and the other automatically. These tests are included as the fourth comparison. Some of the difference in the results may be due to the difference in materials. The tests were also included to illustrate another point, namely, the greater regularity of the manual data when tests are made at temperatures which result in little relaxation. This program and others indicate that, for long-time tests when little relaxation is expected, the manual test with minimum stress steps down is to be preferred to the automatic test. For a short-time test with much relaxation, an automatic machine with a stress recorder is clearly preferable to the manual test.

## Conclusions

1. Automatic relaxation tests and manual relaxation tests give similar results at times of several hundred hours or more if seven or more uniform stress steps down are used.
2. The manual test should be characterized by the upper strain limit.
3. For long-time engineering data, relaxation tests should be characterized and compared on the basis of strain limit rather than initial stress and the results should be presented as remaining stress, rather than relaxed stress.

*Acknowledgment*

We are indebted to R. F. Gill for his interest and contributions to the development of relaxation testing technique in this laboratory. His gentle reminders over a period of ten years have finally resulted in the writing of this paper.

**APPENDIX****Derivation of Formula for Magnitude of Stress Step Down**

- If
- $s$  = stress,
  - $E$  = modulus of elasticity at the test temperature,
  - $e$  = chosen creep strain, having a single value for all constant force creep tests,
  - $t$  = time to attain plastic strain,  $e$ ,
  - $c$  = average creep rate during a constant force test,
  - $f$  = average flow rate at a particular stress level of the manual relaxation test,
  - $\Delta t$  = length of time a particular stress was applied during the manual relaxation test,
  - $a = \Delta t_2 / \Delta t_1$ ,
  - Subscript 0 = maximum stress during the manual relaxation test, and
  - Subscripts 1 or 2 = stress level after the first or second stress step down.

By definition

$$c_1 = \frac{e}{t_1} \quad f_1 = \frac{s_0 - s_1}{E \Delta t_1}$$

$$c_2 = \frac{e}{t_2} \quad f_2 = \frac{s_1 - s_2}{E \Delta t_2}$$

Assume  $c$  and  $f$  are proportional at each stress.

Let

$$s_0 - s_1 = s_1 - s_2$$

then

$$\frac{c_1}{c_2} = \frac{f_1}{f_2} = \frac{t_2}{t_1} = \frac{\Delta t_2}{\Delta t_1} = a \quad (3)$$

If plotted values of  $\log s$  versus  $\log t$  lie on a straight line, then the variables are related by an equation of the form

$$s = kt^n \quad (4)$$

Where  $k$  is a material constant and  $n$  is equal to the slope of the line through the plotted points.

Substituting from Eq 4 into Eq 3

$$a = \frac{t_2}{t_1} = \left[ \frac{s_2}{s_1} \right]^{1/n}$$

$$\frac{s_2}{s_1} = a^n$$

Subtracting 1 for both sides and expanding  $a^n$  by series and retaining only the first two terms

$$\frac{s_2 - s_1}{s_1} = 1 + n \log_e a - 1$$

## References

- [1] Goldhoff, R. M. and Barker, L. B., "Stress Relaxation in Variable Notch Sensitivity Cr-MoV Steel," *Proceedings, American Society for Testing and Materials*, Vol. 62, 1962, p. 1176.
- [2] Schmieder, A. K. and Henry, A. T. in *Elevated Temperature Testing Problem Areas, ASTM STP 488*, American Society for Testing and Materials, 1971, pp. 43-60.
- [3] Gill, R. F. and Goldhoff, R. M. in *Creep Rate Versus Total Creep as a Basis for Design*, ASM Publication No. P. 9-101, American Society for Metals, Oct. 1969, pp. 23-40.
- [4] Gohn, G. R. and Fox, A., *Materials Research and Standards*, Vol. 1, No. 12, Dec. 1961, pp. 957-967.
- [5] Taira, S. and Suzuki, F., *Proceedings, Fourth Japan Congress on Testing Materials*, Kyoto, Japan, 1961, pp. 56-59.
- [6] Coutsouradis, D. and Faurschou, "Cooperative Creep Testing Program," AGARD-R-581-71, Advisory group for Aeronautical Research and Development, Paris, March 1971.

